Prokaryotic Conjugation: Understanding the process of DNA transfer in archaea and bacteria

Leti Beltrán
Charlottesville, Virginia

B.S. Microbiology, Minor: Chemistry, University of Kansas, 2018
M.S. Biological and Physical Sciences, University of Virginia School of Medicine, 2022

A Dissertation presented to the Graduate Faculty of Virginia in Candidacy for the Degree in Doctor of Philosophy in Biophysics

Department of Molecular Physiology and Biological Physics
University of Virginia
April 2024

Table of Contents

Acknowledgements

I'm writing this somewhere in between writing all the other chapters of this dissertation. Mostly because I can't fathom the fact that I'll be completing my doctoral degree, and in bio*PHYSICS*, nonetheless; I hate physics and I hate math, but here I am five years later—Dr. Beltrán, not that I'll have anyone call me by this name. There are so many individuals that I must acknowledge and thank for their support, ceaseless inspiration, pushing me to my limits, investment, time and commitment to me and my training as a scientist. So, where do I begin and with whom? Let me start with Ed Egelman. I doubt that Ed will remember our first meeting—it was during graduate school interviews in February 2019. We talked for our duration of the 20-minute interview about books, Double Helix by James D. Watson and What is Life? By Erwin Schrödinger, his time at the MRC at Cambridge and he gave me a *short* tour of his lab, it is quite small. That was really the last time that I spoke with him until I started graduate school and he gave an impressive talk to the graduate students, informing us he was recruiting for his lab. Prior to joining his lab, I tried to do a co-mentorship with Ed and Dr. Lukas Tamm on a project that was considered too time consuming for a Ph.D. project by Eds standards, and so it was decided that I would solely join Eds lab. When I met with Ed on our follow-up meeting, I told him that I wanted to do other projects outside of ones focusing on helical reconstruction, his expertise, and that I wanted to publish in all the top journals (Nature, Science, and Cell), I believe he laughed a little. I wonder how he would have reacted if I had added that I wanted to be awarded the Nobel Prize, too. I like to joke about it a lot but I often wonder if it is at this point, he may have arrived at the realization that I'd be a bit overly zealous. Ed and I have not always seen eye to eye, if anything I've wanted to poke his eyes out on several occasions, (am I allowed to say this?) but he undoubtedly contributed substantially to my growth during my doctoral training. There are many aspects of Ed's character that I have grown to appreciate, but one of his strongest is his is extreme patience when it comes to teaching. Countless times Ed has been willing to schedule or have impromptu meetings with me to discuss indexing power spectra, going through scripts, calculations, and more recently sitting with me going through a list of potential professors I could complete my postdoctoral training with. Ed has also exhibited flexibility in my predoctoral training research, allowing me time to pursue my interests in single particle cryo-EM, cryo-electron tomography, correlated light electron microscopy, and focused-ion beam milling/scanning electron tomography. Having Ed as my principal investigator unquestionably attributed to my confidence as a scientist, both with my research and as a communicator (written and vocal). And, maybe it is because I have retrospectively seen it now, but I have a genuine appreciation for Ed as a person, and for his passion for research and science. So, thank you Ed for helping mold me into the scientist I am today;

thank you for pushing me to my limits, for your directness and for your commitment to me as my principal investigator.

The next person I want to thank is none other than Fengbin (Jerry) Wang. Oh, Jerry, you have truly been the greatest mentor I've had the privilege to work with; it was you after all that I got my first indexing experience with when I was rotating in Eds lab. You threw more lines on an image with already existing lines and said "you have to calculate the Bessel order first, then you can calculate the helical parameters.", and I nodded my head as if I really understood what you were talking about. After finding the Bessel order you formulated an equation that would help you find the rise and twist for different helical parameters. At the time it seemed like pure magic. Then, you turned to me and said something like, "okay, you can try this now. I'll be in my office. Let me know if you have questions.". Of course, I had questions! I wanted to know what spell you cast so that I could use it too! The pandemic made it difficult with learning, but there is no obstacle you cannot overcome, you generated a presentation highlighting the step-by-step actions of calculating symmetries and sent an email to me saying "Here you go, have fun!"; I was thinking "yes, Jerry, I'll be having *tons* of fun.". It's moments like these that might seem insignificant but made a huge impact on me. The investment, commitment and time you put forward toward making presentations, meeting with me by Zoom, rapidly answering my messages or emails all to help with my learning was more than I could ask for. From you I learned, how to freeze samples, data processing, how to calculate symmetries, model building, and how to outline my first paper. I found myself seeking your advice when I had questions about academics. You were the go-to person; for many in the lab, too. One of my fondest memories is the support you provided to me when you found out that my dog passed away. You sent me links on how to cope and manage the grief of losing a loved one. I believe it was the simple compassion you provided to me during such a hard time that makes the memory so bittersweet and special. You were not just a mentor, but a friend. To this day I feel very grateful that I get to call you a mentor, colleague, and a friend.

Jim, you stepped up at a time when I really needed it. Jerry had recently left to be a professor at UAB and my thesis project was shifting into a more hands-on experimental approach. It would be amiss if I did not mention that my mental health was a bit on the decline after losing my dog and I needed to be in an environment that was both mentally stimulating but also had friendly smiles. From the moment I sent you an email asking if I could use some of the work space in your lab you did not hesitate to get something together with the help of Holly, one of the smartest and most fantastic graduate students I have met. In fact, you went above and beyond to make me feel welcomed in your lab. From allowing me to join lab meetings, to lab lunches, and finally allowing me to add a handmade name tag to your door with all the rest of the lab members. You got to see my quarks as a graduate

student, mostly all the post-it notes and drawings of cartoon rabbits with one fist raised high saying “you got this!”, and I got to see yours as a PI. You have such an inviting demeanor about you that makes it easy to discuss with you both personal and scientific matters. One of the greatest moments that will stick with me is seeing you and the rest of the Trick Dawg band play at the Southern Café. It was unforgettable seeing all the professors in attendance dancing without a care. And, why shouldn’t they dance without a care? They are human after all. You were at an unofficial mentor capacity for me going on about a year and a half and within that time your commitment to teaching and mentoring was (and is) outstanding, no surprise that when I nominated you for the Robert J. Kadner Award I had no difficulty in finding support for your nomination among students and faculty. You are a constant inspiration, Jim. The environment that you create in your lab cannot be rivaled, yet (once I start a lab, I plan on making a collective space where innovative science is done and the researchers feel like people, too). So, I cannot thank you enough for the home you gave to me in your lab, the time you spent on mentoring me at an unofficial capacity and for showing me what a healthy lab culture can look and feel like. Oh! Before I forget thank you Jim for allowing me to bring in all my baked goods. I’m sure the lab will lose weight without my constant baking!

Lastly my family – I cannot have a completed acknowledgements section without thanking them. I’ll just say it; both my mom, Elaine Beltran, and my sister, Lencia Beltran, deserve honorary degrees for the number of times they have heard me present my research or at least having to listen to me talk about it. I’m sure it left their heads spinning a few times. I remember nearly five years ago telling my parents that I was going to graduate school – I come from a low socioeconomic status, Hispanic first-generation family so someone attending graduate school was very new to us all. My mom, and quite honestly myself included, thought it was so backward that I would be getting paid to learn. Why on earth would anyone pay me to make new discoveries, and, well, have fun? I assured her and myself that it was really true and that I was headed to Charlottesville VA to attend school for at least five years. At the onset I struggled to acclimate to this predominately white institution. I felt isolated, lost, and often misunderstood; I struggled with imposter syndrome and questioned whether I belonged alongside my peers who were coming from families with academic or medical backgrounds. I called my sister and my mom quite often in these early days. My dad, Lawrence Beltran, provided constant reminders of his willingness to help in any way that I needed it. I really had a strong family support group that was a constant when everything else around me was changing or was more or less uncertain, as is the norm with science/experiments. My dog, Einstein, passed away a year and a half ago during my fourth year of graduate school. He was my strength and got me through the most difficult years, I’d argue, of graduate school. I love you, pup; thank you for enduring all my mood swings when I couldn’t figure out power spectrum indexing, or when I was stressed about a

presentation; thank you for your unconditional love. My mom believes that my perseverance was all my own doing, and in some ways, yes it was, but mostly my success and perseverance is because I was surrounded by individuals who saw my potential, who encouraged me, pushed me, supported me, cared for me, believed in me. Besides those I have directly mentioned, there are many others: all the other members of my thesis committee: Stefanie Redemann (chair), Kandice Levental, Robert Nakamoto, and Andreas Gahlmann. The members of the BIMS Inclusive and Equity committee: Mary Hall, Ashley Woodard (co-chair with me), Janet Cross and Adrian Halme. A quick aside, I've been such a thorn in Mary Halls side especially during recruitment. Thank you, Mary for buying me Albemarle Baking Co pastries. ***Thank you all for your constant presence.***

Abstract

It cannot be overstated that antimicrobial resistance (AMR) is a global health threat. Underpinning the spread of AMR is the movement of mobile genetic elements such as plasmids, which code for genes that give rise to antibiotic resistance among human pathogens. Bacterial conjugation is a process which plays a key role in mediating the spread of AMR, which is accomplished via the macromolecular machinery complex, the type IV secretion system (T4SS). The T4SS spans both the inner and outer membrane of the bacterial cell wall and also includes the extracellular conjugative pilus. While, many aspects, such as the proteins involved which assist in facilitating the process of conjugation, have been elucidated and their roles have been studied there is still much to understand and discover.

In this work, we used several approaches, including: cryo-electron microscopy (cryo-EM), data processing approaches such as helical and single particle reconstruction, fluorescent light microscopy, cryo-electron tomography, focused ion beam milling/ scanning electron tomography, and correlated light electron microscopy. Using cryo-EM with the helical reconstruction approach we were able to resolve structures of three conjugation pili, two archaeal (*Aeropyrum pernix and Pyrobaculum calidifontis*) and one bacterial from the model system, encoded by the Ti plasmid of *Agrobacterium tumefaciens*. We show that the archaeal conjugation pili are homologous to bacterial mating pili, but function as DNA-import apparatuses. Several published studies state that the stability of the conjugation pili of *A. tumefaciens* is because of its cyclic pilin subunits. In this study we show that the pilin subunit which comprises the *A. tumefaciens* pili is not cyclic and has a similar fold like the pilins of the F-pilus and F-like pilus. Further, upon subjecting the T-pilus to extreme chemical and physical treatment and compared the resiliency to the well-studied F-pilus we found that the F-pilus was more resilient suggesting that the conjugative pilus is generally stable and is not related to the cyclization.

The conjugation pilus is known to facilitate the interaction between the donor and recipient cell by bringing them into direct contact with each other allowing the two bacteria to form stable mating pairs. In previous studies using the model organism *Escherichia coli*, it was discovered that one of the essential T4SS components, TraN, from the donor cell interacts with the recipient cells outer membrane protein A (OmpA). It was not clear how TraN and OmpA were interacting with each other to support the stabilization of mating pairs, and thus leading to efficient conjugation. In our study we used cryo-EM with single particle reconstruction to solve the interaction of TraN from the model organism, carbapenem resistant *Klebsiella pneumoniae* encoding plasmid pKpQIL, and outer membrane protein K36 from *K. pneumoniae* recipients. The structure of the two proteins, solved to 2.6 Å resolution, reveals that loop 3 which is found within the barrel of the OmpK36 porin interacts with TraN through the insertion of the beta-hairpin tip of TraN into a monomer of the OmpK36 porin timer. When a glycine-aspartic acid mutation is introduced to loop 3 the loop extends into the barrel of the porin and there is an observable decrease in bacterial conjugation. The extension of the loop 3 mutation results in a more constricted pore and consequently clashes with the beta-hairpin of TraN. This in effect causes destabilizes between the TraN and OmpK36 interaction, which lowers the number of mating pairs, and efficient conjugation.

One question that arose from the study of stable mating pairs was, what other events are occurring that proceed gene transfer; more specifically to what extent is the conjugative pilus participating in ssDNA transfer? The longstanding debate is that the conjugation pilus assists in the transfer of ssDNA, while others believe the only major role of the conjugative pilus is to facilitate the direct contact of the donor and recipient cells. In this study, we use dam-positive donor, *E. coli* cells harboring the pED208 plasmid that belongs to the IncF family isolated from Salmonella typhimurium that constitutively expresses the *tra* genes, together with dam-deficient recipient cells that contain the SeqA-YFP fusion protein that acts as a biosensor for methylated DNA. By labeling the pED208 pilus TraA subunit with Alexa-Fluor 568 maleimide dye we were able to observe the conjugation pilus with the fluorescent light microscope. Mixing both donor and recipient cells revealed the direct contact of the donor conjugation pilus with a physically distant recipient cell, producing an intense fluorescent foci from the SeqA-YFP binding to the transferred single stranded hemimethylated DNA. From our results we concluded that the conjugation pilus is capable of acting as a conduit for ssDNA between physically distant cells and that establishing stable mating pairs is not essential for conjugative transfer to occur.

List of Figures

Chapter 1: Introduction

1.1 The Type IV Secretion System

A mediator in the spread of antimicrobial resistance (AMR) is by exchange of mobile genetic elements (MGE), containing genes for antibiotic resistance and other adaptive traits, within microbial populations. Movement of genetic material is accomplished by the process of bacterial conjugation. The process of conjugation involves a plasmid encoded megadalton complex known as the type IV secretion system (T4SS) and an extracellular component referred to as the conjugation pilus (Figure. 1). The encoded secretion system is found on the F-plasmid carried by the donor cell and is transferred to the recipient cell as an MGE.

The T4SS is widely studied in diderm, gram-negative, bacteria such as *Escherichia coli*, *Agrobacterium tumefaciens*, and *Klebsiella pneumoniae*, however, they are also found among monoderm, gram-positive, bacteria. These secretion systems are functionally diverse; among transferring genetic material the T4SS is capable of delivering protein and protein-DNA substrates to bacteria or eukaryotic targets (Li Yang, Hu and Christie Peter, Waksman). Archaea also express secretion apparatuses that are homologous to bacterial conjugation machinery but function as DNA import systems rather than as an export mechanism observed with bacteria (Beltran, *et al.*).

Structurally, the T4SS contains about 12 conserved subunit components that build the fully functional system that span the inner- and outer membranes of the diderm bacteria. Collectively these subunits are referred to as VirB1-VirB11, following the nomenclature for the T4SS of the model organism *A. tumefaciens* (1). The conjugation pilus is comprised of the VirB2/TraA protein subunits. Remarkably the conjugation pilus has been the only identified bacterial, and now archaeal, filament to

associate with lipids at a 1:1 or 1:2 pilin: phospholipid ratio for bacteria and archaea, respectively. Many speculations exist for the purpose of the phospholipid association with the pilin. In recently published work, the authors establish that the presence of the phospholipids provide structural integrity to F-pilus which is vital towards the structural adaptivity in biofilm formations, and stability in harsh environments (2).

One clear observation is that these lipids contribute to the electrostatics of the lumen environment of the pilus. The relationship between the overall charge of the lumen and its function is not entirely clear and a suggestion that has been highly considered is that the lumen environment is correlated with the substrates that pass through the pilus. As mentioned previously, many different substrates are able to pass through the pilus, and although it has not been previously directly shown that ssDNA passes through the pilus, it was a widely accepted hypothesis. The negatively charged lumen of the F- and F-like pilus repels the negatively charged backbone of the single- stranded (ssDNA), potentially acting as a lubricant for the passage of DNA. The conjugative pilus, T-pilus, of *A. tumefaciens*, however, has an overall positively charged lumen contradicting the previous thought that the pilus might act as a conduit for DNA transfer. The explanation behind this contradiction is that the T-pilus lumen

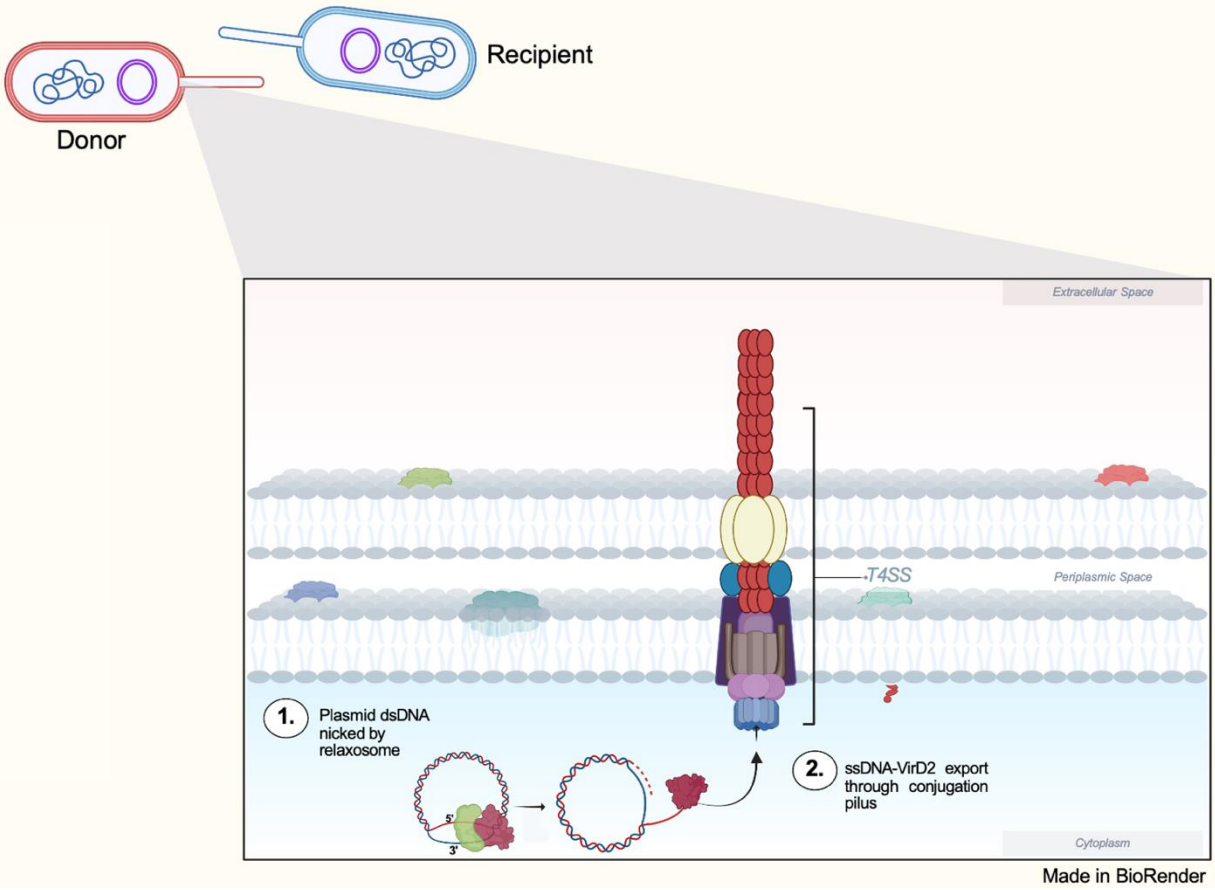

Figure 1. Type IV Secretion System (T4SS). Macromolecular complex that spans the inner and outer membrane of the bacterial cell. The T4SS transports ssDNA, and occasionally protein cargo, from one cell to another cell. The process begins with double-stranded DNA plasmid nicking via relaxasome (step 1) followed by transport of ssDNA through the T4SS to the recipient cell via the extracellular pilus (step 2).

evolved to transfer both negatively charged DNA and positively charged effector proteins (Li and Christie, 2018).

1.2 The process of bacterial conjugation

Comprehensively the historic understanding of the process of conjugation broadly has four steps (Figure. 2). The first step involves the extension of the conjugative pilus from a fertility positive (F+) donor. The pilus probes the environment, and while it is not exactly understood how the pilus is able to detect whether a cell is F+ or F-, once it comes into contact with a recipient cell an interaction is established. Step 2, once the pilus establishes an interaction with the recipient cell the pilus will depolymerize which brings the cells into close proximity to each other. Here, again, it is not clear what receptor, if any, the conjugation pilus recognizes on the surface of the recipient cell or if it is possible that the pilus is able to penetrate the membrane of the recipient cell. Step 3, once the cells are closely positioned stable mating pairs are established along with the formation of a conjugation junction. A copy of the F-plasmid is then transferred to recipient cell. In the fourth step there are now two bacterial cells which contain the F+ plasmid, and this process repeats itself with different cells.

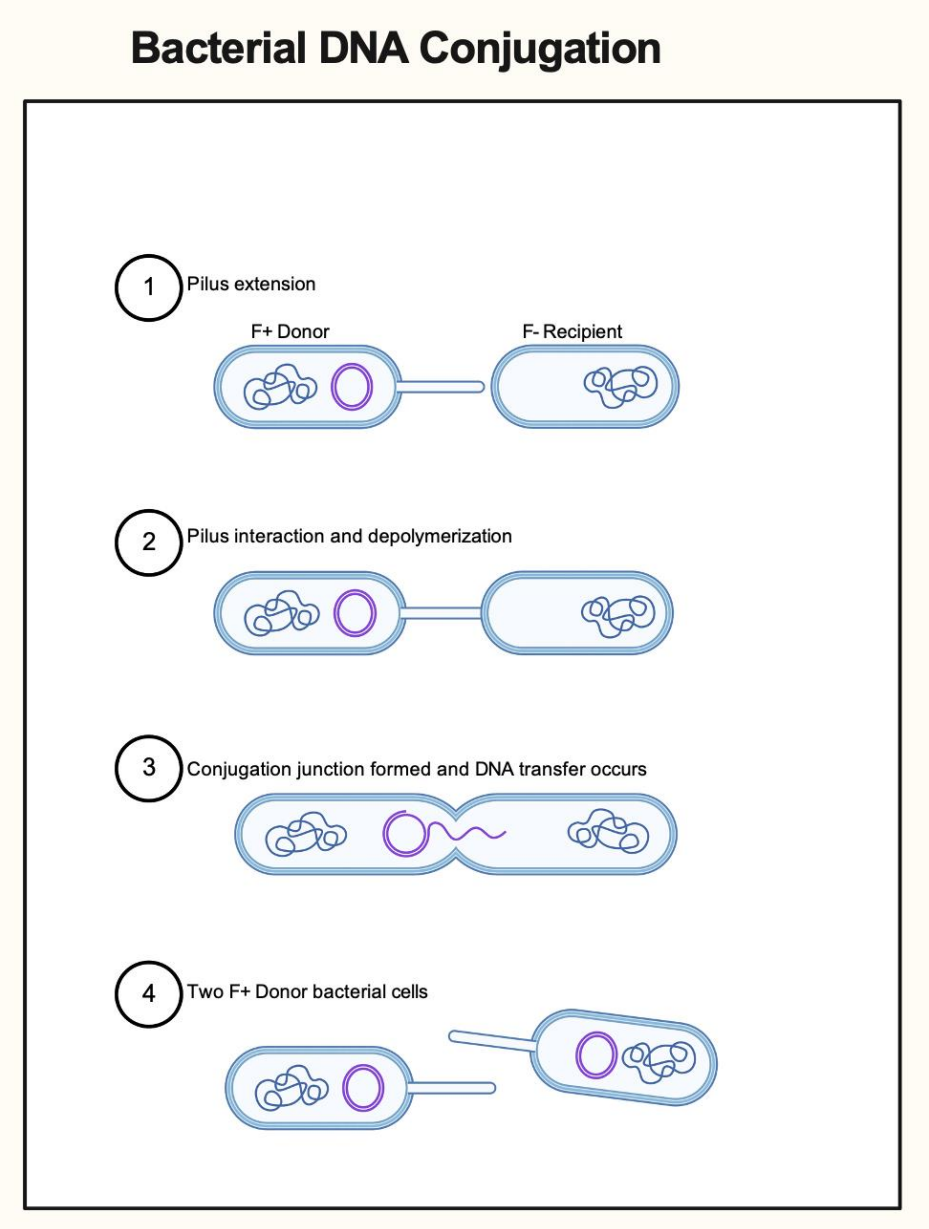

Figure 2. Historical understanding of the process of bacterial conjugation. Simply bacterial conjugation has 3 major steps before both cells contain the fertility (F+) plasmid. Step 1 requires the extracellular conjugation pilus to extend from the donor cell where in Step 2 the pilus will interact with the recipient cell and depolymerize. Step 3 remains less clear, but a conjugation junction is formed and the genetic material is transferred.

Bacterial conjugation requires meticulous steps, which various T4SS associated Vir and DNA transfer replication proteins execute, for successful

conjugation to occur. The double-stranded plasmid requires recruitment and assembly of the relaxasome which nick dsDNA allowing it to unwind to ssDNA-protein complex (Fig 1. Step 1). The relaxase, bound to the 5' end, acts a protective chaperone for ssDNA, preventing the ssDNA from being degraded. Although, the interaction between the escorting relaxase and VirD4, part of the type IV coupling proteins (VirD4+VirB4 ATPase), are not fully understood it has been accepted that the relaxase binds via putative translocation signals which recognize a specific sequence of VirD4 (Li, Y. G. & Christie, P. J.). During conjugation for *A. tumefaciens*, the association of the relaxase with ssDNA transfer to the recipient cell, or host cell, has been suggested to act as a signaling mechanism recruiting proteins in the host cell to help repair ssDNA to dsDNA (Li, Y. G. & Christie, P. J.).

Chapter 2: Domesticated conjugation machinery promotes DNA exchange in hyperthermophilic archaea

This Chapter was reformatted from the journal of Nature Communications:

Beltran, L.C., Cvirkaite-Krupovic, V., Miller, J., Wang, F., Kreutzberger M, A. B., Patkowski, J., Costa, T.R.D, Schouten, S., Levental, I., Conticello V.P., Egelman, E. H., and Krupovic, M. Domesticated conjugation machinery promotes DNA exchange in hyperthermophilic archaea. **Nature Communications**, 14, 666 (2023), 2041-1723.doi:10.1038/s41467-023-36349-8

2.1 Abstract

Conjugation, a major mechanism of horizontal gene transfer promoting the spread of antibiotic resistance among human pathogens, involves establishing a junction between a donor and a recipient cell. The mating pilus plays a prominent role in this process. In bacteria, the conjugation machinery is encoded by plasmids or transposons and typically mediates the transfer of cognate mobile genetic elements. Much less has been known about conjugation in archaea. Here, we determined atomic structures by cryo-electron microscopy of three conjugative pili, two from hyperthermophilic archaea and one encoded by the Ti plasmid of the bacterium *Agrobacterium tumefaciens*, and show that the archaeal pili are homologous to bacterial mating pili. However, the conjugation machinery in hyperthermophilic archaea has been domesticated and mediates the transfer of cellular DNA. We suggest that in extreme environments, pili-mediated DNA exchange between hyperthermophilic archaea facilitates DNA repair by homologous recombination and helps to avoid population collapse.

2.2 Introduction

The importance of horizontal gene transfer (HGT) in microbial persistence and evolution cannot be overstated. Exchange of genetic information is essential for the survival of microbial populations that otherwise succumb to the Muller's ratchet, a process whereby irreversible accumulation of deleterious mutations leads to extinction of an asexual population (3, 4). Furthermore, HGT plays a major role during the adaptation of microbes to constantly changing environmental conditions by providing an immediate access to beneficial traits and promoting cooperation within microbial communities (5). Accordingly, bacteria and archaea have evolved dedicated mechanisms of HGT (6, 7). Traditionally, three major routes of HGT are recognized, namely, natural transformation, transduction and conjugation. Whereas transformation is a natural ability of cells to uptake exogenous DNA from the environment through a dedicated competence system (8-10), the other two HGT mechanisms rely on distinct types of mobile genetic elements (MGE), viruses and plasmids (or integrative and conjugative elements), respectively. An additional HGT route, which is gaining increasing recognition, is intercellular DNA transfer through membrane-bound extracellular vesicles (11-14).

In bacteria, conjugation is one of the main mechanisms for the spread of antibiotic resistance and other adaptive traits (15, 16). Conjugation requires a sophisticated MGE-encoded apparatus, which belongs to the type IV secretion system (T4SS) superfamily, and in diderm bacteria consists of four key components: (i) a conjugative pilus, a multimeric assembly of the major pilin protein, which connects the donor and recipient cells and serves as a conduit for DNA transfer; (ii) the type IV coupling protein, an AAA+ ATPase essential for pilus biogenesis and substrate transfer; (iii) the T4SS membrane-spanning protein complex enabling DNA transfer across the membrane of the donor cell; and (iv) the relaxosome, which nicks the double-stranded DNA (dsDNA), yielding the single-stranded DNA substrate for intercellular transfer (17-21). Conjugative elements have been identified as extrachromosomal plasmids or as integrated elements in certain archaea, including hyperthermophilic archaea of the order Sulfolobales (22-26) and ammonia-oxidizing archaea of the class Nitrososphaeria (27), but the mechanism of conjugation has not been investigated in detail. Notably, none of the archaeal conjugative plasmids encode recognizable homologs of the relaxase or pilus protein and it has been suggested that the mechanism of conjugation in archaea might be different from that operating in bacteria (25).

Hyperthermophilic archaea of the order Sulfolobales have evolved a distinct DNA transfer system, named crenarchaeal exchange of DNA (Ced), which is dependent on species-specific cell aggregation and is inducible upon UV irradiation (28). The Ced system operates in conjunction with the UV-inducible type IV pili operon of Sulfolobales (Ups) system (29). The Ups pili produced upon

UV irradiation mediate cellular aggregation in a species-specific manner, ensured by specific glycosylation patterns on the Ups pili and the protein S-layer, which covers the cellular membrane (30). Both Ced and Ups systems are required for efficient DNA exchange, but the two do not have to be expressed in the same cell (28). Notably, the Ced system mediates unidirectional import of DNA, which is then used as a template for genome repair by homologous recombination; cells that cannot exchange DNA show significantly lower survival rates upon DNA damage (31). Notably, some crenarchaeal species encode the Ced but not the Ups system, whereas others, such as members of the order Thermoplasmatales, have not been found to encode either (28), suggesting alternative mechanisms for DNA exchange.

The Ced system consists of four proteins, CedA, CedA1, CedA2 and CedB (28). CedA contains six or seven transmembrane domains and is believed to form a transmembrane channel for DNA import, whereas CedB is homologous to VirB4/HerA-like AAA+ ATPases and appears to power the DNA translocation across the membrane. The function of CedA1 and CedA2, each with two predicted transmembrane domains, is less clear, but they were shown to form a membrane-localized complex with CedA (28). The Ced system was considered to be unrelated to the bacterial conjugation system because of the opposite directionality of DNA transfer (import versus export, respectively) and the lack of homologs other than VirB4-like ATPase (28). However, how the DNA is transported between the cells within the Ups pili-mediated cellular aggregate and the nature of the channel connecting the donor and recipient cells remained unresolved. It also remained unclear whether the Ced system transfers double-stranded DNA (dsDNA) or single-stranded DNA (ssDNA) substrates.

Here, using cryo-electron microscopy (cryo-EM), we show that a protein from the hyperthermophilic archaeon *Aeropyrum pernix*, a homolog of CedA1, forms a pilus which is structurally homologous to bacterial conjugative pili. We also discover that structurally similar pili, although with no sequence similarity, are produced by members of the Thermoplasmatales, which were previously not considered to encode the Ced-like system. We present high-resolution structures of two putative conjugative pili from hyperthermophilic archaea, *A. pernix* and *Pyrobaculum calidifontis*, and a bacterial conjugation pilus from a model system (32-35), encoded by the C58 Ti plasmid of *Agrobacterium tumefaciens*. It has been previously stated that the pilin subunit in the *A. tumefaciens* mating pilus is cyclic (36, 37), and that this accounts for its robust stability (38). We show that it is not cyclic and is actually similar in fold to other bacterial and archaeal mating pili. Collectively, our results suggest that the archaeal Ced-like systems share a common ancestor with bacterial T4SS conjugation system. However, unlike in bacteria, where conjugation systems are proprietary to mobile genetic elements, in hyperthermophilic archaea the DNA transfer system has

been domesticated, and we propose that this has evolved to ensure survival in extreme environments.

2.3 Results

2.3.1 Identification of putative DNA transfer pili in hyperthermophilic archaea

In Sulfolobales, expression of the ced and ups genes is activated exclusively upon UV irradiation (28). We set out to study the behavior of the Ced system in *Aeropyrum pernix* (order Desulfurococcales), a hyperthermophilic archaeon which grows at temperatures up to 100°C (39) and lacks the Ups system (28). Given that intercellular DNA transfer typically involves extracellular filaments, the extracellular fraction of *A. pernix* cells was analyzed using cryo-EM. In addition to the flagella (40), we identified a new type of filament (Fig. 1A), not previously observed in archaea. The reconstruction of this pilus to 3.3 Å resolution allowed us to determine the pilin identity directly from the cryo-EM map. The pilin was identified as *A. pernix* protein APE_0220a (WP_010865579), an ortholog of the S. acidocaldarius protein CedA1 (WP_011277463), one of the conserved components of the Ced system previously thought to be an integral membrane protein (28).

We have previously shown that *Pyrobaculum calidifontis*, a hyperthermophilic archaeon of the order Thermoproteales (41), which lacks both Ced and Ups systems, is prone to aggregation mediated by bundling pili related to TasA-like fibers, a major component of the biofilm matrix in many bacteria(42). We thus explored whether *P. calidifontis* cells produce pili which could be involved in DNA transfer. Cryo-EM analysis of the *P. calidifontis* filament preparation revealed pili (Fig. 2.D), which following the reconstruction to 4.0 Å resolution (Fig. 1E), proved to be structurally similar to the CedA1 pili of *A. pernix* (Fig. 2. B, Supp. Fig. 1A). While in the *A. pernix* filament the helical rise and twist per subunit were 3.6 Å and 76.5°, respectively, in the *P. calidifontis* filament these parameters were 5.0 Å and 74.2°. From the secondary structure and side-chain information present, we were able to determine the pilin identity directly from the cryo-EM map using DeepTracer-ID (43) to be *P. calidifontis* protein Pcal_0765 (WP_011849449) (Fig. 2. F), which we name TedC (see below). Although TedC displays a similar fold to CedA1 from *A. pernix* (Supp. Fig. 1A), the two pilins are processed differently, with *A. pernix* pilin not being processed and the *P. calidifontis* pilin, similar to bacterial plasmid conjugative pilins, undergoing proteolytic cleavage. Indeed, SignalP analysis (44) predicts that TedC carries a cleavable signal peptide, with the predicted signal peptidase I cleavage site, 22- AQA↓TT-26. Since the atomic model built into the reconstruction starts at residue 38, rather than the predicted residue 25, we conclude that residues 25-37 are disordered and therefore not visualized in the density map. Homologs of TedC were identified based upon protein sequence analysis in members of all five genera of the order Thermoproteales, namely, Pyrobaculum,

Thermoproteus, Caldivirga, Vulcanisaeta and Thermocladium. Genomic neighborhood analysis (Fig. 2 G) showed that the gene downstream of the tedC encodes a protein with seven predicted transmembrane domains, similar to CedA of S. acidocaldarius and *A. pernix*. Although BLASTP searches did not reveal the relationship between Pcal_0766 and CedA, sensitive profile-profile comparisons showed that the two proteins are indeed homologous (HHpred probability: 98.6), despite negligible pairwise sequence identity of 13% (Supp. Fig. 2A). Notably, profile-profile comparisons of Pcal_0766 against the PDB database showed that it is distantly related to VirB6-like proteins encoded by bacterial conjugative plasmids and involved in formation of the mating pore complex (Supp. Fig. 2B). A gene encoding the VirB4-like ATPase was identified transcriptionally upstream of the cedA-like and cedA1-like genes, separated by a few genes (Fig. 2 G). In Thermocladium species, the ortholog of Pyrobaculum virB4-like gene is adjacent to the cedA1-like pilin gene, suggesting that the corresponding proteins function together. Given the high sequence divergence between the components of the Ced system of Sulfolobales and the related system of Thermoproteales, we termed the latter as Ted, for Thermoproteales exchange of DNA system, with the CedA-like, CedA1-like and VirB4-like components as TedA, TedC and TedB, respectively. CedA2 is not conserved even among Ced systems from different species, and homologs or even counterparts of this protein are not identifiable in the Ted system.

Genomic loci containing the Ted system also commonly include genes encoding homologs of HerA helicase and MinD/ParA family ATPases, whereas Pyrobaculum and Vulcanisaeta species in addition carry the rad50 recombinase genes. HerA helicase and Rad50 recombinase play an essential role during homologous recombination in hyperthermophilic archaea (45, 46). The colocalization of these genes with the Ted system suggest a coordination of the DNA import in Thermoproteales and DNA repair by homologous recombination. In the *A. tumefaciens* systems, MinD/ParA family ATPase, known as VirC1, spatially coordinates early conjugative DNA transfer reactions (47). The finding that archaeal Ced and Ted systems form pili suggests that DNA transfer through these systems might be more similar to bacterial plasmid-mediated conjugation than previously recognized.

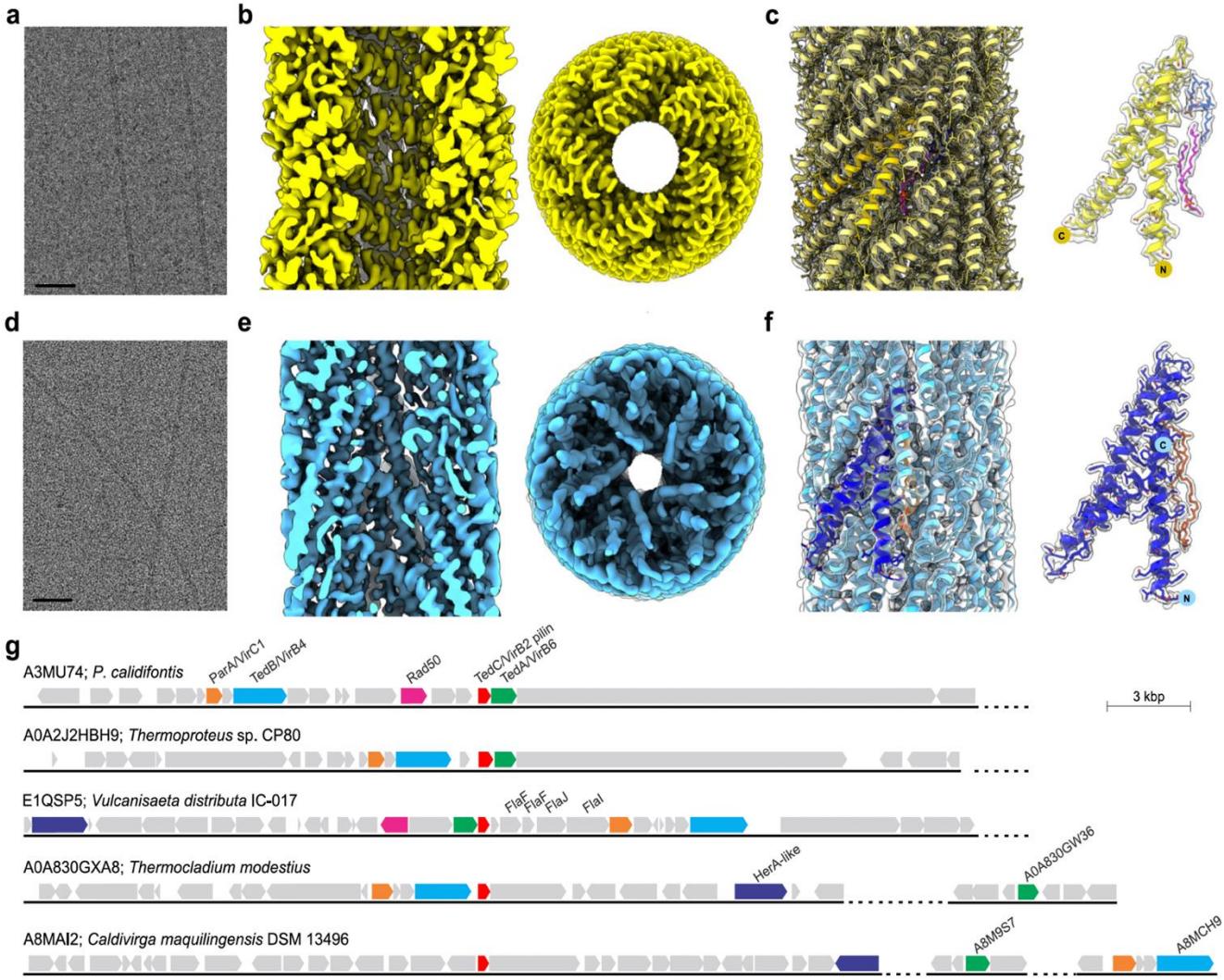

Figure 1. Archaeal conjugative pili. **(A & D)** Cryo-electron micrographs of *A. pernix* and *P. calidifontis* pili, respectively, scale bars 50 nm. **(B & E)** Side and top views of the *A. pernix* (B, yellow) and *P. calidifontis* (E, blue) cryo-EM density maps at resolutions of 3.3 Å and 4.0 Å, respectively. The front half of the filament has been removed in the side views, so that lumens are visible. **(C & F)** Atomic models in ribbon representation of the *A. pernix* (C, yellow) and *P. calidifontis* (F, blue) pili docked within their respective transparent cryo-EM density maps. The asymmetric unit of the *A. pernix* pilin CedA1 (C, bright yellow) shows two bound lipids (magenta and blue), while a single asymmetric unit of the *P. calidifontis* pilin TedC (F, dark blue) shows one bound tetraether lipid (orange). **(G)** Genomic loci encompassing the Ted system in different members of the order Thermoproteales. Each of the five genera within the Thermoproteales (genera Caldivirga, Pyrobaculum, Thermocladium, Thermoproteus and Vulcanisaeta) is represented. Genes encoding the conserved VirB2-like pilin protein TedC, VirB6-like transmembrane channel TedA, and VirB4-like AAA+ ATPase TedB are shown as red, green, and cyan arrows, respectively. Additional conserved

2.3.2 Archaeal conjugation pili are stoichiometric complexes of pilins and lipids

With the atomic models for the pilin subunits docked within the respective cryo-EM maps, we observed unaccounted-for densities between each of the proteins in both maps. These densities were similar to the densities for lipid molecules found in each of the previously reported bacterial conjugation pili, where there is a stoichiometric 1:1 ratio of pilin:phospholipid (48, 49). However, the putative lipid densities in the archaeal conjugation pili were larger. It has been impossible to do the lipidomics analysis for the archaeal conjugation pili, due to our inability at this point to obtain a highly enriched preparation containing just the conjugation pili. However, given that Aeropyrum and Pyrobaculum contain only one membrane, the lipids in the pili must come from the archaeal cytoplasmic membrane.

In *P. calidifontis* the extended density could only be explained by a bipolar cyclic tetraether lipid (Fig. 2A-D). Bipolar archaeal lipids were proposed almost 40 years ago (50), but, to the best of our knowledge, they have never been directly visualized. The cryo-EM map was good enough to identify the cyclic lipid as a glycerol dialkyl glycerol tetraether species (GDGT), a dominant membrane lipid in many hyperthermophilic archaea, including Pyrobaculum species (51), and we have modeled the simplest form, GDGT-0, into the cryo-EM density (Fig. 2B). It is important to note the possibility that more complex forms of GDGT (GDGT-1 through 8) containing cyclopentane rings may fit into the density as well. Both head groups are found to be solvent-exposed, with one of the polar head groups facing the lumen and the other facing the outside of the pilus, while the acyl chains are buried between the hydrophobic helices of the pilin subunits (Fig. 2A). The GDGT-0 lipid is found positioned in the middle relative to helix α1 (Fig. 2A). Most of the pilin-lipid interaction network in the *P. calidifontis* pilus relies extensively on contacts with helix α1 in the asymmetric unit (ASU), but the lipid is sandwiched in between α1 and α2 of a subunit in the neighboring ASU. All contacts are primarily associated with hydrophobic residues apart from one polar electrically neutral serine residue, Ser64 (Fig. 2A). There appears to be minimal contact with the charged head groups. Thus, the protein-lipid interaction stabilization relies heavily on hydrophobic interactions for *P. calidifontis*. While the ASU consists of one protein to lipid there is a total of four lipids which make contact with protein subunit TedC (Fig. 2D).

Interestingly, the lipid density was less resolved for *A. pernix* compared to the lipid density for *P. calidifontis*, even though the overall resolution for the *A. pernix* map was higher, 3.3 Å vs 4.0 Å, as determined by the map:map FSC (Table S1). In *A. pernix*, there are two lipids in every ASU, one of which adopts a partially folded conformation, with one of the isoprenoid chains folding back on itself, while the other has a crescent-like shape (Fig. 2E-G). Unlike most other members of the phylum

Thermoproteota, the membranes of Aeropyrum species contain only a small amount of GDGT lipids. Instead, an unusual C25,C25-diether with a phospho-dihexose head group was the main lipid species observed by mass spectrometry of a cellular membrane preparation of *A. pernix* (Supp. Fig. 3A-B), consistent with previous identification of this lipid in *A. pernix* (52). Both non-protein densities in the *A. pernix* map could be fit with this lipid, suggesting that the same lipid is present in two different conformations (Fig. 2F). The crescent-shaped lipid head group is directed toward the extracellular space with the isoprenoid chains extended and buried between pilin subunits (Fig. 2E). The crescent-shaped lipid primarily contacts helix α1 of the pilin, with one potential hydrophobic interaction with the partially folded lipid (Fig. 2E). The contacts with helix α1 are mediated by leucine-rich hydrophobic interactions and one charged interaction between the phosphate head group and the positively charged Lys15. The second lipid density resulted in a model with bent isoprenoid chains and the phosphate head group directed toward the lumen (Fig. 2E). The isoprenoid chains are buried between the subunits. Contacts with the pilin are made exclusively by the hydrophobic residues leucine, isoleucine and valine from helices α1 and α2 (Fig. 2E). There are no observed contacts between the pilin and the lumen-facing phosphate head group of the second lipid. There are two lipids and one protein subunit in the ASU of the *A. pernix* CedA1 pilus, generating a complex network of lipid contacts for each protein subunit (Fig. 2G-H). In total, each CedA1 subunit will make contacts with 10 lipid molecules (Fig. 2H).

In addition to the lipids, weak peripheral density was observed for both of the archaeal conjugation pili (Supp. Fig. 4) that would be consistent with glycosylation. However, this density was diffuse, and we could not see clear additional density on specific residues such as serines, threonines or glutamines that might be targets of such as serine, threonine, or glutamine that might be targets of such glycosylation.

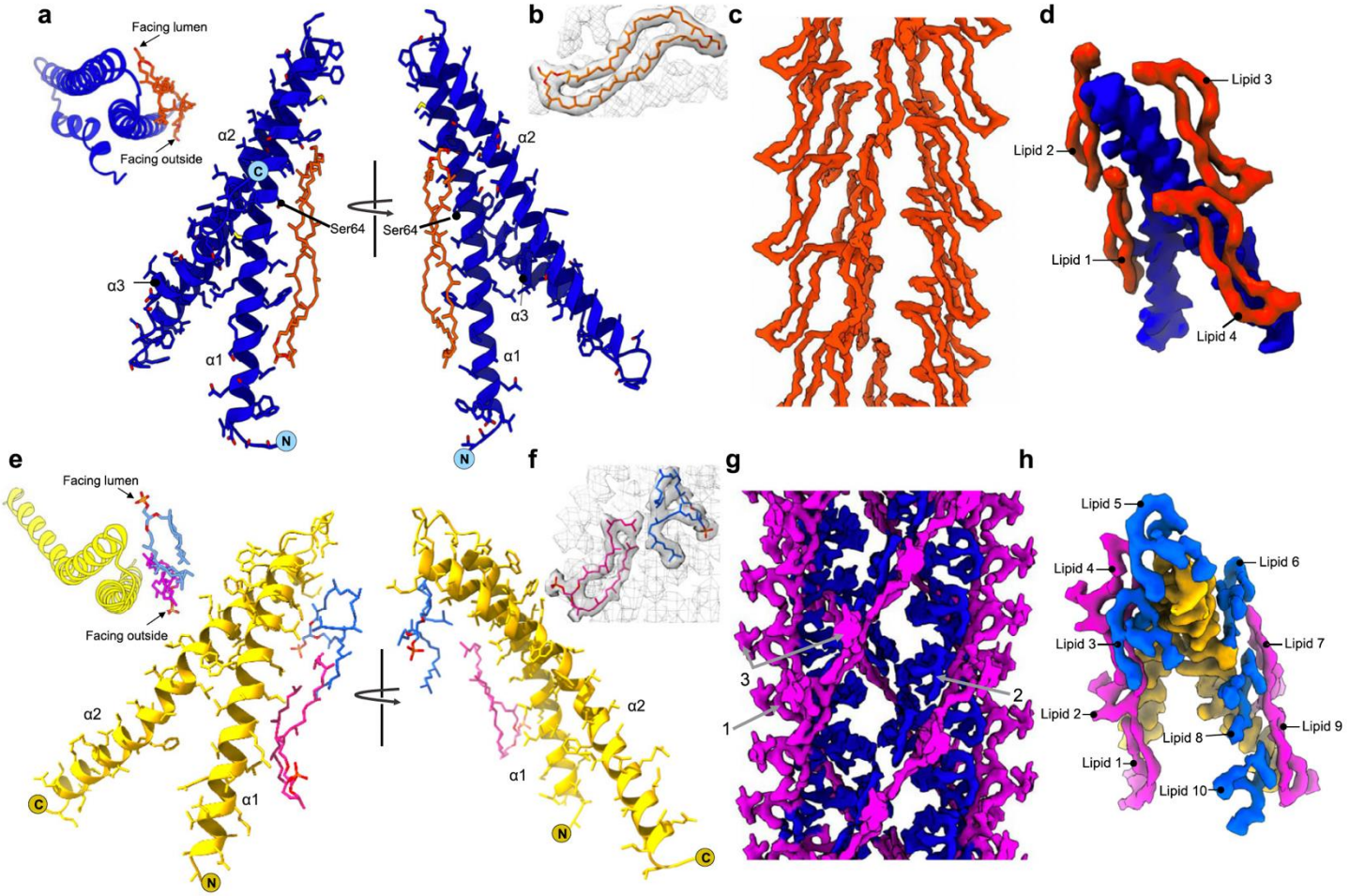

Figure 2. Intricate pilin-lipid interaction networks within archaeal conjugative pili. (A) Front and back views of a single asymmetric unit of the *P. calidifontis* pilus (blue) contains one pilin (TedC) and one phospholipid GDGT-0 (orange). One polar head group of the tetraether lipid faces the lumen and the other faces the outside of the pilus. A top view of a subunit, looking down the helical axis, is shown on the left for orientation. The isoprenoid chains of the GDGT-0 lipids are buried between hydrophobic helices and interact closely with helix α1 of the pilin shown but will also interact with α2 of neighboring pilins. (B) An atomic model of the cyclic GDGT-0 lipid docked within the lipid density. (C) Lipid density from *P. calidifontis* (blue). The density is very well resolved and shows that the GDGT-0 lipids have one head group facing the outside of the filament and the other head group facing the lumen. (D) A single pilin (blue) contacts four surrounding GDGT-0 lipids (orange). (E) The front and back view of the CedA1 pilin (yellow) of *A. pernix*. The asymmetric unit contains two lipids and one pilin, with the lipid in two different conformations: one having a partially folded shape (blue) and the other a crescent-like shape (magenta). The crescent head group is facing the outside of the pilus while the isoprenoid chains are buried between the pilin subunits. The partially folded lipid's phosphate head group is facing the lumen of the pilus and the isoprenoid chains are bent and buried between the subunits. A top view of a subunit, looking down the helical axis, is shown on the left for orientation. For both lipids the contacts with the pilin are mediated by hydrophobic residues such as leucine, isoleucine and valine from helices α1 and α2. The crescent-like lipid has one hydrophobic interaction with the partially folded lipid. (F) Atomic models for the crescent-shaped and partially folded lipid docked into the lipid densities. (G) Lipid density from *A. pernix* (yellow). The lipid density is less resolved than in *P. calidifontis* but shows two C25-C25 diether lipids, one of which forms a crescent-like shape (arrow 1) and the other forms a partially folded shape (arrow 2). Both lipids are capped with extra density (arrow 3) which is likely a dihexose sugar attached to the phosphate head group. (H) A single protein subunit (yellow) makes contacts with ten lipids (five crescent-shaped (pink), and five partially folded (blue)).

2.3.3 Conjugation pili of *Agrobacterium tumefaciens*

To extend the comparison between the archaeal mating pili and the existing structures of bacterial ones, we used cryo-EM to solve the structure of the *A. tumefaciens* T-pilus to 3.5 Å resolution (Fig. 3A, B; Table S1). The T-pilus has a 5-fold rotational symmetry with a rise of 13.7 Å and a twist of 32.5° per subunit. Similar to other bacterial conjugation pili (48, 49), there is a

stoichiometry of one lipid molecule to each protein subunit. However, unlike in pED208 (48) and pKpQIL (49), where each protein subunit contacts five lipid molecules, in T-pilus, each pilin subunit contacts four lipid molecules (Fig. 2C).

We conducted comprehensive shotgun lipidomics by electrospray ionization mass spectrometry (ESI-MS) on isolated pili to identify and detail the lipid species tightly associated with fibrillar pili-forming proteins. The isolated pili were pre-treated with PLA2 to hydrolyze all (contaminating) phospholipids that were not stably associated with pili proteins. As a control, we analyzed isolated pili from pED208, whose associated lipids were previously reported as being two sub-species of the anionic lipid phosphatidyl-glycerol (PG) (Costa et al., 2016). Our analysis (Supp. Fig. 5) confirmed and extended these results, showing that these two species (PG 16:0/16:1 and PG 16:0/18:1) are indeed the most abundant lipids associated with pED208, and that three other similar PG species are also present. Thus, ESI-MS allows quantitative analysis of lipid species associated with bacterial pili. The same analysis applied to VirB2 T-pili (Supp. Fig. 5) revealed a strikingly different set of PLA2-resistant lipids, with >65% of the phospholipids being phosphatidyl-ethanolamine (PE). Interestingly, the acyl chains of T-pilus lipids (PE 16:0/16:1 and PE 16:0/18:1) were similar to those observed in pED208, despite having different chemistry of the headgroup. A minor fraction (< 20%) of PLA2-resistant lipids were phosphatidyl-cholines (PC).

It is important to emphasize the essential need for PLA2-catalyzed hydrolysis of contaminating phospholipids in these assays, as the pili-bound lipids are relatively unabundant and even minor membrane contamination will overwhelm the signal. We therefore expect that in the absence of phospholipase treatment, any lipidomics analysis of the T-pilus will mainly find the lipids present in the contaminating membrane blebs and vesicles. This might explain the large difference between our results, where PE is the dominant lipid in the pili, and that found in two other very recent reports, where either PC(53) or PG(54) were found as the dominant lipid in the T-pilus. In neither of these two studies was phospholipase treatment used to minimize the contribution of contaminant lipids.

The 3.5 Å resolution of the T-pilus map allowed for unambiguous model building and interpretation of the protein subunit, VirB2 (Fig. 3D). The atomic model of VirB2 shows clear structural homology to the TraA subunit of the F-pilus (Supp. Fig. 1B). One clear difference between VirB2 on the one hand, and TraA of pED208 and pKpQIL on the other, is that there are kinks in helix 1 and 3 of the VirB2 subunit, produced by Pro23 and Phe61, respectively (Supp. Fig. 1B). The electrostatic surface for the lumen of the T-pilus generated by the atomic model is overall quite positive. The headgroup of PE is zwitterionic, with a net neutral charge, and addition of the PE lipid into the T-pilus model does not significantly change this electrostatic surface, which results in a more positively charged lumen compared to the lumen of pED208(48) (Supp. Fig. 6). Interestingly, when viewed from

the top there is an alternating positive to negative charge arising from the arginine and the lipid, respectively (Supp. Fig. 6). The T-pilus is known for its diverse substrates, enabling transport of both ssDNA-VirE2(55) as well as effector proteins (56) whose transport is independent of the DNA(32). The inclusion of VirE2 is thought to protect the T-strand from nuclease degradation while in *A. tumefaciens* and facilitate its transfer through the T4SS and T-pilus (55). An AlphaFold prediction for the structure of VirE2 suggests that it would be too large to pass through the lumen of the T-pilus in a natively-folded state. We therefore suggest that it must be partially unfolded to allow for such transport. While the lumen of other bacterial mating pili may have evolved to be optimal for DNA transport, the lumen of the T-pilus, also used for the transport for a diverse set of other substrates, has a positive electrostatic potential that would still allow DNA transfer, but not be optimal due to the greater friction resulting from DNA sticking to the walls. Obviously, this would suggest that the other substrates are likely to have overall positive electrostatic surfaces, and it has previously been noted that the effector proteins, where characterized, carry C-terminal domains that are positively charged (32).

The high resilience of the T-pilus to extreme chemical or physical conditions has been reported in a previous study (38), and its stability was attributed to the putative cyclic nature of the T-pilin (36, 37). Surprisingly, the cryo-EM structure of VirB2 reveals no cyclization of the pilin. Similar to other bacterial conjugative pili and TedC of *P. calidifontis*, VirB2 is proteolytically processed by a signal peptidase (57). In the mature pilin, residues QSAG from the N-terminus and G from the C-terminus are not seen in the density map, most likely due to disorder, and have not been built into the atomic model. The two residues suggested to be covalently linked in the T-pilus (36) were Gln1 and Gln74 (using our numbering for the mature pilin), neither of which are in our atomic model. But the five missing residues would be unable to span the distance of ~ 34 Å between Gly5 and Gly73 (the first N-terminal residue and last C-terminal residue in the model), so it is not possible that the subunit really is cyclic. This leads us to the question of the basis for the resiliency of the T-pilus. To answer this question, we subjected the T-pilus to many of the same extreme chemical or physical conditions reported by Lai and Kado (38) (Supp. Fig. 7, Table S2) and compared the resiliency to the well-studied F-pilus which is known to be non-cyclic. Interestingly, the T-pili look intact under 50% glycerol and 4M urea, flexuous and partially degraded under high temperatures (70 °C) and 0.1% SDS and depolymerized under 1% Triton X-100. In contrast, the F-pili are much more stable and remain intact under all conditions, including 1% Triton X-100 (Supp. Fig. 7 and Table S2). These results suggest that the architecture of bacterial conjugation pili is generally very stable and not related to cyclization. Further, we see no evidence of extensive glycosylation for the T-pilus (Supp. Fig. 4), nor was any potential glycosylation described for previous conjugation pili structures (48, 49), so we can exclude

extensive glycosylation which has been suggested as a mechanism for stabilizing extracellular archaeal filaments in the most extreme environments (58).

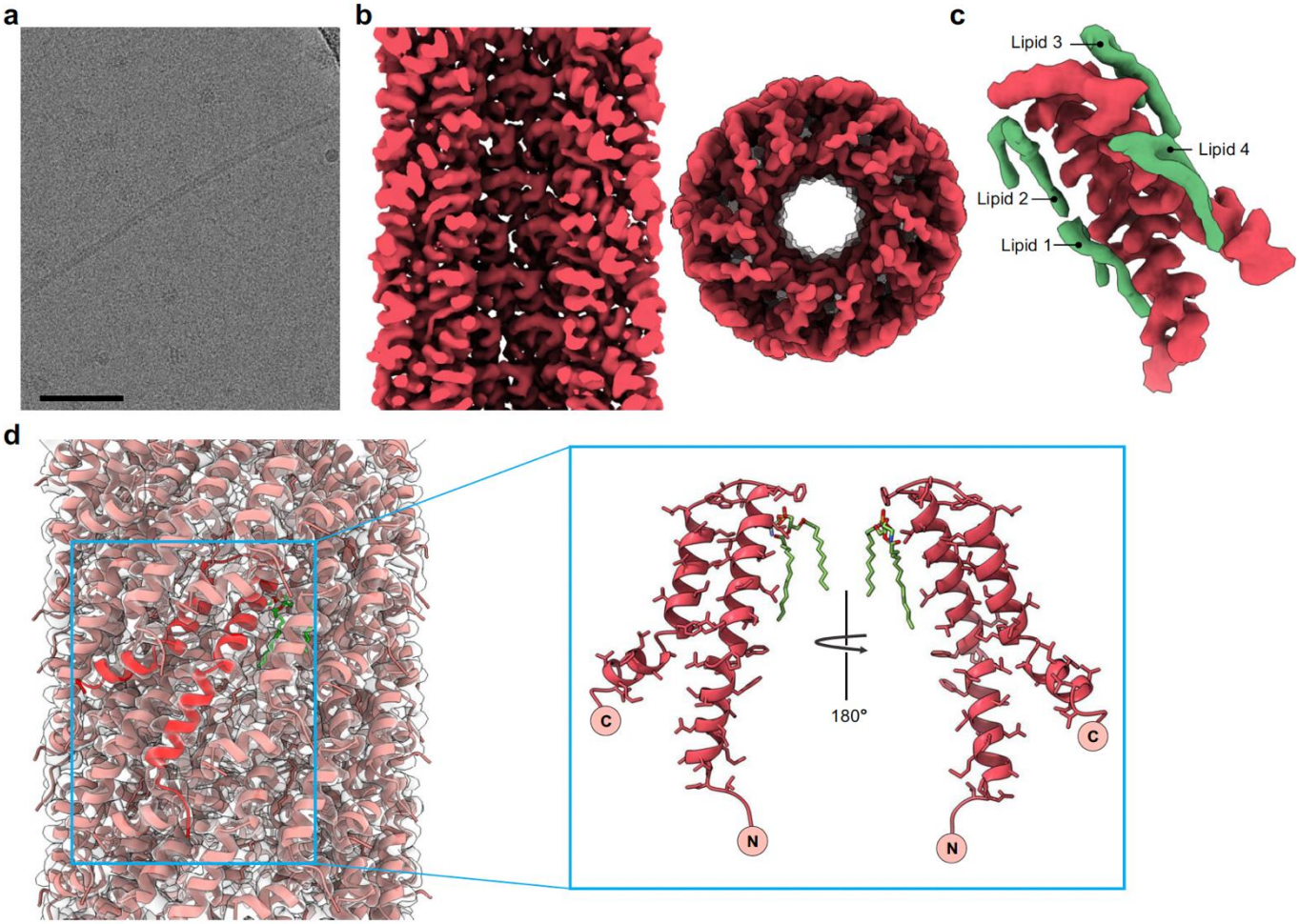

Figure 3. Cryo-EM of A. tumefaciens. A) Cryo-electron micrograph of *A. tumefaciens* T-pilus, scale bar 50 nm. (B) Side and top view of the T-pilus cryo-EM density map at a resolution of 3.5 Å. The front half of the filament has been removed in the side view, and we are looking at the lumen. (C) While there is a 1:1 stoichiometry of lipids to pilins in the filament, a pilin (red) makes contact with four lipids (green). (D) Atomic model of the T-pilus in ribbon representation docked within the transparent cryo-EM density map. A single subunit model is shown in red. An inset on the right shows front and back views of the VirB2 subunit.

2.3.4 The lumen of prokaryotic pili is too narrow to transfer dsDNA

With structures for four bacterial conjugation pili (pED208, F, pKpQIL and Ti from *A. tumefaciens*) and two archaeal ones (*A. pernix* and *P. calidifontis*), it is clear that there is a common architecture for all and obvious homology, despite negligible sequence similarity (Fig. 4A). Each prokaryotic pilin subunit consists of two or three hydrophobic α-helices, with kinks appearing in some of the helices, such as in *A. pernix* and *A. tumefaciens* (Fig. 2A & D, 3D and 4A). When a heat-map of global structural similarity (based upon the Dali server (59) Z-scores) between a single pilin from all known structures of prokaryotic conjugation pili was generated, unsurprisingly a clustering of the archaeal pilins was observed (Supp. Fig. 8). Notably, however, the mature *P. calidifontis* pilin contains an additional

hydrophobic α-helix (α3) compared to pilins encoded by *A. pernix* and bacterial plasmids. Despite the *A. tumefaciens* pilin having high structural similarity with pED208 and pKpQIL, it was clustered with the archaeal pilins rather than bacterial pilins from the F-pilus, pED208, and pKpQIL, which formed a separate cluster. The clustering of *P. calidifontis*, *A. pernix*, and *A. tumefaciens* pilins is likely due to the helix kinks which are absent in the other bacterial pilins.

We compared the external diameters of the archaeal and bacterial (T-pilus, pED208, F-pilus, and pKpQIL) conjugation pili as well as the diameters of their central channels, which allow the transfer of DNA (Fig. 4B and E). It must be noted that all such measurements are quite approximate, as discussed recently (60), and usually ignore the contribution of hydrogens and tightly bound water molecules. Further, structural varicosity in both archaeal pili complicates reducing the diameter to a single number. Nonetheless, with unavoidable approximations, all lumen diameters (Fig. 4B and E), range from 16 Å to 26 Å. The outer diameter of the *A. pernix* pilus more closely resembles the outer diameters of the bacterial F and F-like pili, while *P. calidifontis* has an outer diameter that is approximately the same as the T-pilus. The lumen diameter of *A. pernix* pilus is very similar to that of the T-pilus, whereas the lumen diameter of *P. calidifontis* is considerably narrower (Fig. 4E).

To determine whether dsDNA could pass through the lumen of the prokaryotic conjugative pili, we placed a model for B-form dsDNA within the lumen of the conjugation pili models from *P. calidifontis*, *A. pernix*, and *A. tumefaciens*. We observed extensive clashes between dsDNA and the atomic surface of all models (Supp. Fig. 9). These observations suggest that ssDNA, not dsDNA, passes through conjugative pili, although no experimental evidence exists to support this notion. Indeed, using synthetic nanopores in ultrathin silicon nitride membranes, it has been shown that ssDNA permeates pores with diameters as small as 10 Å (61). Hence, pore diameters of all prokaryotic conjugative pili are sufficiently wide for the passage of ssDNA, but not dsDNA. Previous structural studies have suggested that the lumen of the F-pilus has an overall negative charge which contributes to a repulsive force that will keep negatively charged ssDNA away from the wall of the lumen, effectively lowering friction (48, 49). In *A. pernix* each pilin is bound to two diether lipids with phosphorylated dihexose (i.e., glucose-inositol) head groups. One of these lipids faces the lumen of the central channel where it might also provide similar negative charge to facilitate DNA transfer (Fig. 2E).

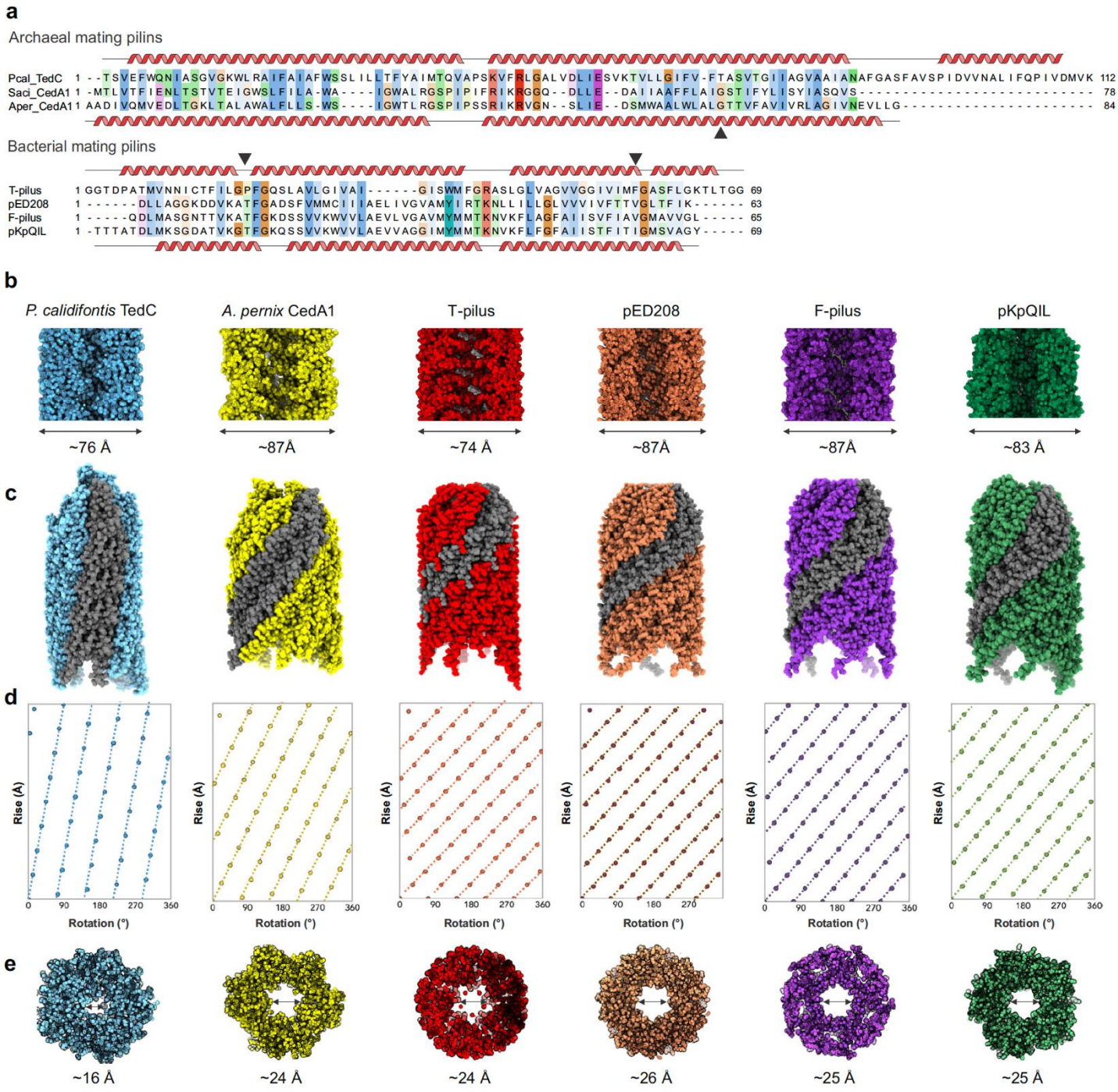

Figure 4. Comparison of archaeal and bacterial conjugative pili. (A) Sequence alignments of archaeal (top) and bacterial (bottom) mating pili. Sequences of mature pilins are shown with the secondary structure elements determined from the structure for the pilins shown above and below the corresponding sequences. Kinks in the α-helices are indicated with triangles. (B & E) Comparison of the lumen and outer diameter of archaeal *P. calidifontis* (blue) and *A. pernix* (yellow) with bacterial pili: *A. tumefaciens* T-pilus (red), pED208 (mauve), F-pilus (purple) and pKpQIL (green). The outer diameters range between 74 Å to 87 Å. The lumen diameters range between 16 Å to 26 Å, but in some cases cannot be easily reduced to a single number. (C & D) Atomic models with a single strand, shown in gray, show connectivity between the subunits. This connectivity is also represented with helical nets for the archaeal and bacterial pili. The helical nets show the unrolled surface lattice viewed from the outside of the filament. Each point represents a subunit, and the dotted lines are drawn to highlight the fact that all have right-handed 5-start helices. All of the pili have substantial connectivity between subunits along these 5-start helices.

2.3.5 Different helical symmetries still allow quasi-equivalent interactions

The twist of the archaeal pili from both *P. calidifontis* (74.2°) and *A. pernix* (76.5°) is similar to that of the pKpQIL pilus from *K. pneumoniae* (77.6°), generating strong connectivity along 5-start protofilaments (Fig. 4C-D). Similar 5-start protofilaments are observed in other bacterial conjugation pili as well, including the *A. tumefaciens* T-pilus reported here, the pED208 F-like pilus (48), and the F-pilus(48). However, those pili have a C5 rotational symmetry rather than the 1-start helical symmetry observed in pKpQIL (49), *P. calidifontis and A. pernix* (Fig. 4C-D). The difference in helical symmetries results in very small differences in intermolecular interfaces, much like what is observed for pED208 and pKpQIL, which have C5 and C1 symmetries, respectively (49). This is similar to the quasi-equivalence phenomenon reported in other helical tubes made of helix-turn-helix subunits, such as in archaeal virus SMV1(62), where very similar interfaces can be preserved even though there are large apparent changes in symmetry (between C7 and C1 in SMV1).

2.4 Discussion

Bacterial conjugation machineries are nearly exclusively encoded by plasmids or integrating and conjugating elements and hence typically promote the transfer of the cognate mobile genetic elements, with occasional transfer of the host DNA, e.g., when the plasmid origin of transfer (oriT) is recombined into the cellular chromosome (63). An exception to this paradigm is the conjugation-like process, dubbed distributive conjugal transfer, described in Mycobacterium species, whereby large fragments of the chromosomal DNA are exchanged between the donor and recipient species(64). However, although superficially this form of DNA transfer is reminiscent of the classical plasmid conjugation, it is mediated by a poorly understood mechanism involving the Type VII secretion system, rather than the T4SS (65). Here we show that the Ced system which imports DNA in hyperthermophilic archaea of the order Sulfolobales (28), and the related Ted system of Thermoproteales described herein, are domesticated derivatives of the T4SS. Both Ced and Ted systems encode homologs of the VirB4 ATPase (CedB/TedB), VirB6 membrane pore (CedA/TedA) and VirB2 conjugative pilin (CedA1/TedC). Nevertheless, the individual components display no recognizable sequence similarity between the Ced and Ted systems, and the assembly pathways might also differ. For instance, whereas the pilins in the Ced system are apparently secreted without processing, the N-terminal signal sequence of TedC appears to be cleaved by a signal peptidase. In this respect, TedC is more similar to the bacterial plasmid VirB2-like pilins. It is interesting to note that the N-terminal region of CedA proteins is homologous to nearly the entirety of the CedA1 pilin (Supp. Fig. 2C), suggesting a common export pathway for CedA and CedA1 and that one has evolved from the other. Notably, the same result was obtained when VirB2 and VirB6 of *A. tumefaciens* were

compared, albeit with a lower significance score (Supp. Fig. 2D). It is not possible to claim with any confidence which of the two proteins is ancestral. However, given the central role of the VirB6-like pore for conjugation and the absence of conjugative pili in monoderm bacteria, it is tempting to suggest that the pilin is a more recent addition to the T4SS apparatus to facilitate the DNA transfer between spatially separated cells. According to this scenario, the stoichiometric incorporation of lipids, a unique feature of bacterial conjugation pili and their archaeal homologs, might be a vestige of the ancestral function of these pilins as bona fide membrane proteins. Notably, our results provide the first direct visualization of archaeal GDGT lipids in the *P. calidifontis* pilus and highlight the flexibility of diether lipids in the pilus of *A. pernix*. The pilins are surrounded by lipid molecules, with most interactions holding the pili together being between pilin subunits and lipids. Thus, in a way, the conjugative pili can be regarded as highly ordered extensions of the cytoplasmic membrane.

Given the direct visualization of horizontal gene transfer between spatially separated bacterial cells using fluorescence microscopy (66), it is clear that bacterial conjugation pili can act as conduits for DNA transfer. However, the possibility still exists that the main role of such pili is to depolymerize and bring two mating cells into physical juxtaposition, and that the bulk of DNA transfer only takes place when this conjugation junction is established. Our structural results cannot address this possibility. Many of the proteins involved in conjugation have been identified in bacteria, such as in *E. coli* (67, 68) and *A. tumefaciens* (69), but these proteins have remained elusive in archaea. Mutagenesis studies in bacteria have shown ssDNA to be the genetic material exported from the donor to the recipient cell via the conjugation pilus (66, 70), where dsDNA is nicked by the enzyme relaxase. Relaxase in complex with several other proteins, known collectively as the relaxosome, is responsible for mediating the unwinding of ssDNA. To our knowledge, there are no apparent homologs of bacterial relaxases encoded in the archaeal genomes or conjugative plasmids. Nevertheless, our data indicate that archaeal pili, similar to their bacterial counterparts, most likely transfer ssDNA. The observation that Ted genes in some genera of Thermoproteales co-occur with genes encoding Rad50 and HerA-like helicase, might hold a clue to this conundrum. In hyperthermophilic archaea, herA and rad50 usually form an operon with the genes encoding nuclease NurA and Mre11 and the four proteins function during DNA damage repair though homologous recombination (71). NurA, an RNase H-fold nuclease, is endowed with the endonuclease and exonuclease activities that are modulated by the HerA helicase (72, 73). The integrated activity of NurA-HerA is responsible for DNA end-resection, a process which generates the 3′ single-stranded tails that are subsequently coated by the Rad50 recombinase to initiate strand invasion and DNA repair. In Sulfolobales, expression of the HerA operon, Ced and Ups systems is activated by DNA damage and all three operons are coregulated by the transcription factor B3 (74). We hypothesize

that the ssDNA substrate for the transfer through Ced and Ted systems is generated by the activity of NurA-HerA system, rather than by a dedicated relaxosome as in the case of bacterial plasmid conjugation systems (Fig. 5). Notably, the Ted system, but not Ced, apparently includes a ParA/MinD-family ATPase related to the VirC1 protein of *A. tumefaciens* plasmid Ti, which functions during the delivery of the relaxosome-bound ssDNA to the T4SS complex (47), and a similar role can be postulated for the homologous protein of the Ted system. The narrower pore in the *P. calidifontis* mating pilus, compared to *A. pernix* and the bacterial mating pili (Figs. 4,5), may reflect the fact that only ssDNA is transferred, rather than a relaxase-ssDNA complex.

Our current study provides new insights into the mechanism of horizontal DNA transfer in hyperthermophilic archaea through the domesticated conjugative T4SS apparatus. Such domestication is a remarkable example of the 'guns-for-hire' paradigm (75), whereby molecular machines evolving at the interface of the interaction between mobile genetic elements and their hosts are captured and repurposed by the competing parties. To our knowledge, the domestication of the conjugative apparatus for DNA transfer has not been reported in other organisms. Many questions remain unanswered, including the generation of ssDNA substrates for intercellular transfer as well as the mechanistic details of the biogenesis and full molecular complexity of the Ced and Ted systems. Notably, none of the species in the orders Thermoproteales and Desulfurococcales, including members of the genera Pyrobaculum and Aeropyrum, are genetically tractable. Thus, our present study further highlights the utility of cryo-EM in gaining important insights into the biology of non-model organisms.

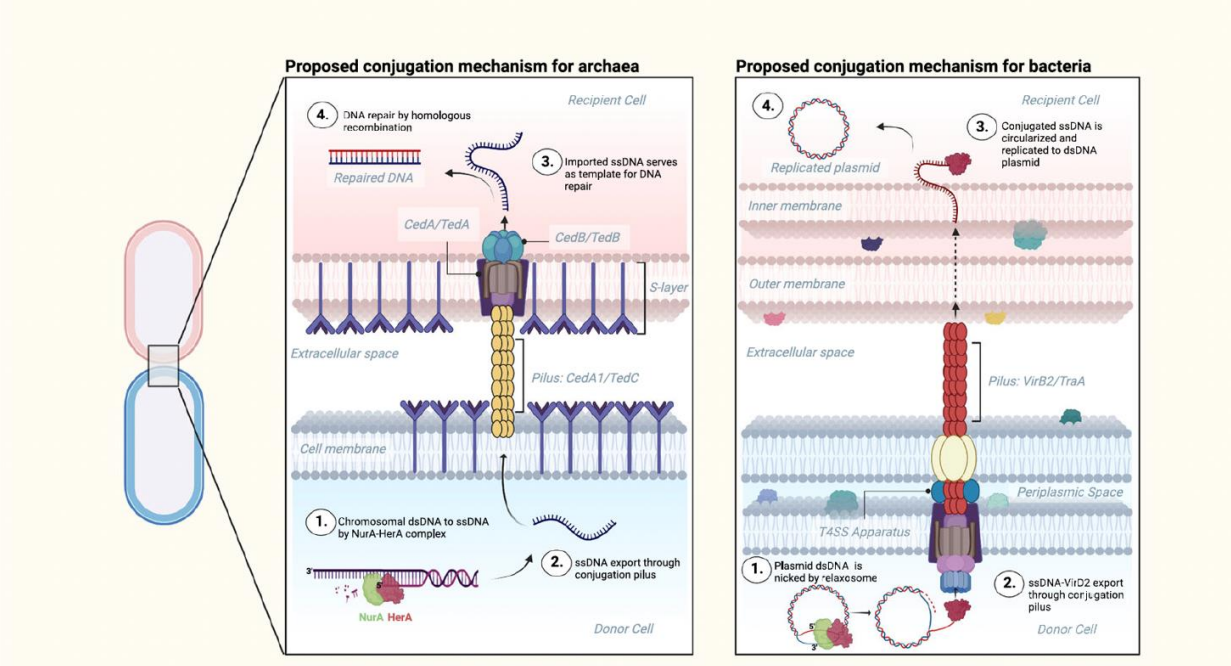

Figure 5. Proposed conjugation mechanisms between donor and recipient cells in archaea (left) and bacteria (right). The schematic shows how ssDNA substrates are generated by the HerA-NurA machinery in the donor archaeal cells and by the plasmid-encoded relaxosome in bacteria. Note that CedA and, potentially, Ted systems function as DNA importers rather than DNA exporters, contrary to the bacterial plasmid conjugative machineries.

2.5 Methods

2.5.1 Cultivation of archaeal cells and preparation of pili samples

Pyrobaculum calidifontis DSM 21063(41) and *Aeropyrum pernix* K1 DSM 11879(39) cells were purchased from the DSMZ culture collection. *P. calidifontis* was grown in 1090 medium (1.0 % tryptone, 0.1 % yeast extract, 0.3 % sodium thiosulfate, pH7) at 90°C without agitation. Pre-culture (30 mL) was started from a 200 µL cryo-stock, grown for 2 days and then diluted into 200 mL of fresh medium. When OD_{600} reached ~0.2, the cells were collected by centrifugation (Sorval SLA1500 rotor, 7000 rpm, 10 min, 20°C). The resultant pellet was re-suspended in 10 mL of phosphate-buffered saline (PBS) buffer, and the cell suspension was vortexed for 15 min to shear off the extracellular filaments. The cells were removed by centrifugation (Eppendorf F-35-6-30 rotor, 7830 rpm, 20 min, 20°C). The supernatant was collected and the filaments were pelleted by ultracentrifugation (Beckman SW60Ti rotor, 38,000 rpm, 2 h, 15°C). After the run, the supernatant was removed and the pellet was re-suspended in 200 µL of PBS buffer. *A. pernix* K1 cells were grown in 3ST medium (35 g/L Sea salts [Sigma], 0.1 % tryptone, 0.1 % yeast extract, 0.1 % thiosulfate, pH7) at 90°C without agitation. Pre-culture (10 mL) was started from a 1 mL cryo-stock, grown for 3 days and then diluted into 60 mL of fresh 3ST medium. After 3 days of growth 100 mL of fresh media was added to the culture and the growth was continued for another 3 days. Then the cells were removed by centrifugation (Sorval SLA1500 rotor, 7000 rpm, 10 min, 20°C) and the filaments were pelleted from the supernatant by ultracentrifugation (Beckman SW60Ti rotor, 38,000 rpm, 2 h, 15°C) and re-suspended in 200 µL of PBS.

2.5.2 pED208 pili purification

The F-pili were purified as described in Costa et al., 2016 with some minor modifications. In short, *E. coli* JE2571 harboring the pED208-plasmid were grown on large (24 x 24cm) LB agar plates overnight. Bacteria were gently collected from the plates with SSC buffer (15 mM sodium citrate pH 7.2 150 mM NaCl) and left to resuspend for 2h at 4 °C with mixing, followed by two rounds of centrifugations at 10,800 x g for 20 min. The pili were precipitated from the supernatant by addition of 500 mM NaCl and 5% PEG 6000, followed by incubation for 2h at 4 °C. Precipitate was rescued by centrifugation at 15,000 x g for 20 min and resuspended in 120 ml of water, followed by another round of precipitation as described above but this time the precipitate was resuspended in 1 ml of PBS (pH 7.4) buffer. The suspension was layered on pre-formed CsCl step gradients (1.0-1.3 g/cm^3) and separated by 17 h centrifugation at 192,000 x g in 4°C. The gradient was fractionated and the fraction

containing the F-pili was dialyzed against PBS (pH 7.4). Purity of the F-pilus was assessed by SDS-PAGE and the presence of the F-pilin (TraA) was further confirmed by mass spectrometry.

2.5.3 *A. tumefaciens* pili purification

Methods for *Agrobacterium tumefaciens* T-pilus isolation and concentration are adapted from Lai and Kado(76). Briefly, *A. tumefaciens* C58ΔvisR (flagella-knockout) was streaked from a stab or frozen culture on LB agar with no antibiotics at 28°C. After colonies appeared, about 2 days, a single colony was cultured overnight in 5 mL 523 media in a covered culture tube with shaking at 19°C. The next day the turbid culture was transferred to a centrifuge tube and pelleted by centrifuging 15 mins at 10000 rpm. Media was aspirated from the culture tube and the pellet was gently resuspended in 25 mL AB/MES with 5% glucose, then incubated at 19°C for four hours. The culture was then spread on 20 petri dishes or six screening trays containing AB/MES with 5% glucose, 200 µM acetosyringone to induce pili growth, 1.2% agar. Agar plates were incubated at 19°C for six days. After a lawn developed on each plate, 1 mL of cold 10 mM sodium phosphate buffer, pH 5.3 was added to each petri dish (or 5 mL for screening trays) and layers of bacteria were scraped off with a cell spreader and transferred to a 50mL Falcon tube on ice. This step was repeated with a second aliquot of buffer added to remove remaining bacteria. The total volume of bacteria and buffer was about 50 mL. The bacterial suspension was pipetted up and down to break up the biofilm then gently pushed through 1 mL of glass wool in a 30 mL syringe to strain out agar gel. The strained bacterial suspension was then forced through a 26-gauge needle eight times total to shear the T-pili off of the bacteria. After shearing, the suspension was transferred to a 0.2 µm disposable filter vacuum flask and filtered on ice to separate sheared pili from whole cells, periodically removing build-up from the filter. The isolated pili were concentrated by a factor of 10 using a 100 MWCO centrifugal filter. The pili were rinsed twice with 10 mM Tris-HCl, 100 mM NaCl, pH 7.5 buffer, resuspended to 10% of the starting volume, and frozen at -80°C for storage.

2.5.4 Cryo-EM Sample Preparation and Data Collection

A 3µL aliquot of sample containing either *Pyrobaculum calidifontis*, *Aeropyrum pernix*, or *Agrobacterium tumefaciens* pili was applied to a plasma cleaned (Gatan Solarus) lacey carbon grid (Ted Pella, Inc.), blotted with automated blotting for 3 s at 90% humidity and flash frozen in liquid ethane using an EM GP Plunge Freezer (Leica). The dataset used for structure determination was collected at the Molecular Electron Microscopy Core at the University of Virginia on a Titan Krios EM operated at 300 keV, equipped with an energy filter and K3 direct electron detector (Gatan). An energy filter slit width of 10 eV was used during data collection and was aligned automatically every

hour. All 8,127 *P. calidifontis*, 598 *A. pernix* and 8,363 *A. tumefaciens* movies were collected in counting mode using EPU v2.4 (Thermo Fisher) at a magnification of 81K, pixel size of 1.08Å, and a defocus range from -2.2 to -1.2μm. Data were collected using a total dose of 50 $e^-/Å^{-2}$ across 40 frames with an exposure time of 2.98s.

2.5.5 Data Processing and Helical Reconstruction

Unless otherwise stated, all data processing was done using cryoSPARC v3.2.0 (77). Movies were corrected for full-frame motion using patch motion correction followed by patch CTF Estimation(78). After CTF estimation, micrographs were sorted and selected based on estimated resolution (0 to 4 Å), defocus (0.6 to -2.6 μm), ice thickness, and total full-frame motion. Initial particles were automatically picked using 'Filament Tracer' with a filament diameter of 100-160 Å and a separation distance of 0.05-0.07 Å. Particles were extracted at a box size of 300 or 320 pixels, followed by 2D classification. Class averages containing filaments distinguishable from noise were selected for template-based particle picking. A total of 549,015 and 427,344 filaments were extracted using a box size of 320 Å, for *P. calidifontis* and *A. pernix*, respectively. A total of 197,531 T-pilus filament segments were extracted using a box size of 300 Å for *A. tumefaciens*. These particles were sorted using two iterative rounds of 2D classification with 50 classes each, number of online-EM iterations set to 20 and a batch size of 100 per class. The final iteration of 2D classification yielded a subset of 71,981, 44,262, and 49,308 filaments for *P. calidifontis*, *A. pernix*, and *A. tumefaciens*, respectively. Reconstructions of archaeal and prokaryotic conjugation pili were generated using the following method: (1) an averaged power spectrum was generated using the raw images of aligned filament segments selected from 2D classification, (2) layer lines were indexed to produce a list of possible helical symmetries, and (3) the correct helical symmetry was determined by trial and error by inspection of an output 3D map looking for obvious structural motifs (i.e., recognizable secondary structural and amino acid side chain densities). Particles were further refined using local CTF refinement, and another round of helical refinement was performed to generate the final reconstruction. The final resolution achieved for *P. calidifontis*, *A. pernix*, *and A. tumefaciens*, were 4.0 Å, 3.3 Å, and 3.5 Å, respectively. The cryo-EM and refinement statistics for each conjugation pilus are listed in Supplemental Table 1.

2.5.6 Model Building and Refinement

The sequence identity of the subunit for *P. calidifontis* and *A. pernix* was unknown. Using AlphaFold(79) the sequence identity for *A. pernix* pilin was narrowed to the one that best fit the cryo-EM density map. Using DeepTracer-ID(40) we were able to determine the pilin identity of *P.*

calidifontis directly from the cryo-EM map. With the sequences identified for their respective map the side chains of each ASU model were adjusted manually in COOT(80) and inspected using UCSF Chimera(81). For the *A. tumefaciens* structure the density was good enough to trace the entire backbone and localize most side chains. The cryo-EM structure of pKpQIL (PDB ID: 7JSV) was used as a starting point for building the *A. tumefaciens* cryo-EM model. Following model completion, side chains of the model were manually adjusted in COOT(80) and inspected in UCSF Chimera (Pettersen et al., 2004). All models were refined using PHENIX real-space refinement (82). Refinement included global minimization, B-factor optimization, and applied secondary structure and Ramachandran restraints. The final models were validated with the MolProbity(83) implementation in PHENIX. Refinement statistics for each filament are listed in Supplementary Table 1. Both cryo-EM maps and atomic coordinates have been deposited with the Electron Microscopy Data Bank and Protein Data Bank with the accession codes given in Supplemental Table 1. Model-map correlation coefficients were also used to estimate the resolution of the reconstructions and are listed in Supplemental Table 1.

2.5.7 Sequence analyses

Multiple sequence alignment of bacterial and archaeal pilins was made using PROMALS3D and manually adjusted(84). Genomic neighborhoods were analyzed using the enzyme function initiative-genome neighborhood tool (EFI-GNT)(85). Profile-profile comparisons and annotation of proteins encoded in the vicinity of TedC pilin in Thermoproteales were performed using HH-suite package v3(86). Profiles of the query sequences were constructed by running three iterations of HHblits against the UniRef90 database and the resultant profiles were compared against various profile databases, including protein family (Pfam) database, the Protein Data Bank (PDB) and the NCBI Conserved Domain database, all available from http://ftp.tuebingen.mpg.de/pub/protevo/toolkit/databases/hhsuite_dbs/(87). Signal peptides were predicted using SignalP v5(44).

2.5.8 Mass spectrometry and lipidomics of *A. pernix*

The freeze-dried cell preparation was extracted using a modified Bligh-Dyer protocol(88). Part of the extract was acid hydrolyzed by refluxing with 5% HCl in methanol for 3 hours to release core ether lipids. Both the Bligh-Dyer extract (containing the intact polar lipids with head groups) as well the hydrolyzed extract was analyzed by ultra-high performance liquid chromatography-high resolution mass spectrometry using a Q Exactive Orbitrap MS following Bale et al.(88) Electron spray ionization

and tandem MS-MS of pED208 F-pilus and pC58 T-pilus lipidomics. Lipidomics were performed at Lipotype, GmbH (Dresden, Germany) as described previously(89-92)

Nomenclature

The following lipid names and abbreviations are used. Cer – Ceramide, Chol – Cholesterol, CL – cardiolipin, DAG – Diacylglycerol, HexCer – Glucosyl/Galactosyl Ceramide, PA – Phosphatidic Acid, PC – Phosphatidylcholine, PE – Phosphatidylethanolamine, PG – Phosphatidylglycerol, PI – Phosphatidylinositol, PS – Phosphatidylserine, and their respective lysospecies: lysoPA, lysoPC, lysoPE, lysoPI and lysoPS; and their ether derivatives: PC O-, PE O-, LPC O-, LPE O-; SE – Sterol Ester, SM – Sphingomyelin, TAG – Triacylglycerol.

Lipid species were annotated according to their molecular composition as follows: [lipid class]-[sum of carbon atoms in the fatty acids]:[sum of double bonds in the fatty acids];[sum of hydroxyl groups in the long chain base and the fatty acid moiety] (e.g., SM-32:2;1). Where available, individual fatty acid composition following the same rules is given in brackets (e.g., 18:1;0-24:2;0).

2.5.9 Lipid extraction

Samples were extracted and analyzed as described(89-93), which is a modification of a previously published method for shotgun lipidomics(90). Briefly, samples were suspended in 150 µL of 150 mM ammonium bicarbonate in water and spiked with 20 µL of internal standard lipid mixture, then extracted with 750 µL chloroform/methanol 10:1 (v:v) mixture for 2 hours at 4°C with 1400 rpm shaking. After centrifugation (3 min, 3000 g) to facilitate phase partitioning, the lower, lipid-containing, organic phase was collected (1st step extract), and the remaining water phase was extracted further with 750 µL chloroform/methanol 2:1 (v:v) mixture under the same conditions. Again, the lower, organic phase was collected (2nd step extract). Extracts were dried in a speed vacuum concentrator. 120 µL of a dried 1st step extract underwent acetylation with 75 µL acetyl chloride/chloroform 1:2 (v:v) mixture for 1 h to derivatize cholesterol. After completing the reaction, the mixture was dried. 120 µL of a dried 1st step extract and a derivatized extract were resuspended in an acquisition mixture with 8mM ammonium acetate (400 mM ammonium acetate in methanol:chloroform:methanol:propan-2-ol, 1:7:14:28, v:v:v:v). 120 µL of the 2nd step extract was resuspended in an acquisition mixture with 30 µL 33% methylamine in methanol, in 60 mL methanol:chloroform 1:5 (v:v). All liquid handling steps were performed using a Hamilton STARlet robotic platform.

2.5.10 PLA2 treatment

0.2U PLA2 was added to Eppendorf tubes containing samples with a concentration of ~18µM of pili from either pED208 F-pilus or pC58 T-pilus. These samples were then incubated for 60 minutes at 37°C and flash frozen in liquid ethane.

Lipid standards

Synthetic lipid standards were purchased from Sigma-Aldrich (cholesterol D6), Larodan Fine Chemicals (DAG, TAG) and Avanti Polar Lipids (all remaining lipids). Standard lipid mixtures were chloroform/methanol 1:1 (v:v) solutions containing:

Cer 35:1;2, (D18:1;2, 17:0;0)

Chol D6

DAG 34:0;0 (17:0;0, 17:0;0)

DiHexCer 30:1;2 (D18:1;2.12:0;0)

HexCer 30:1;2 (D18:1;2.12:0;0)

LPA 17:0;0 (17:0;0)

LPC 12:0;0 (12:0;0)

LPE 17:1;0 (17:1;0)

LPI 17:1;0 (17:1;0)

LPS 17:1;0 (17:1;0)

PA 34:0;0 (17:0;0, 17:0;0)

PC 34:0;0 (17:0;0, 17:0;0)

PE 34:0;0 (17:0;0, 17:0;0)

PG 34:0;0 (17:0;0, 17:0;0)

PI 32:0;0 (16:0;0, 16:0;0)

PS 34:0;0 (17:0;0, 17:0;0)

SE 20:0;0 (20:0;0)

SM 30:1;2 (18:1;2, 12:0;0)

TAG 51:0;0 (17:0;0, 17:0;0, 17:0;0)

2.5.11 Lipid spectrum acquisition

Extracts in acquisition mixtures were infused with a robotic nanoflow ion source (TriVersa NanoMate; Advion Biosciences) into a mass spectrometer instrument (Q Exactive, Thermo Scientific). Cer, DiHexCer, HexCer, lysolipids, and SM were monitored by negative ion mode FT MS. PA, PC, PE, PI, CL, PS, and ether species were monitored by negative ion mode FT MSMS. Acetylated cholesterol was monitored by positive ion mode FT MS. SE, DAG, TAG and species were monitored by positive ion mode FT MSMS.

2.5.12 Lipid identification and quantification

Automated processing of acquired mass spectra, identification, and quantification of detected molecular lipid species were performed by LipidXplorer software(94). Data post-processing and

normalization were performed using an in-house developed data management system. Only lipid identifications with a signal-to-noise ratio >5, an absolute abundance of at least 1 pmol, and a signal intensity 5-fold higher than in corresponding blank samples were considered for further data analysis.

2.5.13 Chemical and physical treatments of pED208 F-pilus and pC58 T-pilus

The following chemical or physical treatments were introduced and incubated at room temperature (23°C) unless otherwise stated for ~10 minutes to samples of either pED208 F-pilus or pC58 T-pilus: 50% glycerol, high temperature (70°C), 0.1% SDS, 1% Triton-X 100, and 4 M urea.

Negative stain transmission electron microscopy of treated pED208 F-pilus and pC58 T-pilus

2 μL of sample either of pED208 F-pilus or pC58 T-pilus subjected to their respective chemical or physical treatment were applied to a carbon grid and stained with 2% uranyl acetate and examined by transmission electron microscopy using a Phillips Tecnai T12 at 80kV.

2.5.14 Data Availability

The atomic model for the *P. calidifontis* pilus was deposited in the Protein Data Bank with accession code 8DFT, and the corresponding map was deposited in the Electron Microscopy Data Bank with accession code EMD-27413. The atomic model for the *A. pernix* pilus was deposited in the Protein Data Bank with accession code 8DFU, and the corresponding map was deposited in the Electron Microscopy Data Bank with accession code EMD-27414. The atomic model for the *A. tumefaciens* pilus was deposited in the Protein Data Bank with accession code 8EXH, and the corresponding map was deposited in the Electron Microscopy Data Bank with accession code EMD-28657.

2.6 Acknowledgements

Cryo-EM imaging was conducted at the Molecular Electron Microscopy Core facility at the University of Virginia, which is supported by the School of Medicine and built with National Institutes of Health (NIH) grant G20-RR31199. In addition, the Titan Krios (SIG S10-RR025067) and K3/GIF (U24-GM116790) were purchased with the aid of the designated NIH grants. We thank Anchelique Mets and Ellen Hopmans (NIOZ) for technical support and mass spectral interpretations, respectively. Special thanks to Clay Fuqua for providing the *Agrobacterium tumefaciens* strain from which we obtained the T-pili. This work was supported by NIH Grant GM122510 (E.H.E.), GM138756 (F.W.) Welcome Trust Grant 215164/Z/18/Z (T.R.D.C). M.K. was supported by l'Agence Nationale de la Recherche grant ANR-21-CE11-0001-01.

2.7 Supplemental Figures

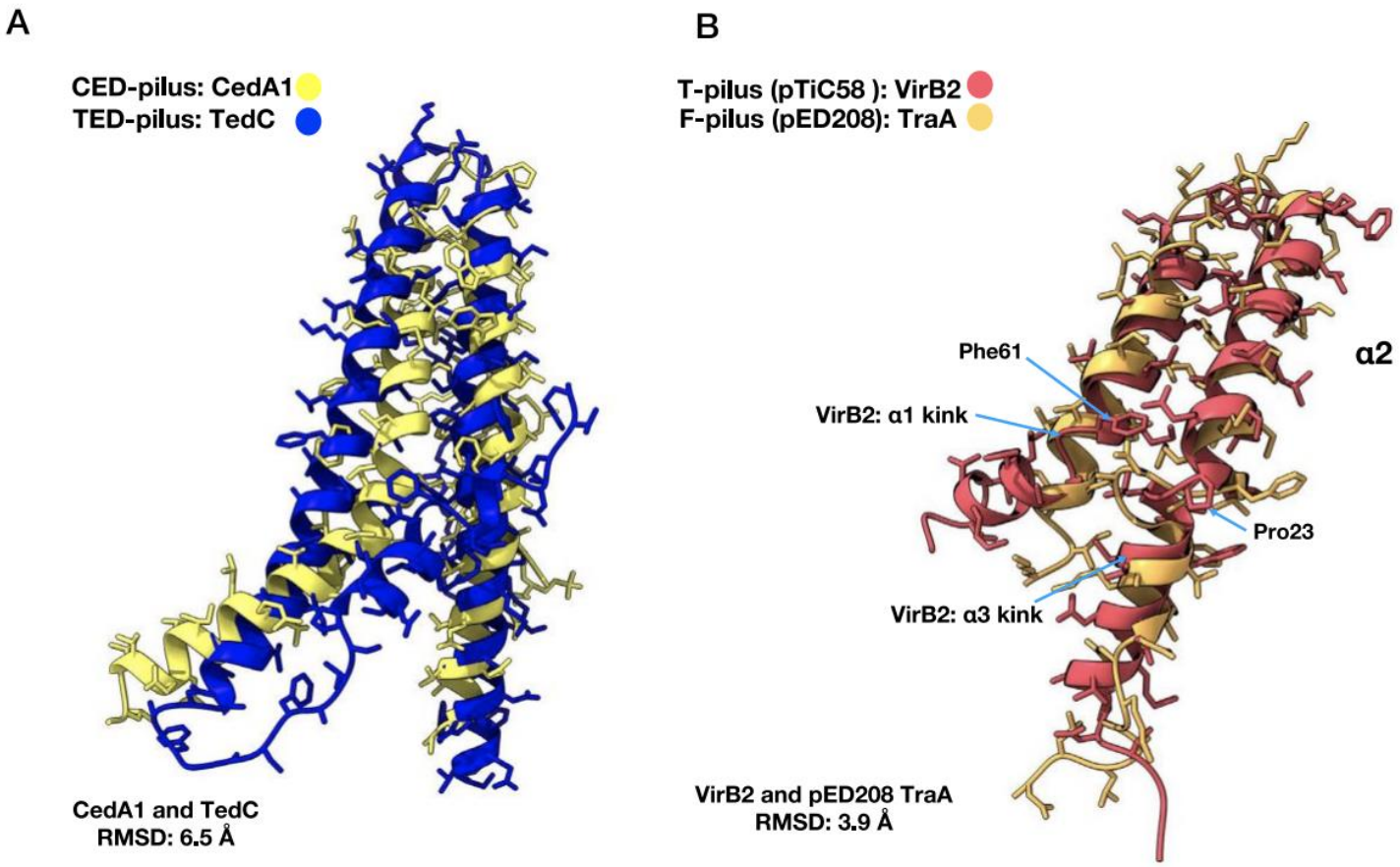

Supplemental Figure 1. (A) An alignment of the CedA1 (yellow) with the TedC (blue) subunits shows an RMSD of 6.5 Å between the two subunits. A distinct kink in helix α2 of CedA1, while the kink in helix α2 of TedC is present but less prominent. (B) Alignment of the VirB2 subunit (red) with the TraA subunits of pED208 (orange). There is a 3.9 Å RMSD between VirB2 and pED208 across 58 atom pairs. There are two distinct kinks in VirB2 not present in pED208. The kink in VirB2 helix α1 occurs at phenylalanine 61 and the kink in α3 occurs at proline 23.

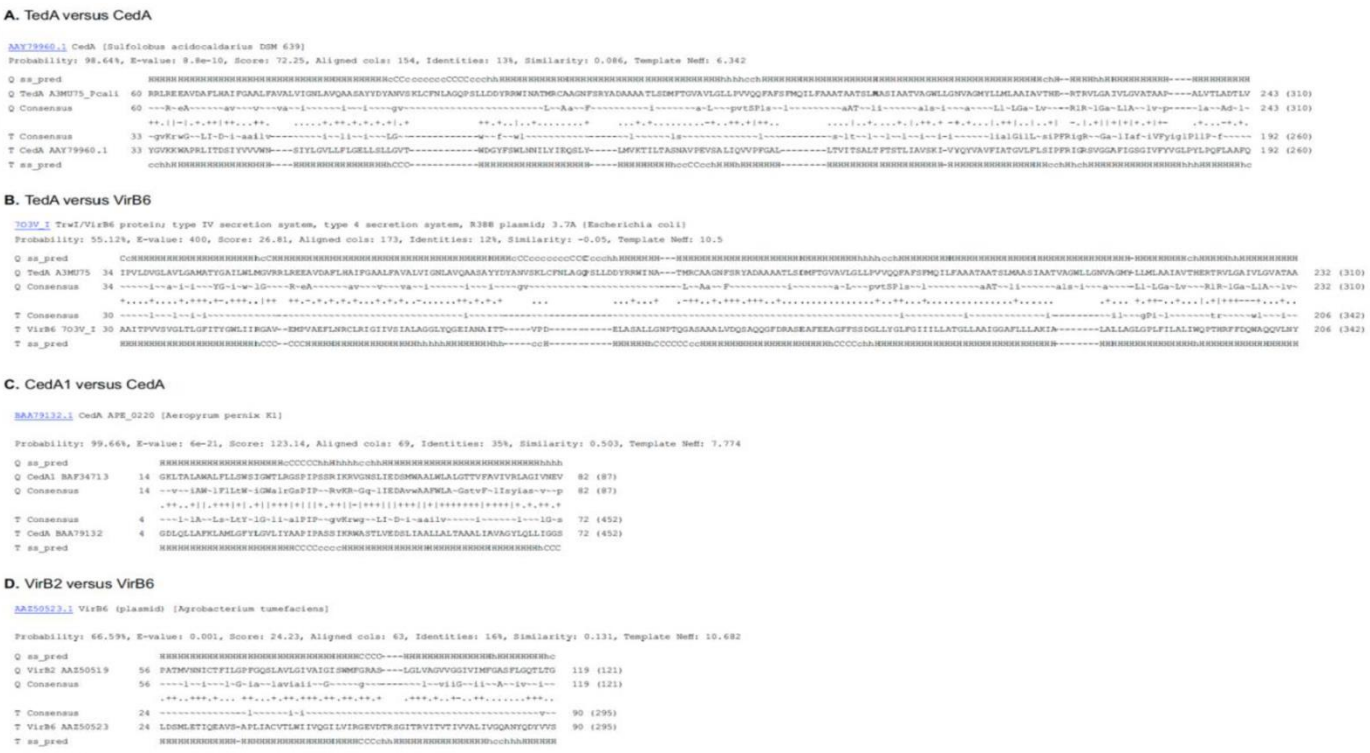

Supplemental Figure 2. Results of the profile-profile comparisons using HHsearch for different components of the conjugative machineries of bacteria and archaea. (A) Comparison of the archaeal membrane pore proteins TedA and CedA. (B) Comparison of the archaeal protein TedA and bacterial protein VirB6. (C) Comparison of CedA and CedA1. (D) Comparison of bacterial conjugation proteins VirB2 and VirB6. H(h), α-helix; E(e), β-strand; C(c), coil.

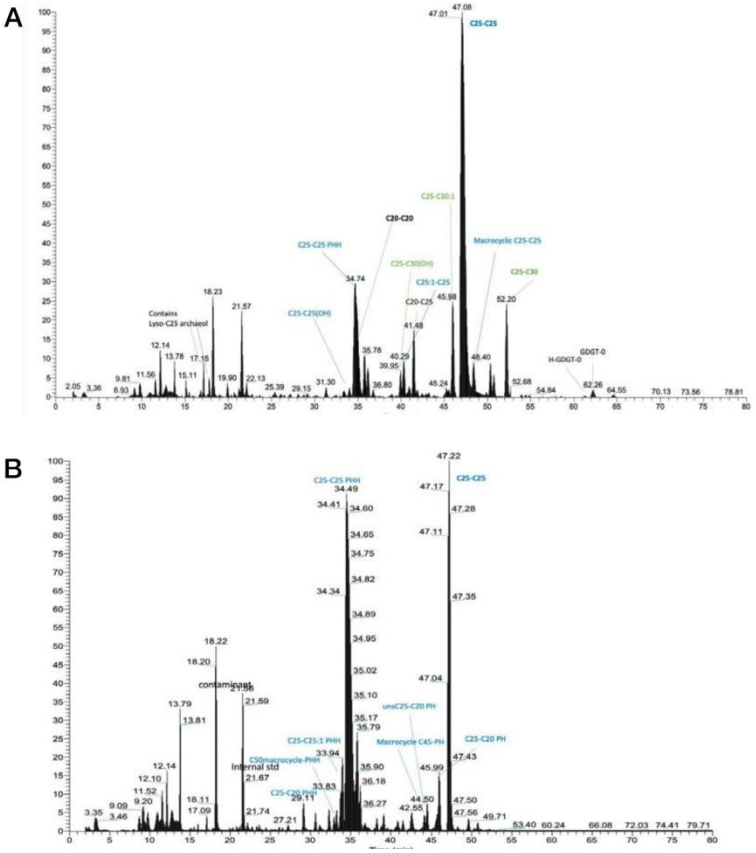

Supplemental Figure 3. Mass spectrometry of the lipids extracted from A. pernix cell culture. **(A)** A chromatogram of the core lipids found in the sample showing C25-C25 diether lipids as the most abundant species. **(B)** A chromatogram of the most abundant lipid headgroups reveals phospho-dihexose, i.e., a dihexose sugar connected to the glycerol by a phosphate group, as the most prevalent lipid headgroup and phospho-hexose, one sugar connected via a phosphate-group, as the second most prevalent.

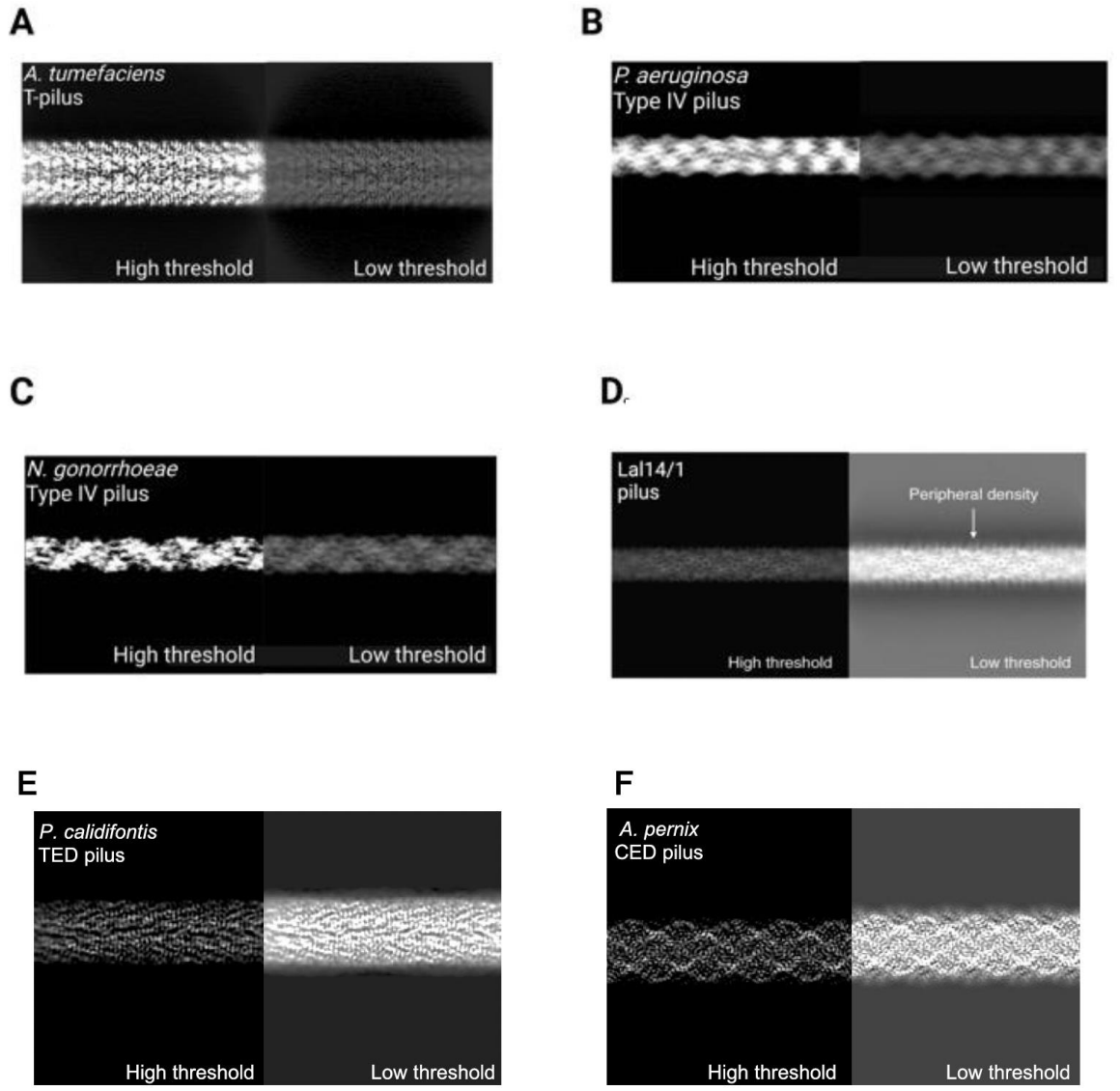

Supplemental Figure 4. Projections of the 3D reconstructions at different thresholds reveal if pili are extensively glycosylated. T4P pili of Neisseria gonorrhoeae (**A**, EMDB deposition EMD-8739, [https://www.emdataresource.org/EMD-8739]) and Pseudomonas aeruginosa (**B**, EMDB deposition EMD-8740, [https://www.emdataresource.org/EMD-8740]) are shown as negative controls, whereas the highly glycosylated type IV pilus of Saccharolobus islandicus LAL14/1 (**C**, EMDB deposition EMD-0397, [https://www.emdataresource.org/EMD-0397]) shows peripheral density at low threshold, and serves as a positive control. Both the Ted pilus of *P. calidifontis* (**D**) and the Ced pilus of *A. pernix* (**E**) show some surrounding density, which could represent glycosylation. In contrast, the T-pilus of *A. tumefaciens* (**F**) shows no obvious surrounding density at low threshold and behaves like controls A and B.

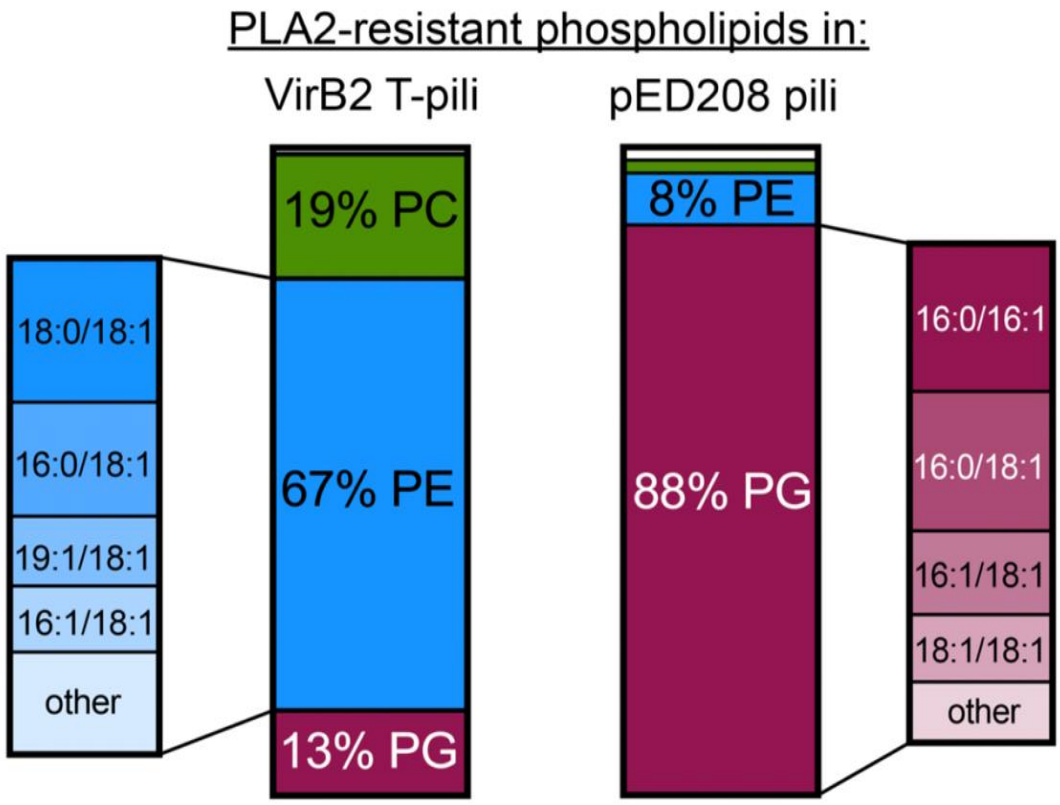

Supplemental Figure 5. Mass Spectroscopy on lipids of VirB2 and pED208. *PLA2 was applied to purified pili from VirB2 and pED208 to digest any unprotected phospholipids. The remaining lipids were extracted, then identified by mass spectrometry and quantified using internal standards. The major phospholipid classes in the pili samples are shown by headgroup class, and the acyl chain compositions are shown for the major headgroup classes (PE for VirB2, PG for pED208). Unlabeled bars represent minor species.*

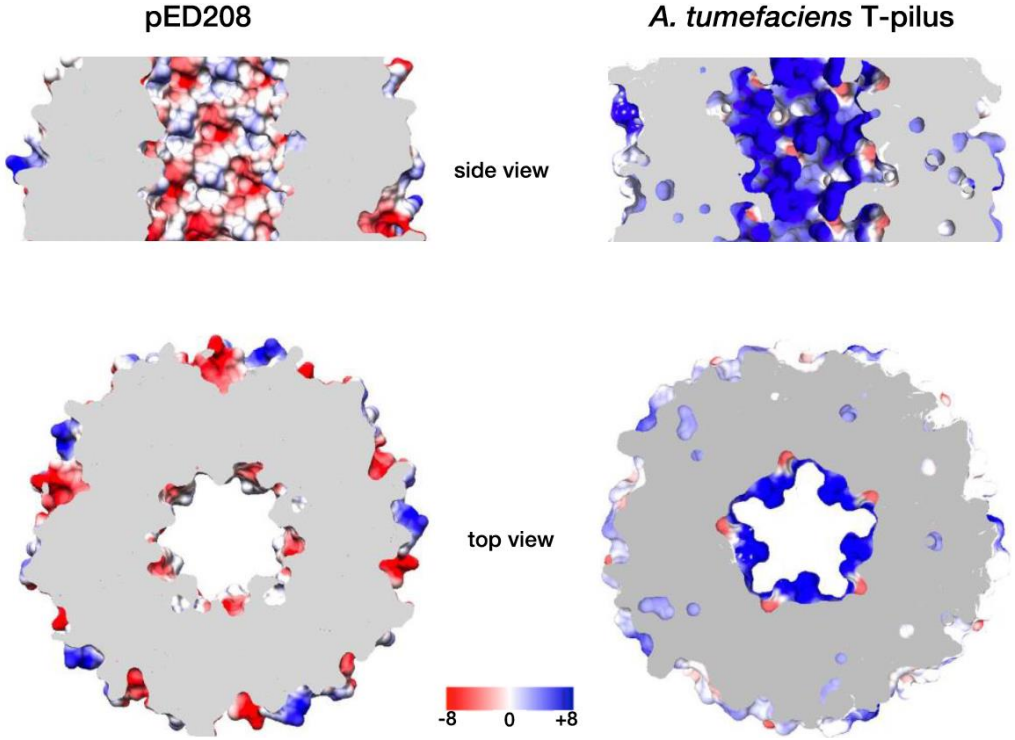

Supplemental Figure 6. Electrostatics of the pED208 and T-pilus lumen. Electrostatic potential surface for the lumen of the pED208 (left) and T-pilus (right). The side and top view of the pED208 pilus shows a more electronegative lumen compared to the T-pilus. The top view of the T-pilus shows an alternating positive to negative charge arising from the arginine and the lipid, respectively. All electrostatic potentials and surfaces were calculated using UCSF Chimera. The units for the potential are kT/e.

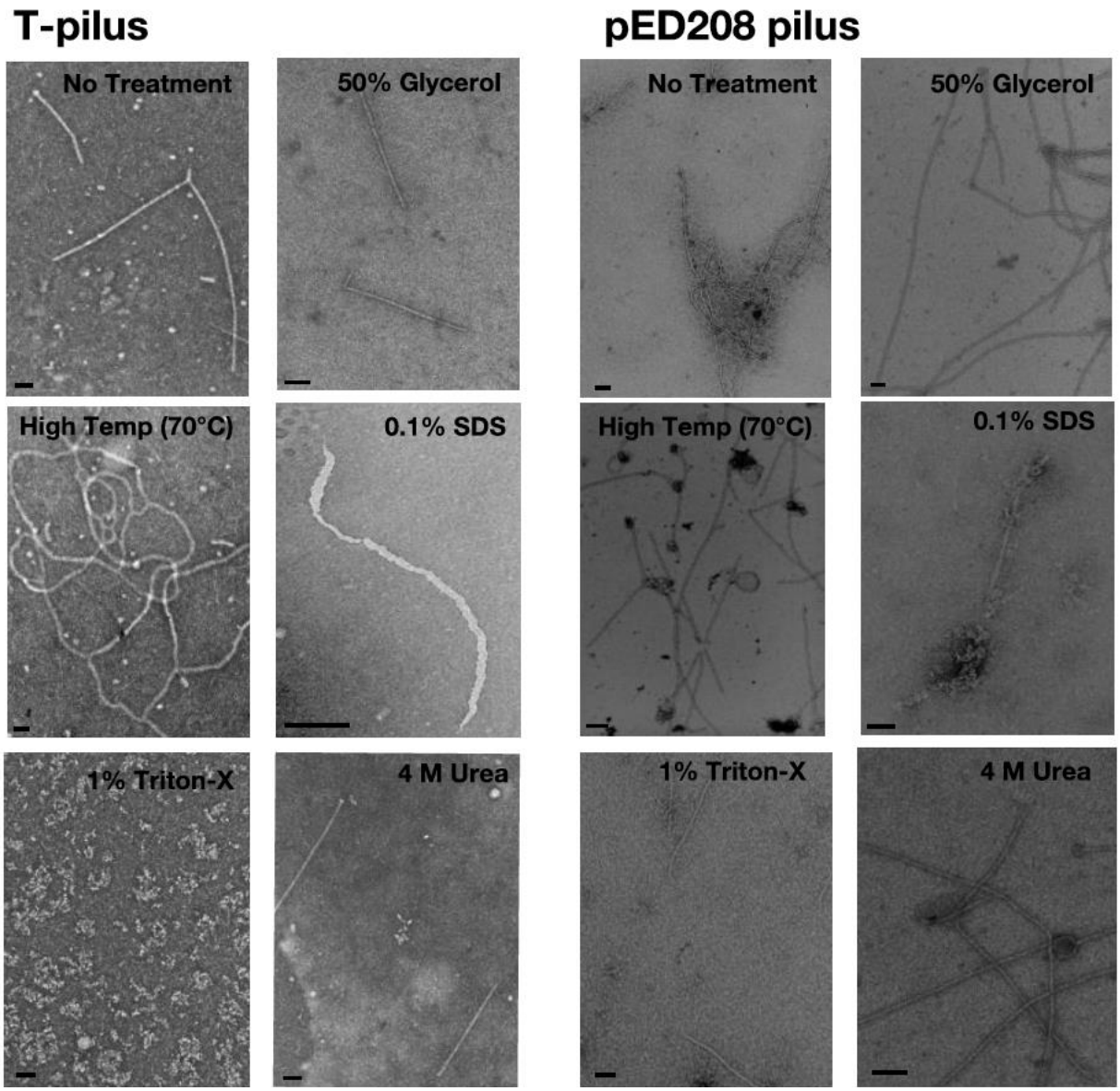

Supplemental Figure 7. Chemical and physical treatment of pED208 andT-pilus. Negative stain electron micrographs showing the effects on pilus structure of different harsh environmental conditions for *A. tumefaciens* T-pilus (left) and *E. coli* pED208 (right), scale bars 50 nm. The morphology of the T-pilus under no treatment, glycerol (50%) and 4M urea appears fully intact. The high-temperature (70°C) and SDS (0.1%) partially degrades the pilus and results in flexuous filaments. Triton-X (1%) fully depolymerizes the filament and creates aggregated clusters. The pED208 pilus morphology is mostly in a flexuous state with partial bundling at the ends of the pilus under SDS (0.1%). Each condition/treatment was replicated three times for both the T-pilus and pED208. Over 15 grid squares were chosen at random and examined for each sample to ensure a broad representation of pilus morphology across the entire electron microscopy grid. See Table S2 for more details.

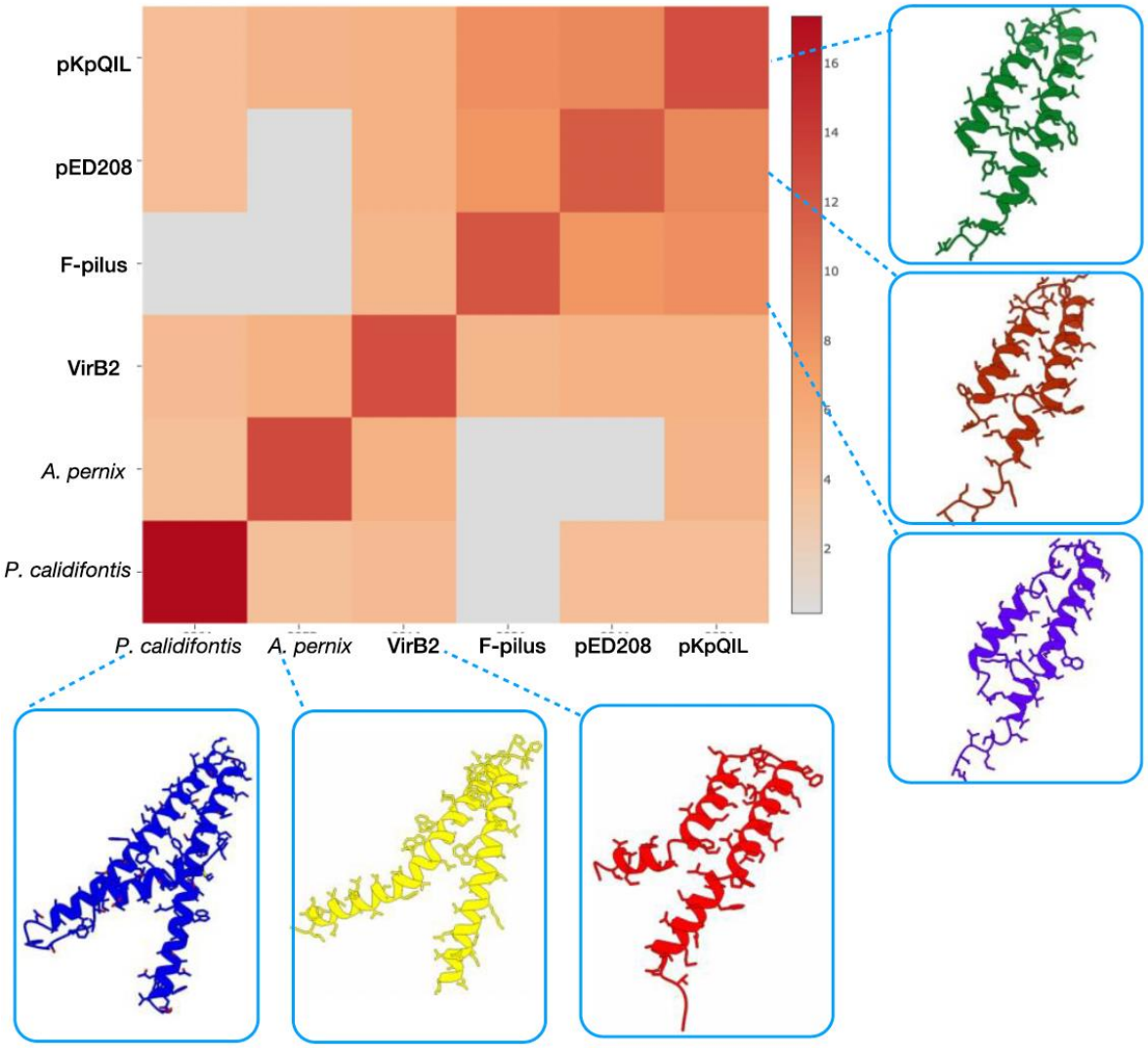

Supplemental Figure 8. Comparison of prokaryotic conjugative pilin subunits. Heat-map of global structural similarity between pilins from all known structures of prokaryotic conjugation pili: *P. calidifontis* (blue), *A. pernix* (yellow), *A. tumefaciens* (red), F-pilus (purple), pED208 (light brown) and pKpQIL (green). The color scale corresponds to the Dali Z-score values. The dark red indicates increased similarity, the lighter red indicates some similarity and grey is no to low structure similarity. Each pilin consists of two or three hydrophobic α-helices with kinks appearing in both of the archaeal pili and the *A. tumefaciens* T-pilin. All share a common helix-turn-helix architecture and have obvious structural homology.

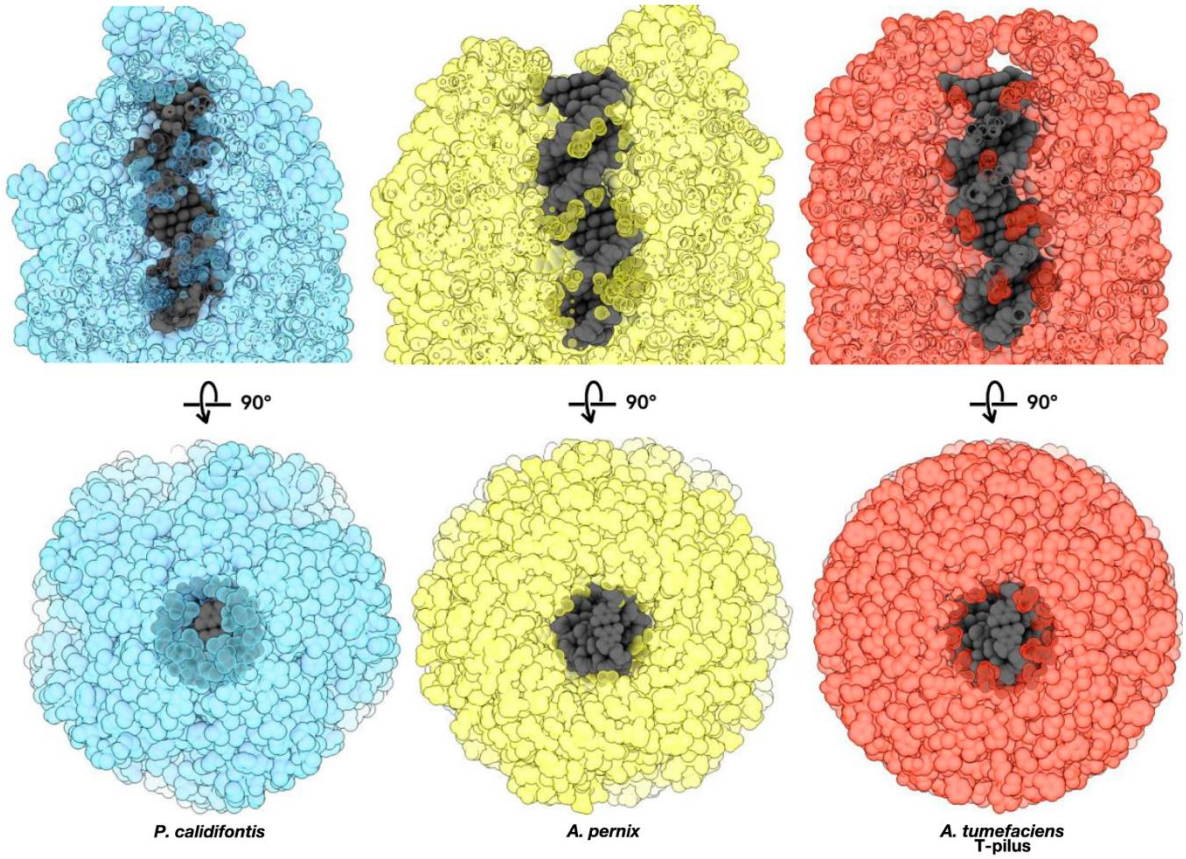

Supplemental Figure 9. dsDNA modeled within lumen of archaeal and bacterial conjugative pilus. Conjugative pili cannot transport dsDNA. Side views (top) and top views (bottom) of the atomic models of *P. calidifontis* (blue), *A. pernix* (yellow), and *A. tumefaciens* (red) with a model for B-form dsDNA placed within the lumen. The narrow lumen of all the prokaryotic conjugative pili would result in extensive clashes with dsDNA suggesting that only ssDNA could be accommodated within the lumen. The atomic model of *P. calidifontis* (blue) does not include a lipid model with phospho-dihexose headgroups. The addition of these sugar headgroups would decrease the pore size and result in even further clashes with dsDNA.

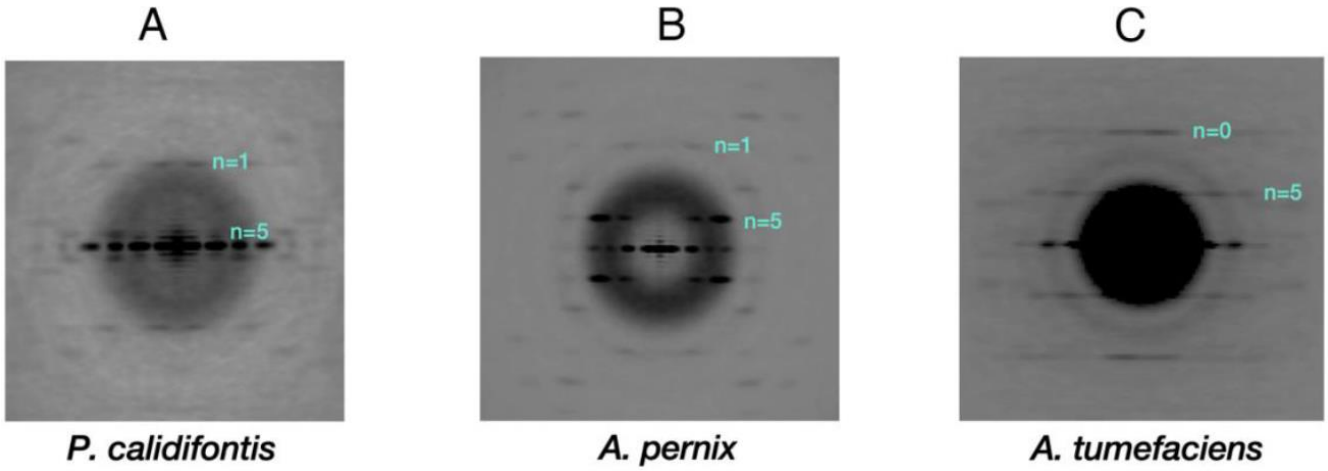

Supplemental Figure 10. Averaged power spectra of the P. calidifontis, A. pernix and A. tumefaciens pili. (A.) Averaged power spectrum generated for *P. calidifontis* from 54,000 segments. Two-layer lines are indexed with their Bessel orders: the n=1 and n=5. (B.) Averaged power spectrum generated for *A. pernix* from 44,000 segments. Two-layer lines are indexed with their Bessel orders: the n=1 and n=5. (C.) Averaged power spectrum generated for *A. tumefaciens* from 49,000 segments. Two-layer lines are indexed with their Bessel orders: the n=0 and n=5. To increase the dynamic range, the log of the intensities is shown for *P. calidifontis* and *A. tumefaciens*.

Parameter	*P. calidifontis* TedC	*A. pernix* CedA1	*A. tumefaciens* VirB2
Data collection and processing			
Voltage (kV)	300	300	300
Electron exposure (e^{-}Å^{-2})	50	50	50
Pixel size (Å)	1.08	1.08	1.08
Segments (n)	71,981	44,262	49,308
Helical symmetry			
Point group	C1	C1	C5
Helical rise (Å)	5.00	3.61	13.68
Helical twist (°)	74.21	76.5	32.45
Map resolution (Å)			
Software (final reconstruction)	cryoSPARC	cryoSPARC	cryoSPARC
Model:map FSC (0.38)	4.2	3.5	3.7
Map:map FSC (0.143)	4.0	3.3	3.5
Refinement and Model validation			
Bond lengths rmsd (Å)	0.004	0.007	0.003
Bond angles rmsd (°)	0.796	0.612	0.632
Clashscore	16.28	3.45	4.3
Ramachandran Favored (%)	97.27	98.78	100
Ramachandran Outlier (%)	0	0	0
MolProbity score	1.85	1.14	1.66
Deposition ID			
PDB (model)	8DFT	8DFU	8EXH
EMDB (map)	EMD-27413	EMD-27414	EMD-28657

Table S1. Cryo-EM and refinement statistics.

Environmental effects on T-pilus and pED208 structure

Agent or condition	Temperature (°C)	Morphology of T-pilus filament[1]	Morphology of pED208 pilus filament[1]
No Treatment	23	Rigid/Fully intact	Flexuous/Fully intact
Glycerol (50%)	23	Rigid/Fully intact	Flexuous/Fully intact
High temperature	70	Flexuous/Partially degraded	Flexuous/Fully intact
SDS (0.1%)	23	Flexuous/Partially degraded	Bundling at the ends of the pilus /Fully intact
Triton X-100 (1%)	23	Aggregated clusters/Fully depolymerized	Flexuous/Fully intact
Urea (4 M)	23	Rigid/Fully intact	Flexuous/Fully intact

[1]For each preparation the sample was negatively stained with 2% uranyl acetate and examined by transmission electron microscopy

Table S2. Environmental effects on pilus structure.

Cer 35:1;2, (D18:1;2, 17:0;0)
Chol D6
DAG 34:0;0 (17:0;0, 17:0;0)
DiHexCer 30:1;2 (D18:1;2.12:0;0)
HexCer 30:1;2 (D18:1;2.12:0;0)
LPA 17:0;0 (17:0;0)
LPC 12:0;0 (12:0;0)
LPE 17:1;0 (17:1;0)
LPI 17:1;0 (17:1;0)
LPS 17:1;0 (17:1;0)
PA 34:0;0 (17:0;0, 17:0;0)
PC 34:0;0 (17:0;0, 17:0;0)
PE 34:0;0 (17:0;0, 17:0;0)
PG 34:0;0 (17:0;0, 17:0;0)
PI 32:0;0 (16:0;0, 16:0;0)
PS 34:0;0 (17:0;0, 17:0;0)
SE 20:0;0 (20:0;0)
SM 30:1;2 (18:1;2, 12:0;0)
TAG 51:0;0 (17:0;0, 17:0;0, 17:0;0)

Table S3. Standard Lipid Mixtures

Chapter 3:

Ompk36-TraN Facilitate Mating Pairs for efficient conjugation

This Chapter was reformatted from the journal of Nature Microbiology:

Low, W.W., Wong, J.L.C., **Beltran, L.C.,** Seddon, C., David, S., Kwong, HK., Bizeau, T., Wang, F., Pe.a, A., Costa, T.R.D,. Pham, P., Chen, M., Egelman, E.H., Beis, K., Frankel, G. Mating pair stabilization mediates bacterial conjugation species specificity. **Nature Microbiology**, 7, 7 (2022), 1016-1027. doi:10.1038/s41564-022-01146-4

3.1 Abstract

Although, not required, the process of bacterial conjugation uses a contact dependent method to transfer genetic material from the donor to recipient cell. This process requires the establishment of stable mating pairs which is mediated by different protein components that make up the type IV secretion system (T4SS). The T4SS component, TraN, is found on the outer membrane of the donor cell and interacts with the outer membrane protein K36 of *Klebsiella pneumoniae* recipients. Using cryo- electron microscopy we solved the structure of TraN and OmpK36 to 2.6 Å resolution. We identified that the beta-hairpin at the tip of TraN inserts into the lumen of one OmpK36 trimeric porins. TraN-OmpK36 are stabilized by non-covalent interactions between the beta-hairpin of TraN and loop 3 of OmpK36. We show that when an insertion mutation (glycine and aspartic acid) is added to loop 3 that the efficiency of conjugation decreases. Upon visualizing crystallographic structure of the OmpK36 GD insertion mutant overlayed with the cryo-EM structures of wild type OmpK36 complexed with TraN we discover that loop 3 of the mutant extends further into the porin lumen and disrupts the beta-hairpin of TraN from inserting.

3.3 Results

3.3.1 Cryo-EM structure of TraN pKpQIL-OmpK36 complex

The structural basis of the OmpK36 and TraN interaction was probed by cryo-EM. Cryo-electron microscopy showed discrete complexes of OmpK36 and TraN, however, TraN was mainly disordered and exhibited an occupancy of less than one molecule for each OmpK36 trimer. A 3D reconstruction for the complex with an overall resolution of 2.6 Å using the map: map approach was generated with density for both the OmpK36 trimer and TraN (Figure. 1A). The crystal structure of the trimeric OmpK36 was placed inside the density with minimal rebuilding; the OmpK36 crystal and cryo-EM

structures display a rmsd. of 0.6 Å over 180 Ca atoms. The additional density above OmpK36 was assigned to TraN (Figure 1. A, B) and it extends into the channel of one subunit of the trimeric porin. The TraN density is weak, present at a low threshold and featureless. Therefore, we have decided not to build the TraN model in this density. The density inside the pore is better defined, showing a loop-shaped appearance with side chains; using the AlphaFold model for TraN pKpQIL, that density corresponds to the predicted b-hairpin of the TraN pKpQIL 'tip' (Figure 1. A, B). With minimal rebuilding of the AlphaFold model and by matching the side chains, a portion of the loop and the two β-strands on either side of the hairpin from the TraN pKpQIL model could be positioned within the density (Figure 1. B). The well-defined density and resulting atomic model for the TraN loop ends with two cysteines forming a disulphide bridge (Figure 1. A, B).

TraN inserts into the OmpK36 pore from its extracellular side and reaches half-way through the channel to L3 (Figure. 2A). The binding/recognition of the TraN b-hairpin is mostly mediated by interactions with L3 of OmpK36. Structural comparison was performed to investigate the disruption in complex formation caused by the L3 GD insertion (Figure. 2B).

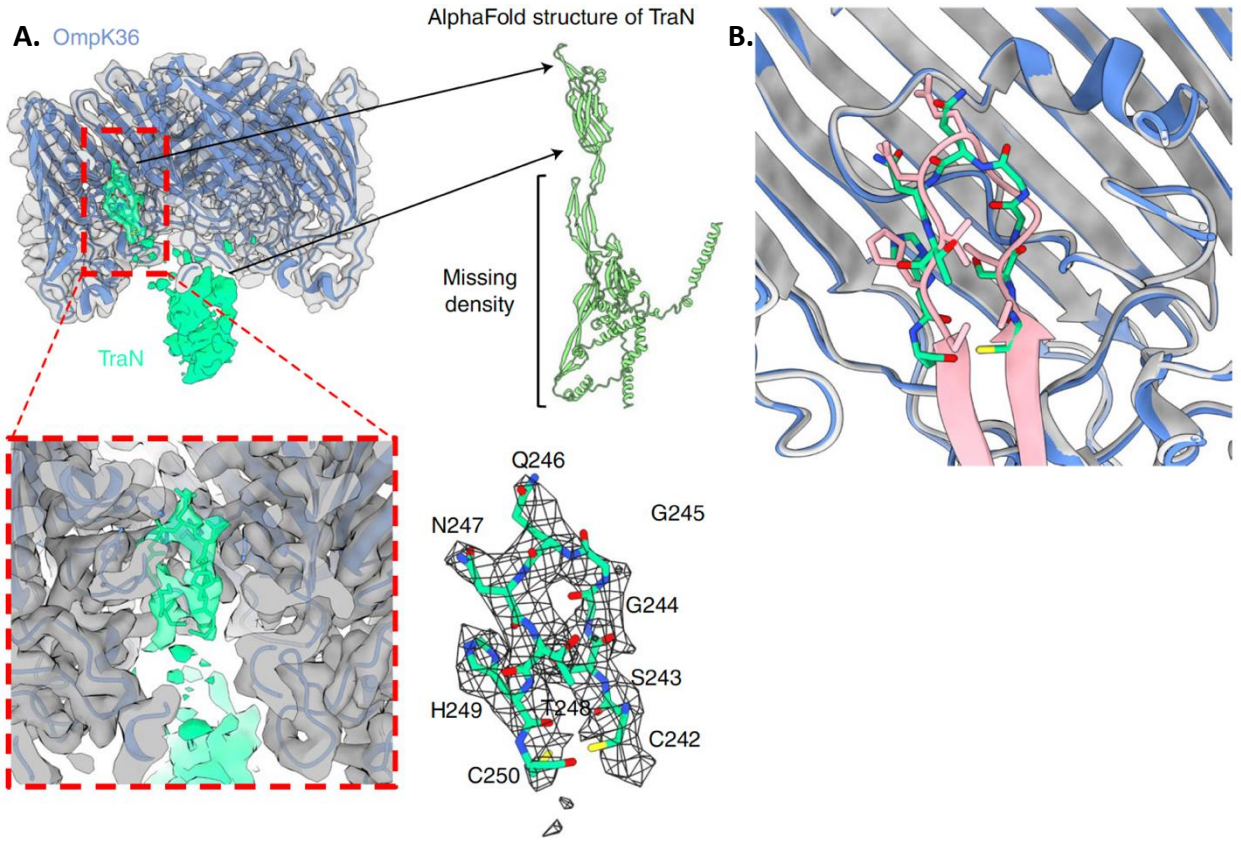

Figure 1. CryoEM structure of OmpK-36 and TraN. **(A.)** Cryo-EM reconstruction of the complex at 2.6 Å resolution. The reconstruction (left) shows Coulomb potential density for the OmpK36 trimer (transparent grey density) and TraN (green density). The front view of the reconstruction perpendicular to the OM has been omitted to reveal the TraN density within the channel. The OmpK36 and TraN atomic models have been fitted inside the reconstruction. The predicted AlphaFold structure of TraN is shown as cartoons (right). The TraN density accounts for the β-hairpin and β-sandwich domains; however, density is missing for the remainder of the predicted AlphaFold structure. Close-up view of the TraN β-hairpin model fitted inside the density (red box and bottom right). **(B.)** AlphaFold predicted a very similar complex formation with the β-hairpin inserting inside the OmpK36 pore. The cryo-EM complex (OmpK36 in blue/TraN in green) and AlphaFold model (OmpK36 in grey/TraN in pink) can be superimposed without any major deviations.

Using the TraN-OmpK36WT model as a reference, the structure for OmpK36WT+GD (PDB 6RCK) (35) was superimposed onto the complex (Figure. 2B). This showed a clash between Gly115 and Asp114 of OmpK36 from L3, and Ser243' and Gly244' of the TraN b-hairpin (Figure. 2B). These clashes would destabilize the interactions between OmpK36 and TraN, lowering the affinity of TraN for OmpK36.

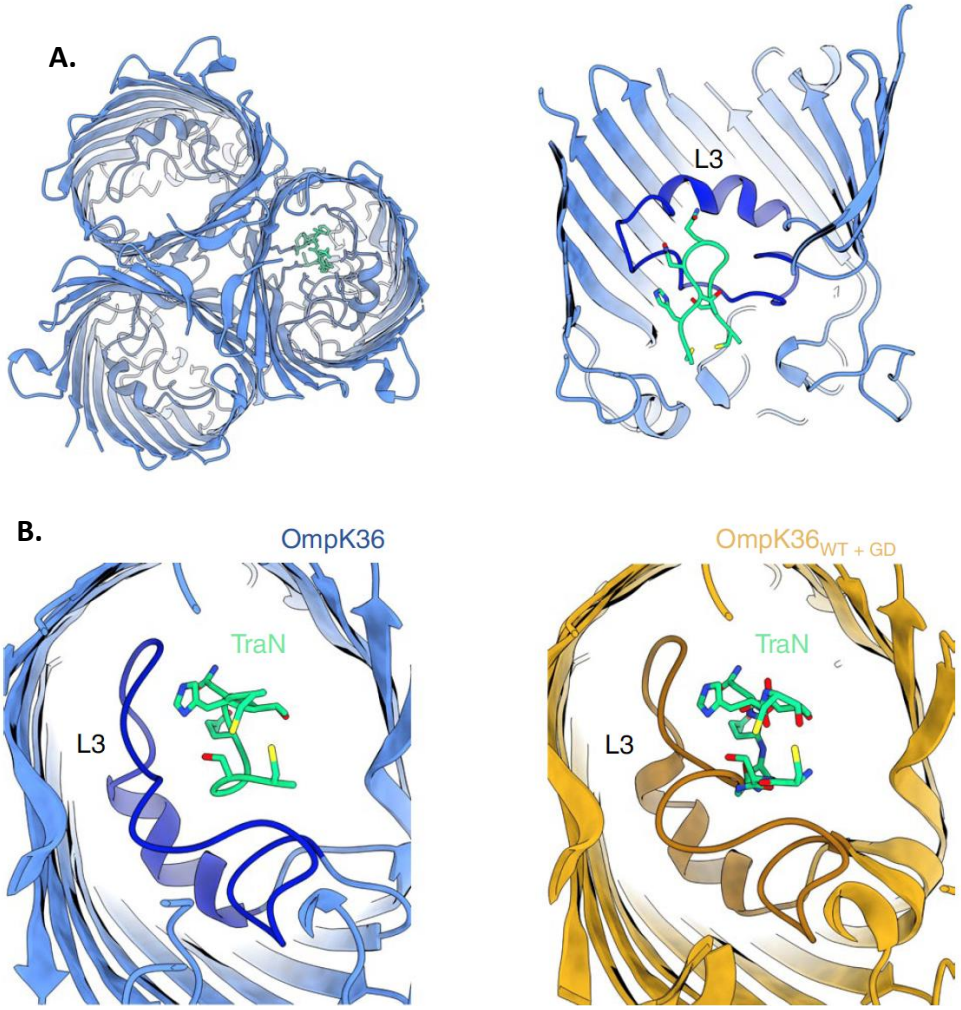

Figure 2. Model of OmpK36 and TraN compared to OmpK36 mutant and TraN. **(A.)** Top view of OmpK36 (blue) interaction with the β-hairpin of TraN (green) (left). TraN inserts halfway inside the OmpK36 channel to interact with L3 (right); the front face of the OmpK36 barrel has been omitted for clarity. **(B.)** The conformation of the OmpK36WT L3 can accommodate the TraN β-hairpin (left), whereas the L3 GD insertion results in steric clashes (right) that prevent complex formation.

3.4 Discussion

Although it had been previously discovered that conjugating *E. coli* cells use TraN and outer membrane protein A to establish mating pairs, their direct interactions were not known (Babić, A.,et al., 2008). In our work we establish TraN's continuous role in stabilizing mating pairs using clinically relevant carbapenem resistant *K. pnuemoniae*. Distinctively, *K. pnuemoniae* recipient cells express an outer membrane protein, OmpK36, which interacts with the tip of TraN at the beta-hairpin. Through non-covalent interactions the two proteins form a stable complex which allows the donor and recipient cells to form close contacts with each other; this close contact site is termed a conjugation junction. It is unclear whether these contacts establish direct membrane-membrane contact between the two cells once stable mating pairs have formed and a conjugation junction has been established. However, these are the first outer membrane proteins identified in opposing cells which we show cooperate to mediate bacteria-bacteria interactions.

Interestingly, when donor cells were mixed with recipient cells containing the OmpK36 GD insertion mutation to loop 3 conjugation was not completely abolished. Suggesting that there must be an alternative method that bacteria use if stable mating pairs are unable to be established. Although controversial, a possibility is that the conjugative pilus facilitates the transfer, acting as a conduit for ssDNA. There is no direct evidence that the pilus acts as a conduit, however, Babić et al show indirectly that genetic transfer occurs at long range distances. Further, in cryo-EM structures of the F- and F-like pilus the lumen environments are negatively charged which would repel ssDNA and act as a lubricant to facilitate the passing of ssDNA (Costa et al., 2016).

While this research provides compelling evidence for events that precede DNA transfer many questions arise from our results. One such question is, what signals the release of TraN from OmpK36 once ssDNA has been successfully transferred? One possibility is that the attachment of TraN to OmpK36 triggers a signal cascade, within either the donor or recipient cell, that results in the detachment of the TraN beta-hair pin from OmpK36, this trigger can be thought of and recognized as a mechano-sensing mechanism. More work needs to be completed to consider this hypothesis with more certainty. This data provides foundational understanding for stabilization of mating bacteria, in context of clinically relevant carbapenem resistant *K. pnuemoniae*. Our data describing the considerable disruption of conjugation by the extension of OmpK36's loop 3 offers new strategies to consider for targeting multidrug resistant microbes.

3.5 Methods

3.5.1 Cryo-EM Sample Preparation and Data Collection

Sample containing OmpK36-TraN at a concentration of 0.33 mg/mL was diluted 1:6 in SEC buffer: 50 mM NaCl, 10 mM HEPES, 0.03% DDM. In brief, a 4 µL aliquot of sample was applied to a plasma-cleaned (Gatan Solarus) graphene oxide-coated Cu 300 mesh 1.2/1.3 holey carbon grid (Quantifoil), blotted with force 6 for 4.5 s at 90% humidity and flash frozen in liquid ethane using a Vitrobot Mark IV (FEI). The dataset used for structure determination was collected at the Molecular Electron Microscopy Core at the University of Virginia on a Titan Krios EM operated at 300 keV, equipped with an energy filter and K3 direct electron detector (Gatan). An energy filter slit width of 10 eV was used during data collection and was aligned automatically every hour. All 13,668 movies were collected in counting mode at a magnification of 81K, pixel size of 1.08 Å, and a defocus range from -2.2 to -1.2 µm. Data collection was performed using a total dose of 50 e- Å-2 across 40 frames at a rate of 4.78 s/movie.

3.5.2 Data Processing

Unless otherwise stated, all data processing was completed using cryoSPARC v3.2.054. Movies were corrected for full-frame motion using Patch Motion Correction followed by Gctf 585 CTF Estimation. After CTF estimation, micrographs were sorted and selected based on estimated resolution (better than 4 Å), defocus (-1 to -2.5 µm), ice thickness, and total full-frame motion. Initial particles were automatically picked using „Blob picker" with minimum and maximum particle diameters of 200 and 256 Å, respectively. Particles were extracted at a box size of 256 pixels, followed by 2D classification. Class averages of trimeric OmpK36 alone, and OmpK36 with TraN were selected for template-based particle picking. A total of 13,780,567 particles were extracted using a box diameter of 256 Å. These particles were sorted using three iterative rounds of 2D classification with 50 classes each, number of online-EM iterations set to 100 and a batch size of 1000 per class. The final iteration of 2D classification yielded a subset of 3,412,946 particles.
To differentiate particles containing only OmpK36 or OmpK36 + TraN, multiple 3D maps were generated using Ab-initio reconstruction", class size set to 4. Output 3D maps were inspected for the presence of TraN. Particles were further refined using two iterations of heterogeneous refinement with input volumes created by multi-class ab initio. The highest resolution class from the second iteration of heterogeneous refinement contained 359,314 particles, which allowed for a ~2.6 Å map to be reconstructed using non-uniform refinement (Extended Data Fig. 8 and Supplementary Table S5).

3.5.3 Model Building and Refinement

The density for the trimeric OmpK36 allowed us to trace the entire backbone and built most side chains throughout the structure. The OmpK36 crystal structure (PDB ID: 6RD3) was used for building the cryo-EM model which only had small differences relative to the starting model. The predicted TraN AlphaFold model was used for initial interpretation of the loop-shaped density found within the lumen of one porin channel. The loop and the two β-strands on either side of the hairpin of the AlphaFold model could be fit into the density. Two cysteines at either side of the hairpin fit into the TraN density and were used as a starting point for matching larger sidechains within the density. Model building including adjusting side chains were performed in Coot. The model was refined in Phenix, using Real-space refinement with `ignoring symmetry conflicts` turned on. Refinement included global minimization, B-factor optimization, and applied secondary structure and Ramachandran restraints. The final model had a MolProbity score of 1.39, with 96% and 0.1% in the Ramachandran favored and outlier regions, respectively (Supplementary Table S5).

3.6 Acknowledgments

Cryo-EM was done at the University of Virginia Molecular Electron Microscopy Core facility, which is supported in part by the School of Medicine and built with NIH grant G20-RR31199. The Titan Krios (S10-RR025067) and K3/GIF (U24-GM116790) were purchased in part or in full with the designated NIH grants.

3.7 Supplementary Figures

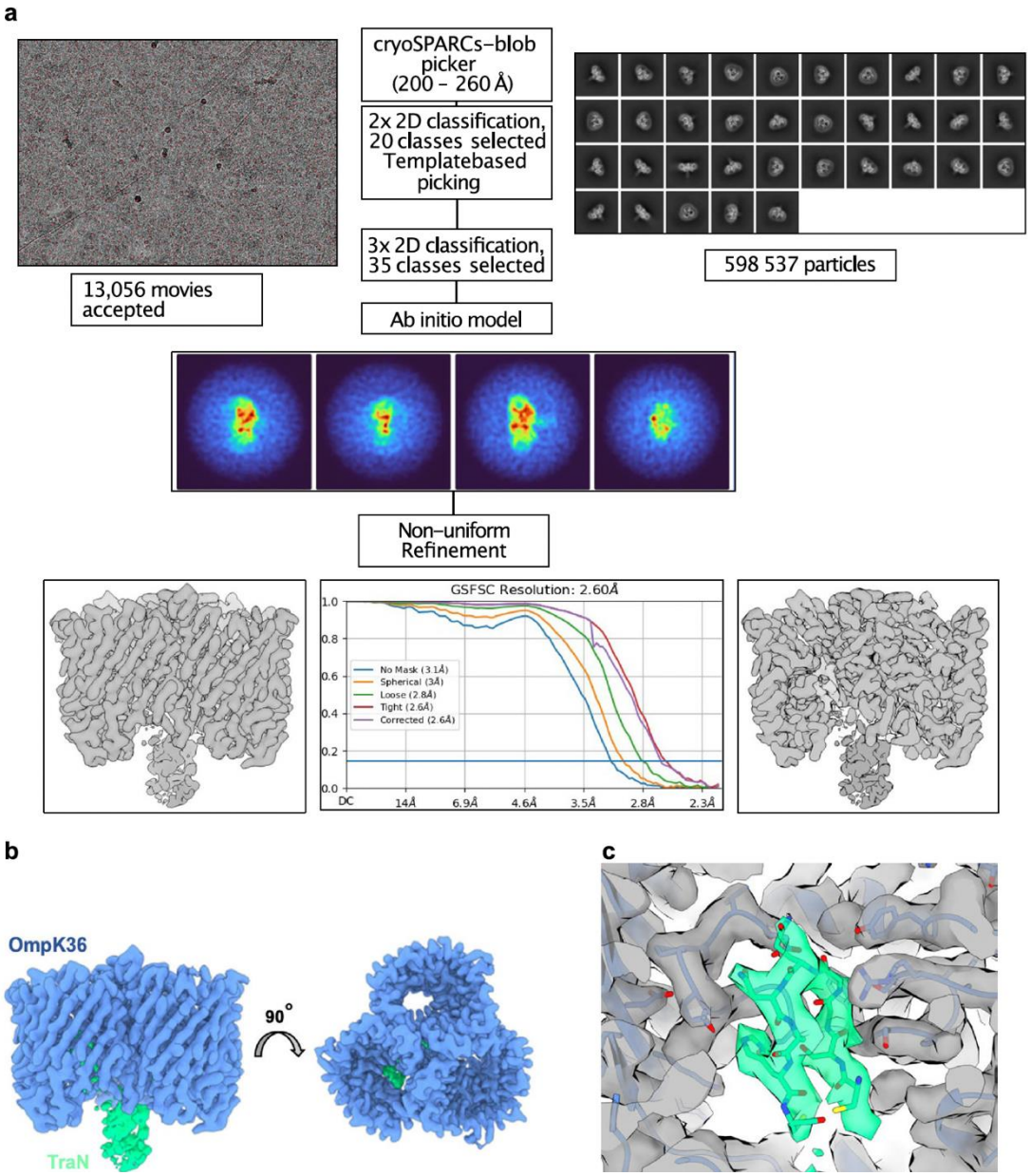

Supplemental Figure 1. Cryo-EM and single-particle analysis of OmpK36-TraN. **a** Overview of the image processing workflow done in cryoSPARC v3.2.0. 13,056 movies were selected based on estimated resolution, defocus, ice thickness, and full-frame motion. Accepted micrographs were subjected to automated particle picking 'blob picking' and 2x 2D classification to obtain template references. Template-based picking followed by 3x 2D classification was completed, resulting in 508, 537 particles. Particles were then used for Ab initio reconstruction; the best output reconstruction generated by Ab initio reconstruction was further refined using Non−uniform Refinement. The results of non-uniform refinement yielded a reconstruction with an estimated resolution of 2.6 Å. **b** Coulomb potential density for the OmpK36 trimer (blue density) and TraN (green density). **c** Close up view of the density for the OmpK36 and TraN 'tip' side chains.

Chapter 4: The mating pilus of *E. coli* pED208 acts as a conduit for ssDNA during horizontal gene transfer

This Chapter was reformatted from the journal of mBio:

Beltran, L.C., Torsilieri Holly, Patkowski, Yang Jae., Casanova James, Costa, T.R.D, Wright Elizabeth, Egelman, E.H., The mating pilus of *E. coli* pED208 acts as a conduit for ssDNA during horizontal gene transfer. **mBio**, 0(0), e02857-02823.doi:10.1128/mbio.02857-23

4.1 Abstract

Bacterial conjugation, a process of horizontal gene transfer, plays a key role in promoting the spread of antimicrobial resistance among human pathogens. The mechanism of conjugation involves the development of a conjugative pilus that forms a physical bridge between two bacterial cells, and the subsequent unidirectional transfer of single-stranded DNA complexed with a protein from the donor to the recipient cell. Atomic structures exist for many of the components of the type IV secretion system (T4SS), responsible for the nucleoprotein secretion, but little is known about the events preceding gene transfer, specifically: what is the extent of the participation of the conjugative pilus in ssDNA transfer? There has been a longstanding debate about whether its main role is to bring a donor and recipient cell into physical juxtaposition and form a mating junction that allows for ssDNA transfer via the T4SS machinery complex, or whether ssDNA is actually transferred through the lumen of the pilus. Here, through a combination of maleimide-labelling of the conjugative pilus, and SeqA-YFP-labelling of the transferred ssDNA, we visualize the process of bacterial conjugation in real time. We discover that the conjugative pilus is capable of transferring the ssDNA at a distance, between physically separated cells, and thus conclude that a physical mating junction is not essential for conjugative gene transfer.

4.2 Introduction

Horizontal gene transfer (HGT) is a common process employed by populations of bacteria and archaea to exchange genetic material. For human pathogens, these transfers often involve genes coding for virulence factors and/or antibiotic resistance. The worldwide spread of antimicrobial-resistance is a concern for human health as many strains are fast becoming resistant to last-line defense therapeutics. The primary contributor to HGT is bacterial conjugation – a process that involves establishing a physical junction between two bacterial cells, the donor and recipient, which allows for transfer of DNA. Bacterial conjugation is mediated by the type IV secretion system (T4SS)

– a membrane-embedded nanomachine capable of producing a hollow extracellular appendage, known as the conjugative pilus, which projects from the outer membrane of the donor cell and is responsible for interaction with the recipient cell (95). In Gram-negative bacteria many high-resolution structures have been determined using cryo-electron microscopy (cryo-EM) for components of the secretion system, including the parts of the T4SS associated with both the inner and outer membranes and the pilus, for model organisms such as *Escherichia coli*, *Agrobacterium tumefaciens*, *Klebsiella pneumoniae*, and *Legionella pneumophila* (48, 68, 95-102). The conjugative pilus has a lumen diameter of approximately 15 Å and is composed of many copies of the TraA subunit which folds into an all α-helical structure containing three α-helices. Although the lumen size is an approximation and does not take into consideration the contribution of hydrogens and tightly bound water molecules which might further reduce the diameter, it has been shown that ssDNA is capable of permeating through pore diameters as small as 10 Å (103). While these structures have led to many new insights regarding the function of these components and ultimately the mechanism of conjugation, many aspects of conjugation are still not very well understood.

The contribution of the F-pilus to bacterial conjugation is still unclear. It has been argued that the F-pilus only serves to bring the donor and recipient cells into direct contact with each other and that the conjugation pilus is fully depolymerized when DNA transfer occurs (104). On the other hand, Babić et al. showed using real-time microscopy that conjugative DNA transfer can occur over distances up to 12 μm (105). While this provided support for the notion that the pilus itself was acting as a conduit for the long-range transfer of the DNA (106), the evidence was indirect. The atomic structures of the F-pilus and related conjugation pili revealed a negatively charged lumen, interpreted as acting to repel negatively-charged DNA from the walls of the lumen, potentially lubricating the passage of DNA (48, 98). This was viewed as consistent with the role of the pilus in transferring DNA. But the structure of the *Agrobacterium tumefaciens* T-pilus revealed a positively-charged lumen (96, 97, 107), seemingly in conflict with this notion of DNA transfer. An explanation was suggested that the properties of the T-pilus lumen may have evolved as a compromise between transferring negatively-charged DNA and positively-charged effector proteins (97, 108).

A significant question that remains to be answered is, how does the DNA get through the recipient cell's outer membrane, periplasmic space and inner membrane when cells are conjugating at a distance? There have been studies that suggest that bacterial conjugation is a two-step mechanism for DNA transport whereby the pilus is fully depolymerized and a pilot protein is involved (104). The model called ‘shoot and pump’ implicates the T4SS as a system that shoots the pilot protein, attached to the DNA, through one or both of the recipient cell membranes (104). Given the extreme flexibility of ssDNA, with a persistence length that is only a few bases (109), it is

impossible to imagine such a mechanism when mating cells are at a distance from each other, and it is still very difficult to imagine how such a mechanism would be possible even when cells have established a tight mating junction.

Here, using fluorescence light microscopy together with an experimental technique that allows us to see transferred DNA, we show direct evidence that the conjugative pilus is present when mating cells are conjugating at a distance. We show that the length of the pilus is variable when cells have not formed mating pairs. In this study we use *E. coli* cells harboring the pED208 plasmid which belongs to the IncF family isolated from Salmonella typhimurium which constitutively expresses the tra genes. With the Alexa-Fluor 568 maleimide labeling of the pED208 pilus TraA subunits, our observations show TraA reinsertion into the inner membrane of the donor cell after depolymerization of the pili, evidenced by the intense fluorescence of the cell body which is not observed in the mutant strain lacking the pED208 TraA protein. Collectively our results show that pili, with variable lengths, are present between actively mating pairs.

4.3 Results

4.3.1 Light microscopy of pED208 WT, pED208 ΔtraA, and MG1655

Using a labeling scheme that allows us to attach Alexa-Fluor 568 C_5 maleimide dye to TraA subunits of the donor cell, *Escherichia coli* harboring the pED208 plasmid, we were able to directly target fluorophore attachment to the extracellular donor cell pilus (Fig. 1 A-C). Our images (without any quantification) suggest that the number, distribution, and length of pili per donor cell appear to be stochastic, in agreement with other published studies of bacterial conjugal pili (110, 111) (Fig. 1 A, Movies 1 and 2, Supp. Fig 5 A & B and Supp. Movie 1). F-pili are dynamic structures that undergo extension and retraction (111). Extension allows the pilus to survey the surroundings and attach to a recipient cell and then retract, pulling the recipient cell into juxtaposition, followed by the formation of stable mating junctions defined by the contact of the mating pairs' cell envelopes (Movie 1, Supp Movie 1 and Supp Fig 5C) (95). All solved structures of conjugation pili, both bacterial and archaeal, show a tight association of lipids with TraA subunits, with a 1:1 stoichiometric ratio for bacterial pili (48, 96-98, 107). It was suggested that one of the functions for this pilin:lipid association would be to facilitate reinsertion of the pilus subunits within the membrane during retraction events (48). However, subsequent studies have shown that there is a 1:1 lipid: pilin association in T-pili, where there has been no evidence of retraction, so the role of the lipid may be more general. Mutant *E.coli* cells lacking the traA gene (pED208 ΔtraA) were labeled with Alexa-Fluor 568 C_5 maleimide dye which appears to either weakly associate, or not all, with the cell membranes when compared to the WT pED208 cells which are brightly labeled (112) (Fig. 1 A-F, Supp Fig. 1 A-B). This suggests a

correlation between labeled TraA and reinsertion within the membrane of the donor cells, discussed in further detail below. It is possible that the weak association of the maleimide dye observed with pilus-deficient pED208 ΔtraA is due to transiently available cysteines from other proteins found on the membrane surface, since this strain lacks pili compared to the wild-type strain, as shown by negative-stain EM (Supp Fig. 2 A-B). Recipient cells, fully characterized by Babić et al, contain a SeqA-YFP fusion protein that recognizes and binds with high affinity to hemimethylated ssDNA, enabling us to specifically and permanently label only transferred ssDNA (105). It is important to note that dam-positive donor cells generate hemimethylated DNA which is transferred to dam-deficient recipient cells that do not contain nor can generate methylated DNA, but contain the SeqA-YFP fusion protein that acts as a biosensor for methylated DNA. Diffuse and weak fluorescence throughout the cell body has been attributed to the dam-deficient SeqA-YFP recipient cells (Fig. 1G,H,I) (105).

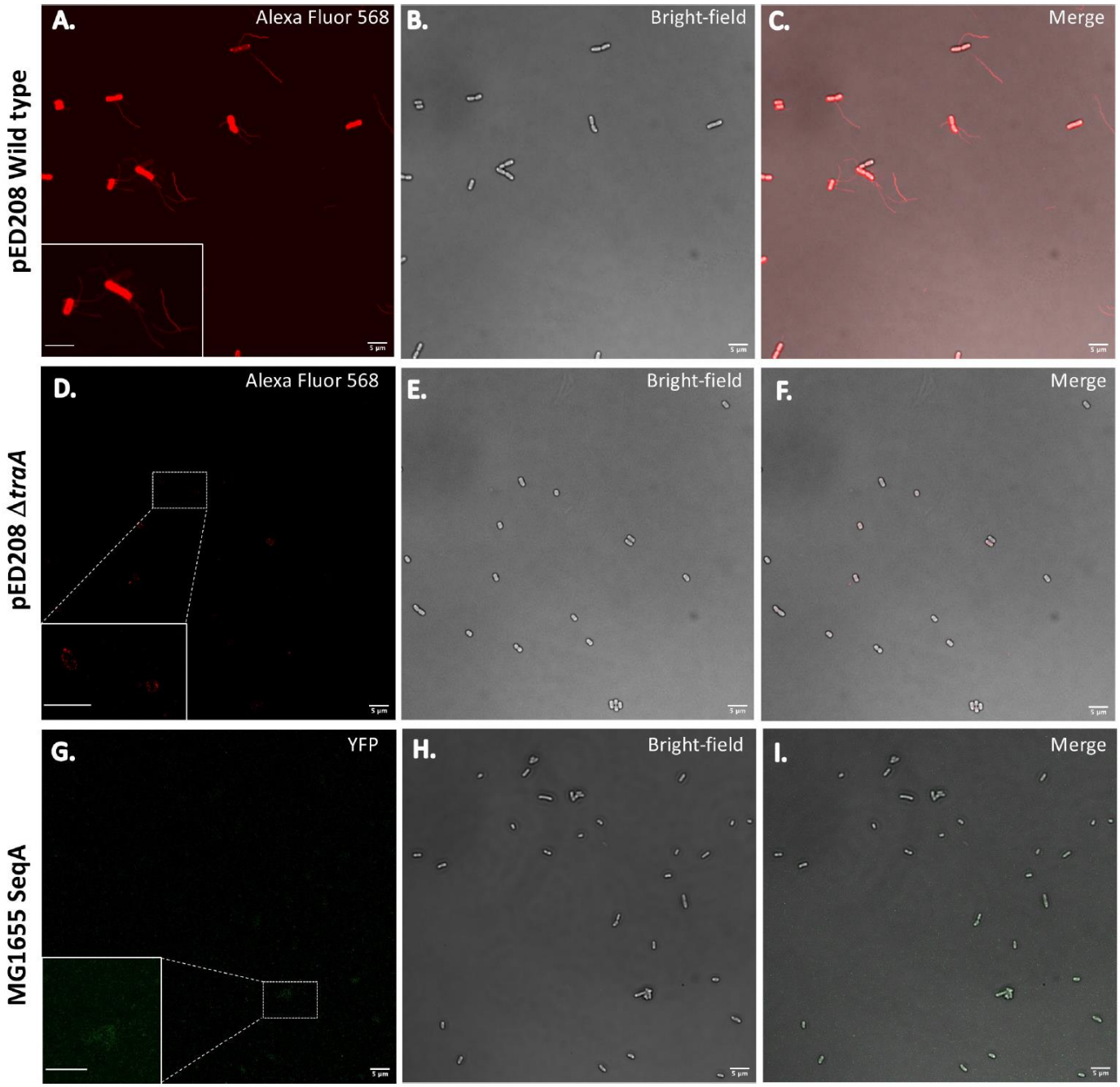

Figure 1. Light microscopy of pED208 WT, pED208 ΔtraA, MG1655 SeqA-YFP. (A-C) Fluorescence microscopy image of WT *E. coli* harboring pED208 plasmid (AF-568 labeled cells and F-pili). Brightfield image of the same WT *E. coli* with the pED208 plasmid in (A). Overlay of the fluorescence (AF-568 labeled cells and F-pili) and brightfield images (A, B) of WT *E. coli* with the pED208 plasmid. (D-F) Fluorescence microscopy image of mutant *E. coli* harboring pED208 ΔtraA (AF-568 labeled cells and F-pili). Brightfield image of mutant pED208 ΔtraA. Overlay of the fluorescence (AF-568 labeled cells and F-pili) and brightfield images of mutant pED208 ΔtraA. (G-I) Fluorescence microscopy image of the recipient cell strain, MG1655 (SeqA-YFP fusion). Brightfield image of the same MG1655 cells. Overlay of the fluorescence and brightfield images of MG1655 (SeqA-YFP fusion). Scale bar 5 μm.

4.3.2 Conjugating bacteria

Similar to observations made by Babić et al., mixing maleimide-labeled donor cells with the SeqA-YFP recipient cell led to the visualization of conjugally transferred DNA in the recipient cells (105). Conjugally transferred DNA is indicated by intense fluorescent foci (green puncta) in recipient cells from SeqA-YFP. The YFP foci seen in recipient cells were often observed at the poles or septum of the cells. During live cell imaging, a mixture of conjugating cells that formed mating junctions, as well as cells conjugating from a distance, were observed (Fig. 2 A & B). The donor pilus colocalization with the bright foci of SeqA-YFP within the recipient cell provides direct evidence that the pilus is actually transferring ssDNA between two cells separated by many micrometers. This process of conjugal transfer of DNA through a mating pilus connecting donor and recipient cells has never been directly visualized, to the best of our knowledge. When the traA gene is knocked out of the pED208 strain, puncta are no longer present in the SeqA-YFP strain when donor and recipient strains are mixed (112) (Fig. 1 C, Supp. Fig. 1A-C & 2A-C). Interestingly, during the experiments it was observed that not all donor cells used the same method to transfer ssDNA to the recipient cell. Some mating cells were ~2 μm apart and did not form mating junctions (Movie 1, blue arrow, Supp. Fig 4 A & B, Supp. Movie 1 and Supp Fig 5 A), while other donor cells used the pilus to probe the volume of the environment, attach to a recipient cell and pull it closer (Movie 1, yellow arrow, and Supp. Fig 5 B). Also observed were mating cells which formed stable mating junctions (Movie 1, green arrow, Supp. Movie 1 and Supp. Fig 5 C). These observations suggest that not all mating pairs evolve to form mating junctions. Further, donor cells can express multiple F-pili, some of which are seen to attach to recipient cells while others appear to survey the environment (Fig. 1, Movie 1 & 2). Due to the limited

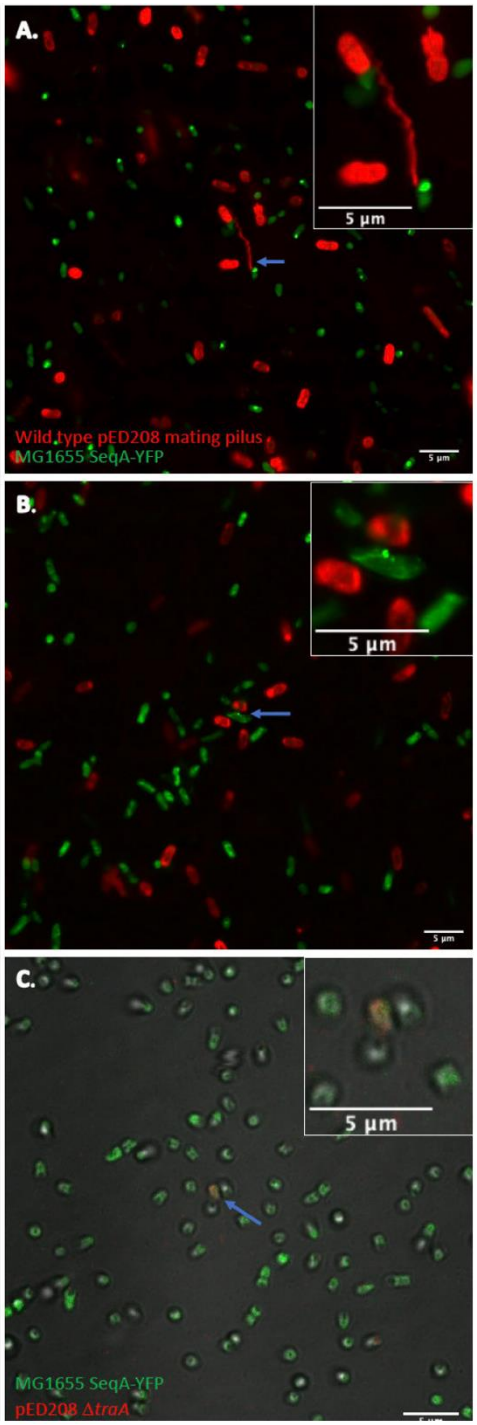

Figure 2. Bacterial conjugation of pED208 WT across multiple spatial scales in comparison with pED208 ΔtraA. (A) The blue arrow points to a WT donor and recipient cell conjugating from a distance (> 5 μm). Donor pilus (red) spans the extracellular space and formed an attachment to the recipient cell passing hemimethylated DNA (green puncta). (B) Blue arrow points to a WT donor and recipient cell in the process of conjugation after mating pairs have formed. The donor (red) has passed hemimethylated DNA (green puncta) to the recipient cell. Puncta are located at polar ends or the septum. (C) Blue arrow points at pair of cells close by, pED208 ΔtraA is weakly labeled red as this strain does not express pili, while recipient cells are green and contain no puncta. Scale bar 5 μm.

resolution of light microscopy, we were unable to directly observe whether any part of the pilus remained once stable mating junctions were formed. A largely depolymerized F-pilus may assist in stabilizing mating pairs together with the TraN-OmpA complex, which is a necessary interaction for efficient conjugation to occur (95, 113, 114). The presence of the F-pilus without type IV secretion system machinery attached has been shown in cryo-EM data (115). Since such pili would presumably be unable to undergo further cycles of polymerization and depolymerization, it was suggested that these static pili might play a role instead in biofilm formation.

4.3.3 Pilin reinsertion to the cell membrane

Conjugation pili are the only known bacterial filaments where protein subunits are tightly bound to a lipid with a stoichiometric ratio of 1:1. The function of the lipid has been difficult to investigate, however, it has been suggested that the lipid plays a critical role in the stability of the pED208 pilus during both conjugation and biofilm formation (116). When the donor strain carrying the WT pED208 was labelled with maleimide, the pili are easily observed by confocal microscopy, along with strong fluorescence from the cell body (Fig 1 A-C). When the knockout strain lacking the pilin subunit TraA was treated with maleimide, there is a significantly weaker fluorescent signal when compared to that of the WT pED208 strain (Fig 1 A-C, D-F, Supp Fig 2 A & B). Since the labeling of the pilin subunits only occurs when the polymerized pilus is extracellular, the presence of labeled subunits in the donor cell body provides direct evidence for the reinsertion of the pilin subunit into the membrane (117).

4.4 Discussion

After ~50 years of investigation, it is evident that there is still much to be understood about bacterial conjugation. Most importantly, we do not understand how the donor cell DNA enters the recipient cell. This study clearly shows that the pED208 pilus is involved in DNA transfer between donor and recipient cells separated by small or large distances. A physiological basis for conjugation at a distance may be supported by the mechanical robustness of the pili as it forms a resilient protective casing (or shaft) for DNA transfer between cells (97, 116). This still leads to many unanswered questions. For example, does the mating pilus penetrate through both the outer and inner membranes of the recipient cell? Or, just the outer membrane? If so, is there a protein or complex that assists in shuttling the DNA into the cytoplasm of the recipient cell? And, when cells have established mating junctions what happens to the pilus? We describe four possible models for this aspect of bacterial conjugation (Fig. 3). The first shows a fully depolymerized pilus, which could only arise after a stable mating junction has been established. The second, third, and fourth models could exist when mating junctions are established, or they could also apply to when mating cells are

physically separated and connected only by the pilus. The second model has the pilus running from the donor cell to the outer membrane of the recipient cell, the third model has the pilus extending into the periplasmic space of the recipient cell, while the fourth model has the pED208 pilus penetrating through both the outer and inner membranes of the recipient cell into the cytoplasm.

The first, second, and third models require the presence of a translocation system in the recipient cell for DNA to be pumped into the cytoplasm, as no force provided by the donor cell would be able to propel extremely flexible ssDNA through either the outer or inner membranes of the recipient cell. The role of ComEA/ComEC as a translocation system, moving ssDNA from the periplasm to the cytoplasm, has been directly shown in the process of natural transformation and it is possible that ComEC functions similarly for the process of bacterial conjugation (118-120). If a recipient cell translocation system is not employed, the fourth model seems the most likely, as the pilus would be positioned to transport ssDNA to the recipient cytoplasm. Such a model for the pilus would be consistent with both transfer at a distance as well as transfer when stable mating junctions have formed.

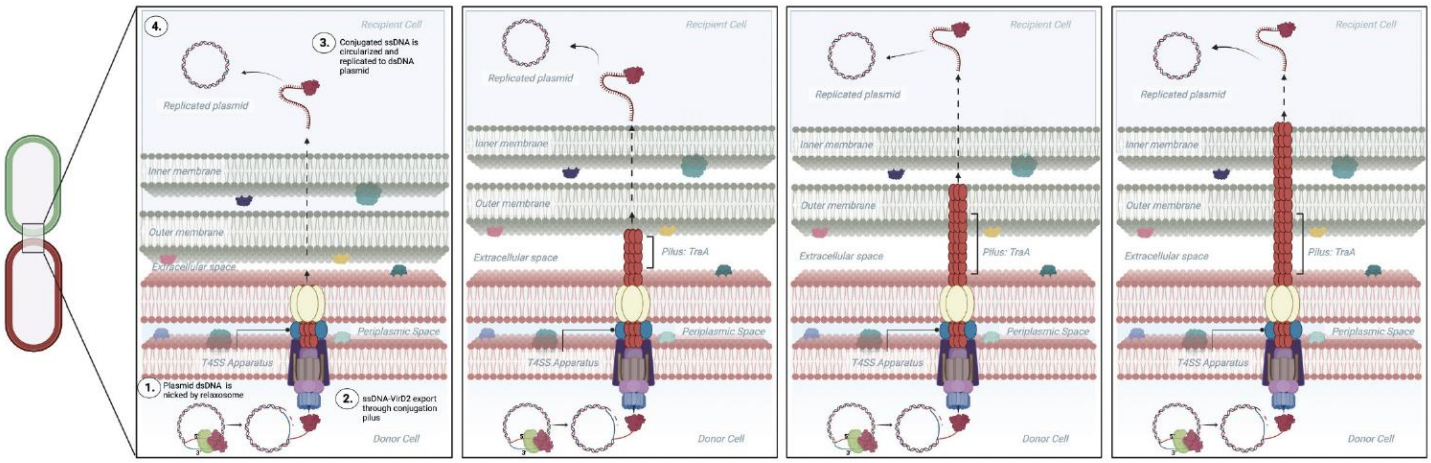

Figure 3. Proposed models of conjugation. Cartoon depicting possible conjugation mechanisms. Models left to right: (1.) Model reflects the donor cell T4SS apparatus without the mating pilus. The pilus has been fully depolymerized and the T4SS acts as the portal for which ssDNA and a pilot protein pass through to the recipient cell cytoplasm. (2.) The mating pilus extends into the extracellular matrix only. The ssDNA traverses, with a pilot protein, through the outer membrane, periplasmic space and inner membrane to the recipient cytoplasm. (3.) A mating pilus perforates the recipient cell outer membrane, and ssDNA passes with a pilot protein through the periplasmic space and inner membrane to the cytoplasm. (4.) The mating pilus perforates the recipient cell outer membrane, periplasmic space, and inner membrane and delivers ssDNA directly to the cytoplasm.

Our results provide a direct visualization of pilin reincorporation into the donor cell membrane that must result from depolymerizing labeled pili. While it may be possible that pilin subunits depolymerize at the distal end into the recipient cell membranes, we do not observe any significant fluorescence from the membranes of the recipient cell, making such a possibility unlikely. Our observations show unambiguously that the mating pilus does actually serve as a conduit for DNA transfer, validating the original hypothesis (108).These results provide a rationale for directly targeting

the pED208 pilus by therapeutics, and such an approach might aid in combatting the spread of antibiotic resistance in bacterial populations.

4.5 Methods

4.5.1 Generation of the cysteine-rich F-pilus variants

To enhance the fluorescence intensity of the maleimide-labelled F-pilus, the number of surface exposed thiol groups had to be artificially increased beyond that natively present by the single cysteine in the mature F-pilin polypeptide. Based on the 3D structure of the F-pilus (Costa et al., 2016), four threonine residues were chosen as candidates for substitution by cysteine residues. Consequently, the T69C, T111C, T112C, T116C mutants of F-pilin (TraA) were generated through site-directed mutagenesis by inverse PCR according to Takara In-Fusion® Snap Assembly protocol. Primer pairs P1 and P2, P3 and P4, P5 and P6, P7 and P8 were used with pBAD_TraA as template to yield constructs pBAD_TraA:T69C, pBAD_TraA:T111C, pBAD_TraA:T112C, pBAD_TraA:T116C, respectively. Primer sequences used in the study are listed in Supplementary Table 1, and all used constructs summarized in Supplementary Table 2.

Table S1. List of primers used in the study

Primer	In-house label	DNA sequence 5’ to 3’
P1	T69C F	GAAAGCCTGCTTCGGTGCCGACTCATTCG
P2	T69C R	CCGAAGCAGGCTTTCACATCATCCTTGCCC
P3	T116C F	CGGTCTTTGCTTCATCAAATGATAAGAGAGCTTGG
P4	T116C R	ATGAAGCAAAGACCGACGGTAGTGAAGAC
P5	T112C F	CTTCACTTGCGTCGGTCTTACCTTCATCAAATG
P6	T112C R	CCGACGCAAGTGAAGACGATAACCACAACCAG
P7	T111C F	CGTCTTCTGCACCGTCGGTCTTACCTTCATC
P8	T111C R	ACGGTGCAGAAGACGATAACCACAACCAGGC

Table S2. List of constructs used in this study

Name of construct	Description	Source
pBAD_TraA	pBADM-11 cloned with traA gene from pED208 plasmid under arabinose-inducible promoter, Amp^R	Costa et al., 2016

pBAD_TraA:T69C	T69C substitution mutation of pBAD_TraA	This study
pBAD_TraA:T111C	T111C substitution mutation of pBAD_TraA	This study
pBAD_TraA:T112C	T112C substitution mutation of pBAD_TraA	This study
pBAD_TraA:T116C	T116C substitution mutation of pBAD_TraA	This study

4.5.2 Complementation assay of cysteine-rich F-pilin variants

To test the generated constructs for functional complementation, a pilus-specific phage spot assay was employed. pBAD_TraA encoding the wild-type F-pilin together with the different substitution variants were transformed into *E. coli* strain DH5α harboring the pilin-deficient pED208:ΔtraA plasmid and grown to OD_{600}=0.5. Expression was induced with 0.2% (w/v) L-arabinose and allowed to proceed for 2 hours at 37°C before being plated on LB-agar plates supplemented with 0.2% (w/v) L-arabinose. Then, 2 µl of the F-pilus specific phage F1 was spotted on top of each of the freshly dispersed bacterial inoculum, and the plates were incubated at 37°C overnight. The next day, formation of bacteriophage plaques on the plates was examined. Positive complementation with the F-pilin and substitutions, e.g., presence of the F-pilus, was determined when F1 phage plaques were observed. Cells harbouring the pBAD_TraA:T116C variant produced plaques identical to those with the wild type pBAD_TraA, therefore this construct was chosen for further maleimide labelling and imaging.

4.5.3 Cultivation of *E. coli* strain harboring pED208 plasmid and labeling of pilus, pED208 ΔtraA or dam deficient seqA-YFP strain

A culture of *E. coli* DH5α(F^+) dam^+ harboring the pED208 plasmid was grown at 37 °C and 180 RPM to an OD_{600} of ~1.1 in 100 mL of LB media containing 50µg/mL kanamycin and 100 µL of 0.1% of ampicillin. 2 mL of 10% arabinose was added for a final concentration of 0.2% to induce the pBAD plasmid expressing the TraA cysteine knock-in. Culture of *E. coli* JE2571(F^+) harboring the pED208 plasmid was grown at 37 °C and 180 RPM to an OD_{600} of ~1.1 in 100 mL of liquid LB with 50µg/mL kanamycin. Culture of *E. coli* MG1655 (F^-) dam^- harboring the SeqA-YFP fusion gene was grown at 37 °C and 180 RPM to an OD_{600} of ~0.6 in 100 mL of liquid LB with 25µg/mL chloramphenicol.

4.5.4 Negative Stain Transmission Electron Microscopy

2 µL of sample containing either of *E. coli* DH5α(F^+) harboring the pED208 + pBAD inducer, pED208 ΔtraA, or *E. coli* dam deficient seqA-YFP strain were applied to a 200-mesh carbon coated grid and stained with 2% uranyl acetate and examined by transmission electron microscopy using a Tecnai-T12 at 80 kV.

4.5.5 Fluorescence Microscopy and Image Analysis

5 μl of sample containing either Alexa-Fluor 568 labeled *E. coli* DH5α(F^+) + pBAD donor cells mixed with the recipient *E. coli* dam deficient seqA-YFP strain, or pED208 ΔtraA donor cells mixed with recipient *E. coli* dam deficient seqA-YFP strain, or samples only containing *E. coli* DH5α(F^+) harboring the pED208 + pBAD, pED208 ΔtraA, or *E. coli* dam deficient seqA-YFP strain were applied to 25 X 75 mm 1.0mm thick glass microslide with or without an agar pad and covered with a 22 x 22 mm micro cover glass slide. The specimens were imaged using a Nikon Ti2-E inverted microscope with AX-R confocal microscopy system, 25 mm FOV resonant scanner, 25 mm FOV Galvano scanner, and an NSPARC detector unit. Images were captured using photomultipliers and the Nikon NIS Elements C software. Live cell imaging was performed at 23°C and the samples were viewed using a 100X/NA1.52 oil objective with perfect focus during live image acquisition. Captured images and movies were processed using Elements Denoise.ai followed by compiling in FIJI software (121).

4.6 Movies and Supplementary Figures

Movie 1.

The blue arrow denotes the location for conjugation from a distance. Pilus is seen to attach to the recipient cell and transfer hemimethylated ssDNA recognized by seqA-YFP producing punta (top). The yellow arrow indicates a donor cell with the appearance of two separate pili, one pilus attaches, then retracts, pulling in a recipient cell (middle). The green arrow shows conjugation between mating pairs (bottom). The scale bar is 5 μm.

Movie 2.

The yellow arrow marks the point where a red punctum is colocalized on a recipient cell. Frame 0:03.79 reveals a visible donor cell pulling itself toward the recipient cell. Top left yellow arrow marks a donor cell which has two separate pili which appear to be surveying the environment at frame 0:04.88. The scale bar (far right) is 5 μm and the time is 1 minute every 10 seconds.

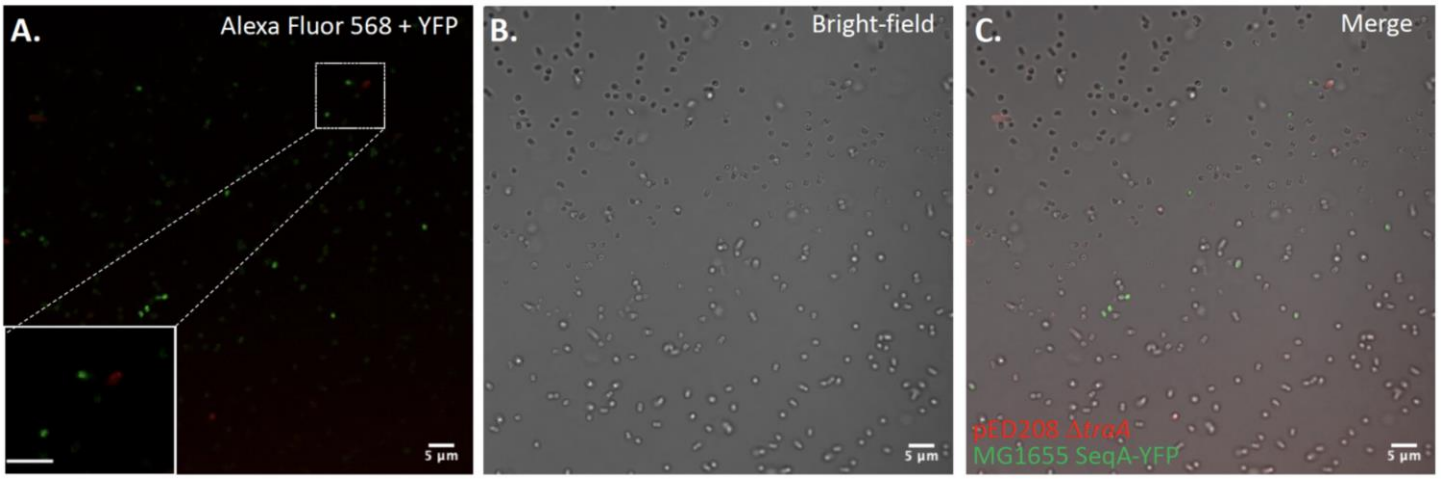

Supplemental Figure 1. pED208 ΔtraA strain mixed with MG1655 SeqA-YFP recipient strain. (A) Fluorescence microscopy image of *E. coli* harboring pED208 *Δ*traA plasmid (labeled with AF 568) mixed with MG1655 SeqA-YFP recipient strain. (B) Brightfield image of pED208 DtraA plasmid mixed withMG1655 SeqA-YFP recipient strain. (C) Merge of the fluorescence and brightfield images of *E. coli* harboring pED208 *Δ*traA mixed with MG1655 SeqA-YFP recipient strain.

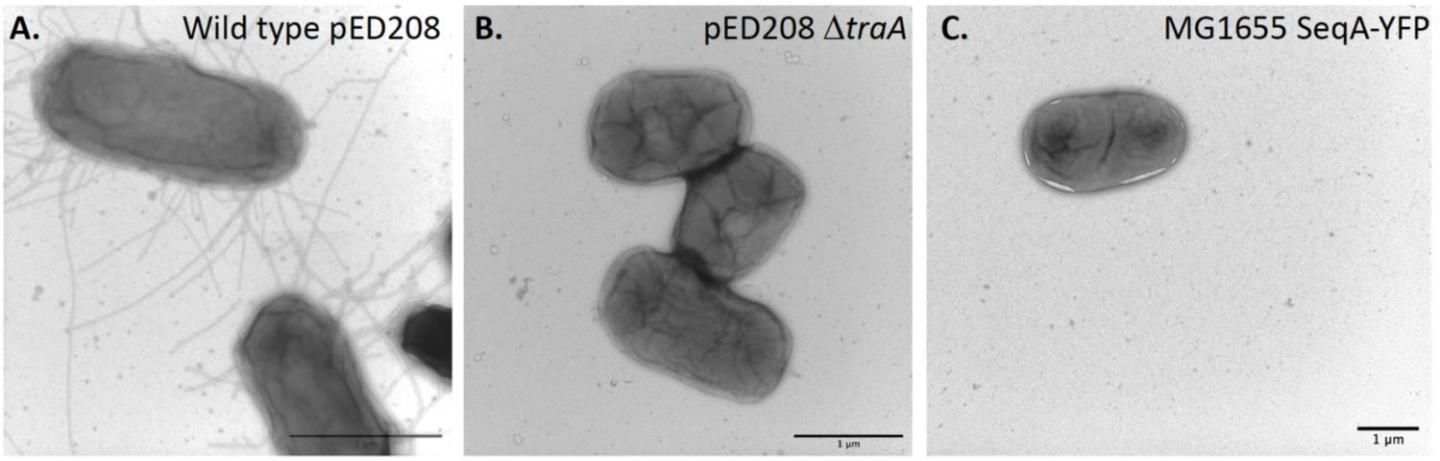

Supplemental Figure 2. Negative stain TEM images. (A) Wild-type *E. coli* strain JE2571 harboring pED208 plasmid and labeled with Alexa Fluor 568. (B) Mutant *E. coli* strain JE2571 ΔtraA, pED208 ΔtraA and labeled with Alexa Fluor 568. (C) *E. coli* strain MG1655 nalR dam::FRT seqA-yfp::Cm.

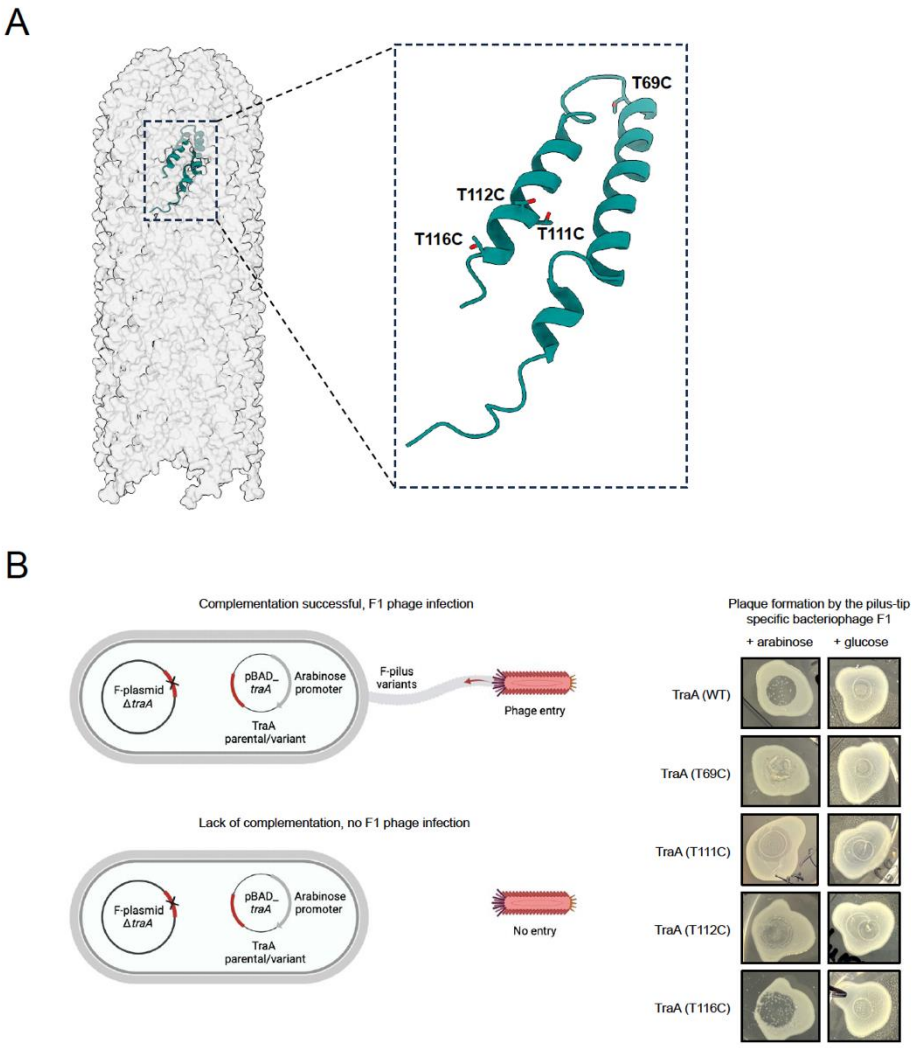

Supplemental Figure 3. Schematic for labeling pED208 TraA subunits. (A) PDB: 5LEG pilus of wild-type *E. coli* strain JE2571 harboring pED208 plasmid. The yellow stars indicate the maleimide deriva2ve targets of Alexa Fluor 568, residues T116 & C79 for attachment. The predictive relative surface accessibility (RSA) is 67% and 54% for T116 and C79, respectively. (B) F1 phage plaque assay to validate that the point mutation cysteine knock-in for T116 was successful. F1 phage binds to accessible F-pili. Clear F1 phage plaques indicate successful knock-in.

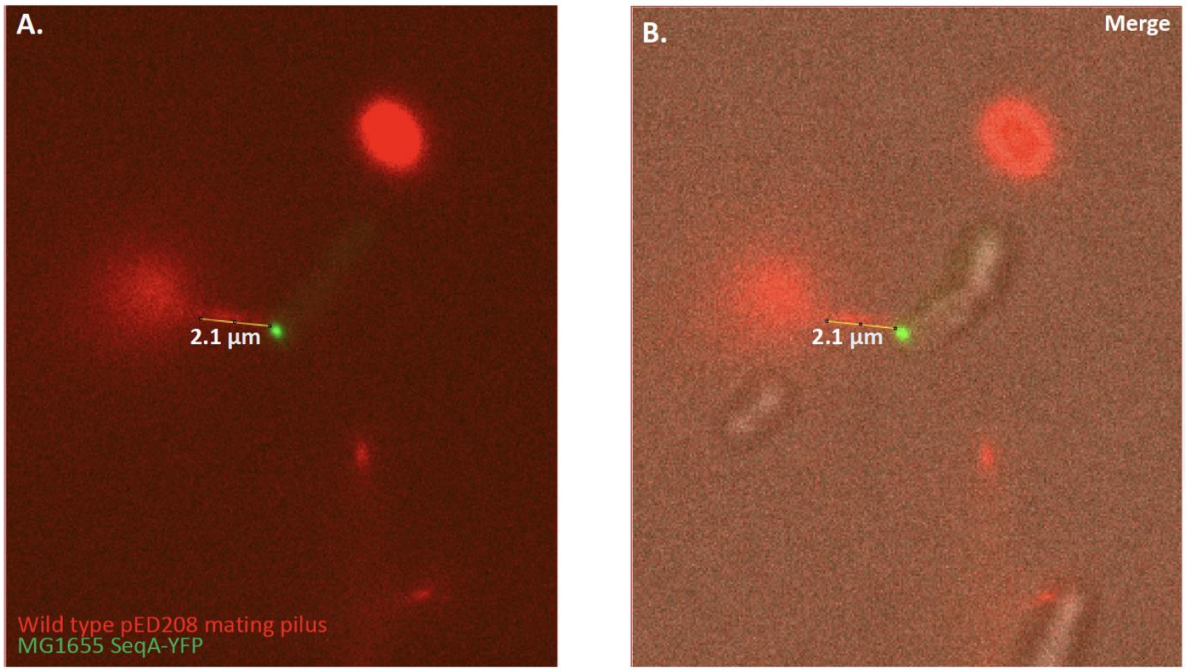

Supplemental Figure 4. Measurement of mating pilus when mating pairs have not formed mating junctions but transferred ssDNA at a shorter distance ~2 micrometers. (A) Fluorescence images of donor cell pED208 (AF 568 – red) and recipient cell (SeqA-YFP fusion - green). Bright puncta indicate the transfer of ssDNA to recipient cell. (B) Brightfield overlay of panel A for better visualization of cells.

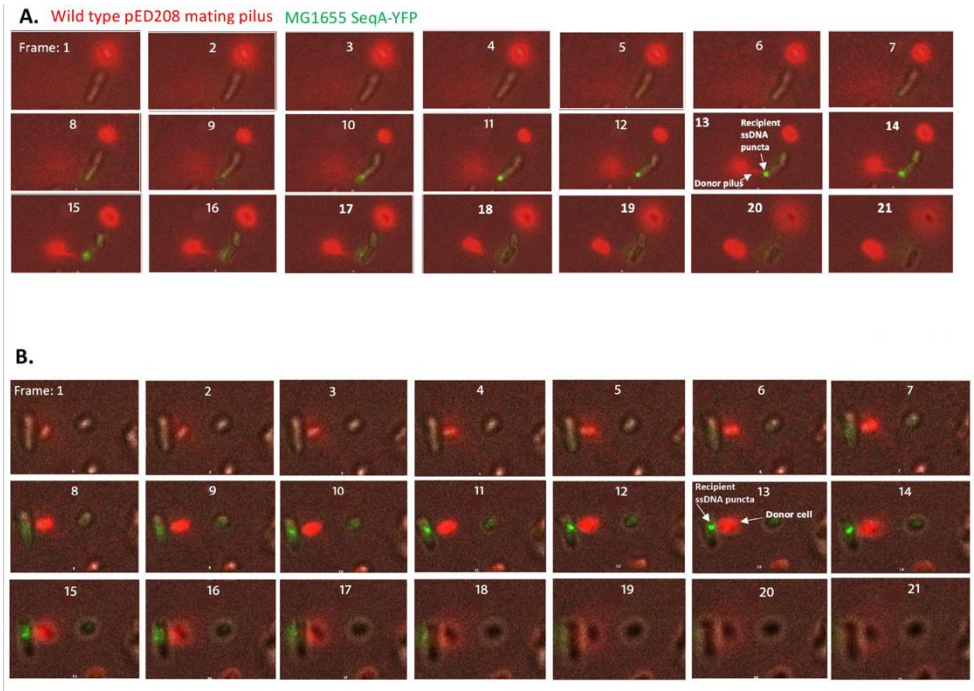

Supplemental Figure 5. Frame-by-frame montage of the three different events happening in Movie 1 at blue, yellow, and green arrows respectively. (A) At the blue arrow, conjugation happening at a distance between donor (red) and recipient (green) cells. Frames 10-17 show green puncta, the SeqA-YFP which specifically recognizes and targets hemi-methylated ssDNA. By frames 12-17 the labeled donor cell pilus can be seen to colocalize in the same region as the green puncta of the recipient cell. After frame 17 the green puncta slowly disappear which is likely the bacterial cell leaving the z-plane of view. (B) At the yellow arrow, donor cell pili are seen to attach to recipient cell and pull the recipient cell towards itself. The donor cell body is out of the z-plane and is not directly observed to be connected to the pili, however, it is evident that the recipient cell is being pulled out of the plane of view in frames 7-21. (C) At the green arrow, conjugation occurring once mating junctions have formed. Donor cell appears to form an attachment to recipient cell starting in frame 1 and transfers the ssDNA to the recipient cell in frame 10, indicated by formation of green puncta. The fluorescence appears to wane after frame 16 and is likely due to cells leaving the z-plane of view.

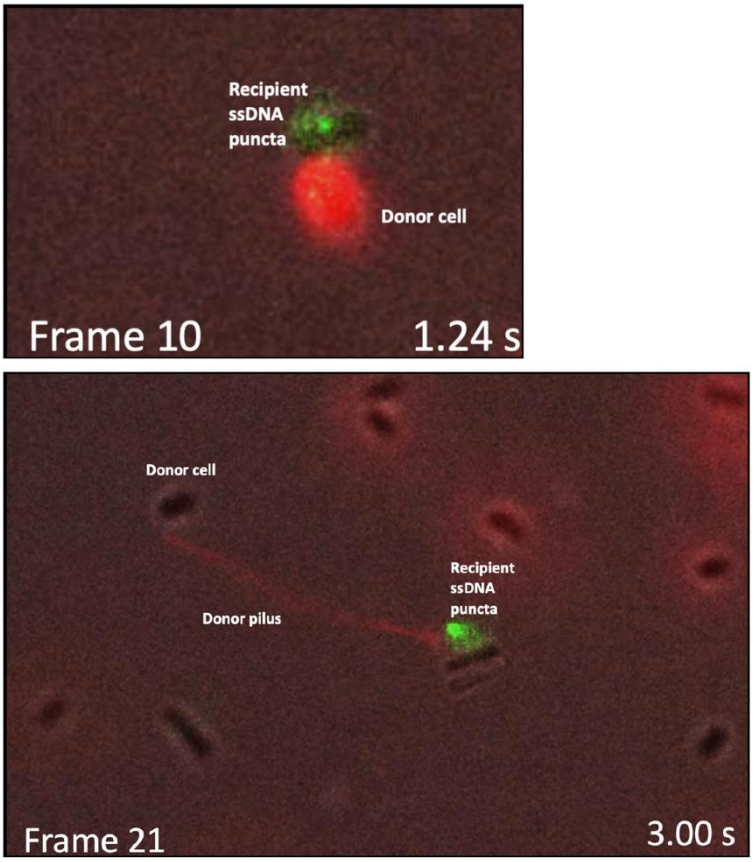

Supplemental still Movie 7. The zoomed-in field of view, black box from Supplemental Movie 6.

Link for all Movies (including Supplemental Movies)
https://journals.asm.org/doi/10.1128/mbio.02857-23

Supplemental Movie 1.
The blue arrow denotes the location for conjuga2on at a distance. A pilus is seen to attach to the recipient cell and transfer hemimethylated ssDNA recognized by seqA-YFP producing puncta (top). The yellow arrow indicates a donor cell with the appearance of two separate pili, one pilus attaches, then retracts, pulling in a recipient cell (middle). The green arrow shows conjugation between matng pairs (bottom). The scale bar is 5 μm.

Supplemental Movie 2.
A zoomed in field of view of the region of interest, blue arrow from Supplemental Movie 1, which shows conjugation happening at a distance. The donor cell pilus is seen to attach to the recipient cell and transfer hemimethylated ssDNA recognized by seqA-YFP producing puncta.

Supplemental Movie 3.
A zoomed in field of view of the region of interest, green arrow from Supplemental Movie 1, showing conjugation between two cells which appear to have formed stable mating pairs.

Supplemental Movie 4.
A zoomed in field of view of the region of interest, yellow arrow from Supplemental Movie 1, which shows the appearance of two separate pili, one pilus attaches, then retracts, pulling in a recipient cell, followed by green fluorescence colocalized to the event.

Supplemental Movie 5.
The yellow arrow marks the point where a red punctum is colocalized on a recipient cell. Frame 0:03.79 reveals a visible donor cell pulling itself toward the recipient cell. Top left yellow arrow marks a donor cell which has two separate pili which appear to be surveying the environment at frame 0:04.88. The scale bar (far right) is 5 μm and the elapsed 2me is 1 minute every 10 seconds.

Supplemental Movie 6.
This movie shows conjugation at a distance in a large field of view. The black box indicates the region of interest where conjugation events, both mating at a distance and nearby, are occurring (Supplemental Movie 7). Snapshots of these two conjugation events were taken from frames 10 and 21 which include the time in seconds the event occurs in the movie. In frame 10, the donor cell pilus is labeled by C5 maleimide dye Alexa-Fluor 568 and the cell body can be observed to fluoresce red. In frame 21, the cell body of the donor cell is not labeled, only the long pilus is, and the recipient cell body has green background fluorescence with ssDNA indicated by a green punctum.

4.7 Acknowledgements
This work was supported by NIH GM122510 (to E.H.E) and NIH U24 GM139168 (to E.R.W).

Chapter 5: Conclusions

5.1 Summary of results

While many aspects regarding the process of bacterial conjugation is fundamentally understood there are many facets that are still unclear. Our results have challenged the historic understanding on many details of conjugation. Specifically, the longstanding debate regarding the main purpose of the conjugative pilus, the events preceding DNA transfer, such as what is occurring at the conjugation junction, and identifying that archaea have DNA import apparatuses that are homologous to bacterial conjugation machinery, suggesting horizontal gene transfer via conjugation in archaea might be more similar to bacterial conjugation than previously recognized. This work uses a comprehensive approach to understand conjugation structurally and biochemically.

In our first study we uncovered new data about archaeal genetic transport mechanisms. While, there is a paucity of knowledge and understanding regarding genetic transport in archaea we

identified two, previously unknown, pili from *A. pernix and P. calidifontis* which we termed CedA1 and TedC, respectively. We used a method involving the cryoEM density, secondary structure and side-chain information, and a tool, DeepTracer-ID to determine the sequence identity of the two pili. With the sequence information we found homologs of these proteins and through genomic neighborhood analysis showed that there were genes encoding T4SS homologous proteins; highly suggestive that the DNA transfer mechanism between archaea and bacteria are very similar. The high-resolution of the two pili cryoEM maps revealed extra density unrelated to the pilin protein which we identified to be lipids. The archaeal lipid associations are unique in that they have not been shown directly before in a structure. The *P. calidifontis*, TedC, subunit associates 1:1 (pilin: lipid) with a bipolar cyclic lipid which we show to be a GDGT species. The *A. pernix*, CedA1, subunit associates 1:2 with C25-C25 diether lipids which are capped with extra density found to be phospho-dihexose group. We also challenged previous beliefs on the stability of the *A. tumefaciens* conjugation pilus. Previous hypotheses surrounding the *A. tumefaciens* pilus stability were based on the thought that the pilin subunits were cyclized, and that this folding, unique to that of the *A. tumefaciens* T-pilus and not the F-pilus, made the pilus itself more robust. Our cryoEM results show that the T-pilus has a similar fold to that of the F-pilus and F-like pilus. Subjecting the T-pilus and F-pilus to harsh physical and chemical conditions, like that of those published by Lai and Kado, revealed that the F-pilus was more resilient that the T-pilus, which was contradictory to previously published results. Our data supports that the conjugation pilus is generally very stable, and that the stability has no relation to cyclization.

We also investigated other components of the T4SS to understand more clearly what happens when the donor and recipient cells have come together to establish stable mating pairs. Our model organism, carbapenem resistant *K. pnuemoniae*, showed that the TraN protein, believed to associate with the T4SS at the outer membrane of the donor cell, interacts with outer membrane protein K36 of the recipient cell. The interactions between TraN-OmpK36 were first shown by biochemical data. Using size exclusion chromatography, the purified protein complex revealed that the stochiometric ratio of TraN: OmpK36 was 1:3. Our cryoEM data agrees with the stochiometric ratio of TraN: OmpK36. We show that the trimeric OmpK36 interacts with one TraN protein, at the beta-hairpin tip of TraN, which inserts into the lumen of one OmpK36 porins. Within the lumen the TraN beta-hairpin is stabilized by non-covalent interactions with loop 3 of OmpK36. When an insertion mutation (glycine and aspartic acid) is introduced to loop 3 it extends loop 3 further into the lumen of the porin and blocks the insertion of the TraN beta-hairpin. The inherent blocking of loop 3 results in a decrease in conjugation and overall efficiency for conjugation to occur. With this understanding we were able to propose that the pilus pulls the donor and recipient cells close by, and that the beta-hairpin of TraN

inserts into the lumen of one of the trimeric OmpK36 porins facilitating the stability needed for the duration that the genetic material is transferred from the donor to the recipient cell.

Finally, we show direct evidence that the conjugation pilus is capable of transferring ssDNA to recipient cells at long range distances. Using live cell fluorescent light microscopy (FLM) and a labeling scheme where the conjugation pilus is tagged with a maleimide dye (Alexa-Fluor 568) and a recipient cell containing a YFP labeled SeqA protein, known to recognized and bind tightly to single stranded hemi-methylated DNA, we showed that there was a distinct bright foci within the recipient cell colocalized with the pilus of the donor cell. The FLM data provided evidence to suggest that the pilin proteins reinsert back into the cell membrane of the donor cell. This is apparent as the cell body of the labeled donor cell fluoresces whereas with the cell body of the control donor, a mutant lacking the conjugation pilus, does not fluoresce with the same intensity. There does appear to be background fluorescence, however, it is possible there are exposed cysteines at the surface of the cell body that the maleimide dye is transiently binding to. These findings really challenge the notion that the pilus serves only to act as a mechanism that pulls the donor and recipient cells into close proximity, while strengthening previous data that show the lumen of the F-pilus is negatively charged which might act as a lubricant for DNA transfer. The reinsertion of the pilin into the cell membrane might also explain the advantage of having associations with phospholipids.

5.2 Impacts and future directions

Bacteria are constantly exchanging DNA, which constitutes horizonal gene transfer. While some of this occurs by a non-specific process called natural transformation, some occurs by a particular mating mechanism between a donor and a recipient cell. In specific conjugation, the mating pilus extends from the donor cell to make contact with the recipient cell, using *Escherichia coli*, we show that DNA can be transferred through the pilus between a donor and recipient cell that have not established a tight mating junction, providing new insight for the role of the conjugative pilus. In our research we show that bacterial pairs stabilize, using the TraN (OmpA homolog in *E. coli*) and TraN, to have higher rates of genetic transfer. Lastly, we discovered that the archaeal genetic transfer mechanism is similar to that of bacterial conjugation. Although archaea have not been found to cause disease in humans, they are part of the human microbiota and therefore share a symbiotic relationship to us, their host. Additionally, archaea live in other harsh conditions, i.e., high acidity, alkalinity or temperature and understanding the mechanisms that archaea employ to survive in these harsh conditions are of particular interest. Whether the process of conjugation is taking place with archaea or bacteria our discoveries challenge previous thoughts and notions of conjugation. These insights contribute towards textbook knowledge and what is taught within academic institutions.

With the rise of antibiotic resistance, the importance of identifying novel antibiotics or therapeutics cannot be overstated. A major roadblock for antibiotic research is the high production cost towards identifying potential antimicrobial agents when bacteria incline toward generating mutations towards the antimicrobial agent within a short span of time to survive thus leading to cost losses for pharmaceutical companies. A conceivable therapeutic direction is to target a process that does not require bacterial fitness and instead target the process of conjugation. If there is a way to disrupt the transfer of mobile genetic elements, plasmids, which carry antibiotic resistance genes, this could lead to lower levels of *effective* genetic transfer between bacteria. To begin considering this as a possibility a clear and complete understanding of conjugation should be understood. And while our research provides a better understanding of the conjugation process there is still plenty of room for questions which arise from our new understanding and perspectives.

Some of these questions might be whether DNA is transferred through the pilus or by other mechanisms involving the T4SS complex with exclusion of the pilus. More directly stated, what is doing the transferring once stable mating pairs have been established (is it the T4SS channel or the pilus)? It is not clear what signals, if any, are needed to convey the completion of conjugation and the removal of TraN from the lumen of the OmpK36 porin. Perhaps the non-covalent interactions between the beta-hairpin and loop 3 are weak enough that there is destabilization after a duration of time. Or possibly the mating pairs remain in close contact with each other after.

Once we established that the pilus can function as a conduit for transferring ssDNA, we wanted to know what was happening at the membrane of these mating pairs. Specifically, could we identify whether the pilus was still present once mating pairs have established; perhaps in a shorter retracted state. In 2000, researchers performed electron tomography on conjugating bacteria which formed mating pairs, a quick aside it is not clear how they differentiated between mating and non-mating cells which formed close contacts, and found that the intersectional space of both cells were very electron dense (Samuels A Lacey., *et al.,* 2000). They concluded that this denseness was caused by many localized proteins in this location. Analyzing cellular membranes can be challenging and there has not been a *highly efficient* way to probe these regions using cryo-EM due to sample thickness and lower resolution information obtained by micrographs. Further, identifying cells that are actively conjugating would require a unique approach to study the events of conjugation using cryo-EM, one can think of it as looking for a needle in a haystack.

We developed an approach to bypass sample thickness and identify mating pairs that are actively conjugating so that we could probe with specificity mating cells. The bacterial cells used in this approach are *E. coli* cells with an Alexa-Fluor 568 tag attached to the conjugative pilus via maleimide chemistry (donor) or cells which contain a SeqA-YFP gene (recipient). A 1:1 ratio of donor and recipient cells were incubated together for half an hour on Quantifoil Au 200 mesh R 2/1 (2 µm holes spaced 1 µm apart) grids, coated with 8 nm of carbon in humid conditions so that the droplet did not dry. The grids were then plunge frozen using the Leica EM GP and taken to the Thunder Imager for cryo- correlated light electron microscopy (Figure 1a). A fluorescent montage of the grid was completed to identify regions of interest, ones which show both donor and recipient cells, and correlated back to the low magnification map of the grid. Higher magnification of grid squares with potential regions of interest (ROI's) were taken (Figure 1b). If the region containing potential ROI's were less dense only tilt series were collected (Figure 1b). Once, ROI's with densely packed bacteria

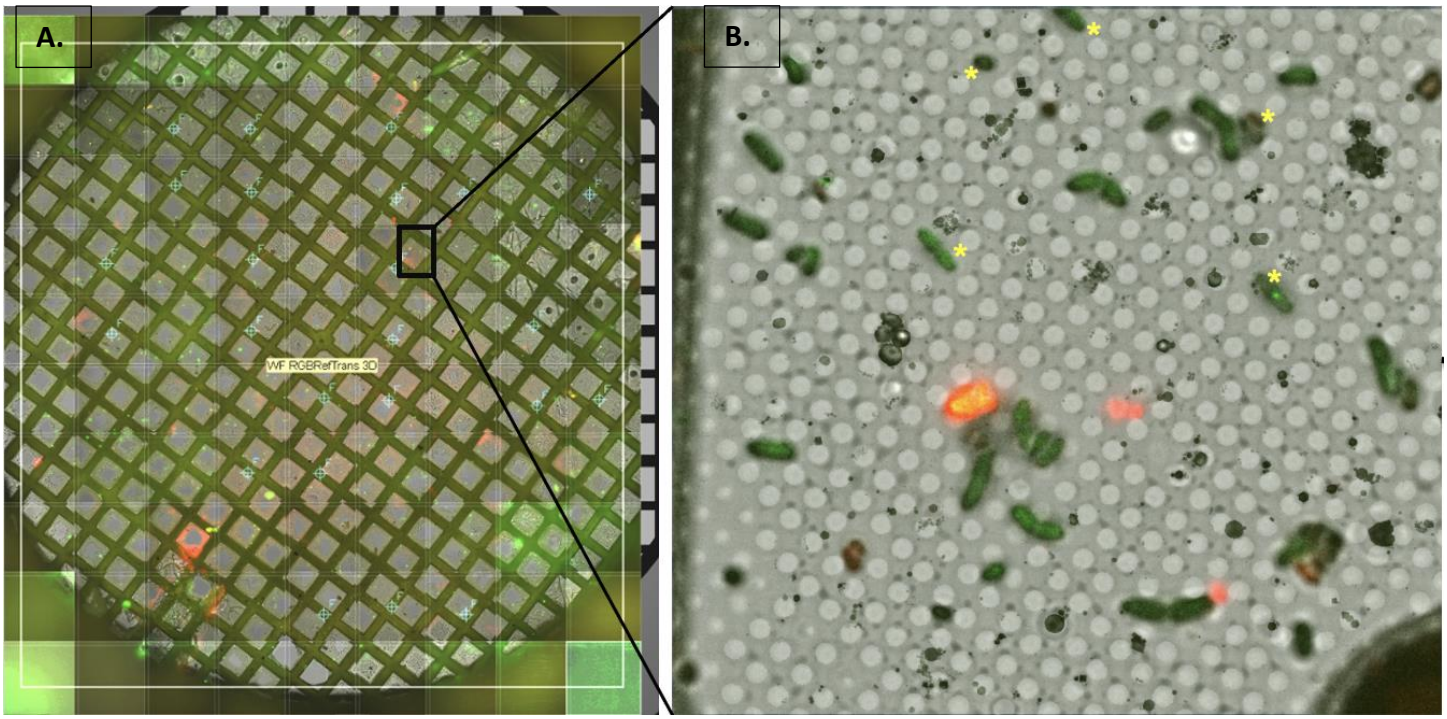

Figure 1. Correlated light electron microscopy. **(A.)** CLEM fluorescent montage overlay of the EM grid. The red signal from Alexa-Fluor 568 iindicates donor cell and brigh green signal from SeqA-YFP indicates recipient cell. The background has a greenish autoflourescent signal. The fluorescent overaly allows specific regions of interest (ROI) to be located and the location to be marked for electron microscopy. **(B.)** Specific location of RIO (A, black box) was chosen and mapped directly on the electon microscope and an image of the grid square was taken. The fluorescent signal from CLEM can be overlayed to the bacteria of the grid square.

were identified the grids were taken the Aquilos for milling. Scanning electron tomography paired with integrated fluorescent light microscopy allowed us to identify our ROIs for milling (Figure 2a&b). Due to the lower signal of the fluorescent light of the iFLM feature signals of smaller magnitude objects, like the donor pilus will be masked by the higher signal of the larger object, the recipient cell. Regardless, one can identify areas of the lamella where there are red patches indicating that there are pili (or a pilus) at these regions (Figure 2c).

About 12 lamellas were imaged on the Titan Krios and tilt series were collected (+30/-30). Tomograms were reconstructed from the tilt series using IMOD Etomo. Interestingly, all tomograms show cells which contained dense spherical-like density at the inner-, or outer, and on the periphery of the cell membrane (Figure 3 a&b). Identifiable cellular components were present, example ribosomes, however these spherical-like densities appear to be a smaller size comparatively and selective for proximity at the cell membrane. The *K. pneumoniae* OmpK36 membrane protein of recipient cells are known to trimerize at the membrane of conjugating cells, which would result in a ~120kDa complex. It is probable that the homologous membrane protein, OmpA, of *E. coli* cells also trimerize at the recipient membrane resulting in a trimer of roughly the same size allowing a protein complex large enough to visualize via the tomograms.

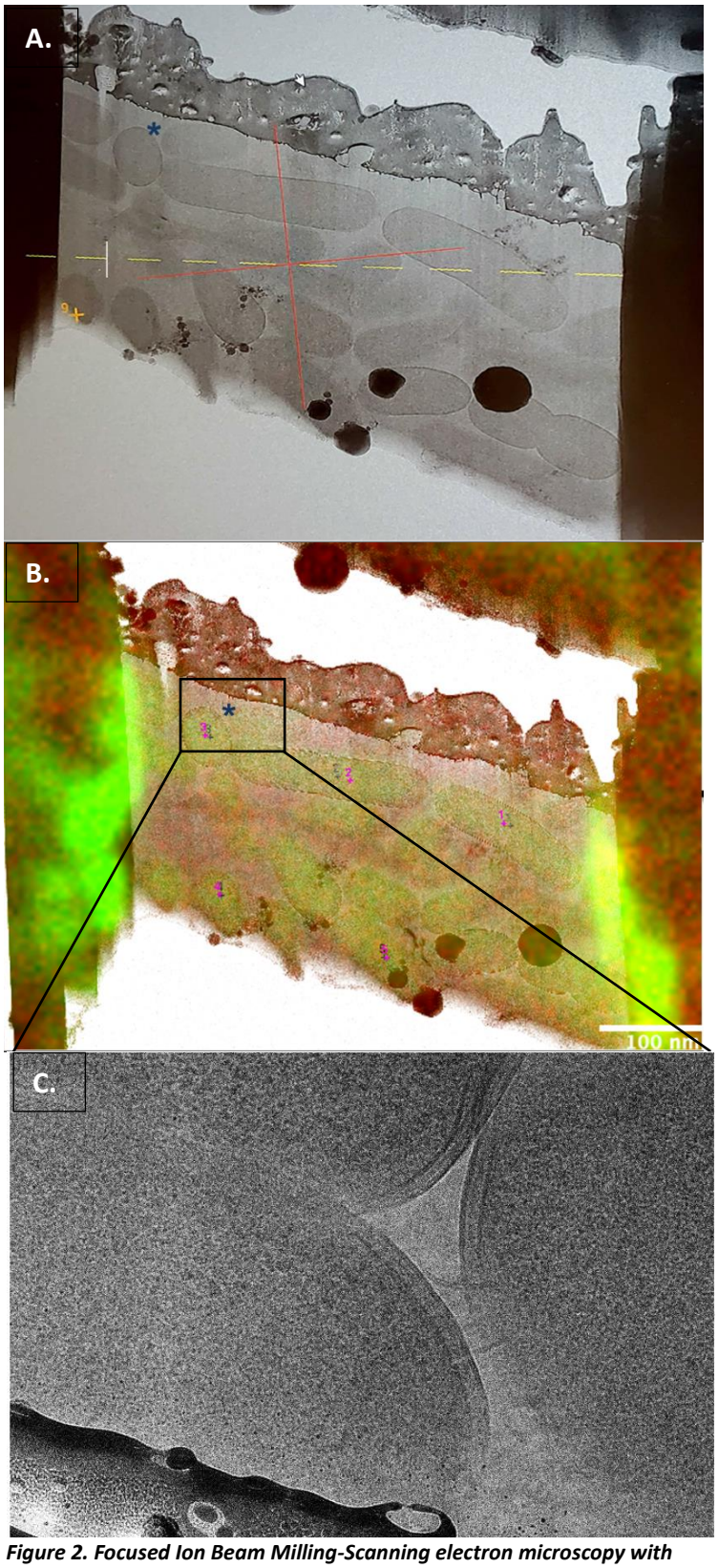

Figure 2. Focused Ion Beam Milling-Scanning electron microscopy with integrated fluorescent light microscopy. **(A.)** Scanning electron microscope image of a 200 nm thick lamella. The blue asterik indicates an ROI where tilt series were collected. **(B.)** The same lamella shown in panel A with the inclusion of the integrated fluorescent light (iFLM). The iFLM was crucial for identifying areas on the grid with ROI and for milling. **(C.)** Tilt series (at zero degrees tilt) of the ROI (blue asterisk) reveals pili at the membrane of bacterial cells.

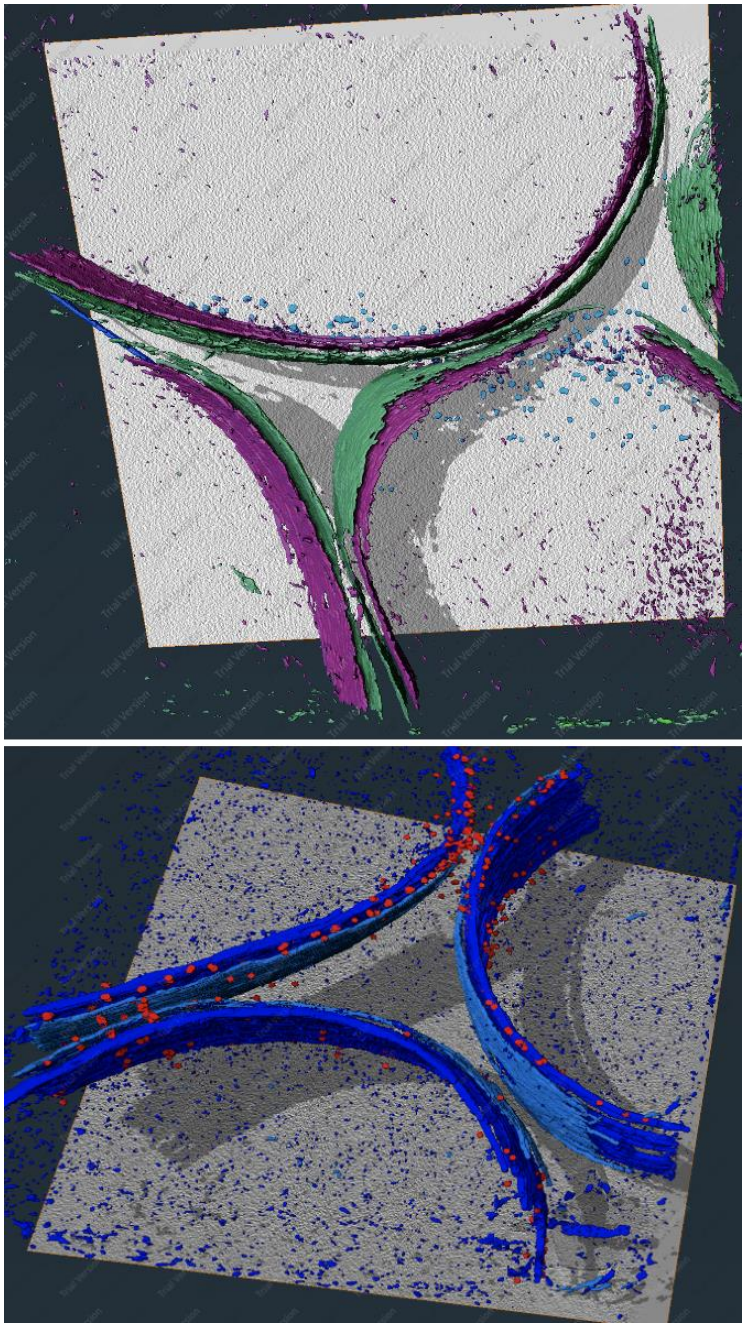

Figure 3. Segmentation of tomograms of two lamella. Inner and outer membrane of bacteria are shown (green or light blue, magenta or dark blue, respectively). Top, a lamella which shows a pilus spanning the inner/outer membrane and superficially interacting with a neighboring cell membrane. Both top and bottom lamella show spherical-like density positioned at the periphery of the inner-, intermembrane space, and outer membrane (light blue, top and red, bottom). Bottom, the spherical-like densities appear to span inner-, intermembrane space, and outer membranes to form a bridge between neighboring cells.

To confirm that the identity of these unknown spherical-like densities is OmpA subtomogram averaging together with conditional knock-downs of the recipient OmpA would need to be performed. The possibility exists that these spherical-like proteins are not OmpA, and may not be related to conjugation. Grids have been prepared which contain the following controls: (a) donor wild-type with Alexa-Fluor 568 labeled pili, (b) donor traA mutant (ΔtraA) not expressing the conjugative pilus, (c) recipient containing the gene which expresses SeqA-YFP, (d) donor ΔtraA mixed with recipient cell containing the SeqA-YFP gene. Low magnification maps of these grids have been taken to ensure high bacterial density; however, these grids have not been milled or imaged. Without the controls it is difficult to discern if these spherical-like densities are a direct correlation and effect of conjugation or completely unrelated. It is therefore suggested to take the hypothesis that these spherical-like densities are related to conjugation as an unverified claim.

The tomograms also reveal obvious filament features. When an overlay of the fluorescent signal is placed on the tomogram the low signal of the Alexa-Fluor 568 is correlated with the filament; identifying the filament as the conjugative pilus. The signal from the Seq-YFP also distinguishes which cell is the recipient cell from the donor cell. In this instance this information helps identify the cell where the pilus is seen extending from as the donor. As the bacteria were not distributed as a monolayer on the grid it is difficult from looking solely at the tomogram if a pilus is making direct contact with an opposing cell. Segmentation provides a separate

structure model for individual protein components of a cell, and if segmentation is done accurately protein contacts are visible. The pilus from one segmentation shows direct contact between the two cells (Figure 3a). The contact is superficial for one cell whereas the other cell the pilus appears in the intermembrane space of the inner and outer membrane (Figure 3a). Additionally, the spherical-like densities are observed in both of the segmentations. Interestingly, the spherical-like densities do not appear in the cell which the pilus is found extending from the intermembrane space. There are what appears to be “bridges” forming between cells which might be coming from the spherical-like density, but it is not clear that all spherical-like densities are homogenous, or the same protein, but might be different types of proteins with similar density shape. The grids containing the controls would need to be imaged and analyzed to make any conclusion that these events are related to conjugation. It is clear that these preliminary results yield interesting data which need to be examined further, but also prompt questions such as: what are these spherical-like densities?, Are they related directly to conjugation?, If we eliminate, OmpA do the spherical-like densities disappear or are they still there?, If they are still present does that indicate that the densities are heterogeneous? As observed in the segmentations the spherical-like densities appear to cluster towards the nearer polar end of the cell. Does conjugation preferably occur at the polar end of cells? If so, does cell curvature (or particular shape of the lipid at the poles) have a preferential effect?

Chapter 6: References

Chapter 2:

1 Takeuchi, N., Kaneko, K. & Koonin, E. V. Horizontal gene transfer can rescue prokaryotes from Muller's ratchet: benefit of DNA from dead cells and population subdivision. G3 (Bethesda) 4, 325-339, (2014). PMC3931566

2 Muller, H. J. The Relation of Recombination to Mutational Advance. Mutat Res 106, 2-9, (1964).

3 Lee, I. P. A., Eldakar, O. T., Gogarten, J. P. & Andam, C. P. Bacterial cooperation through horizontal gene transfer. Trends Ecol Evol 37, 223-232, (2022).

4 Thomas, C. M. & Nielsen, K. M. Mechanisms of, and barriers to, horizontal gene transfer between bacteria. Nature reviews. Microbiology 3, 711-721, (2005).

5 Gophna, U. & Altman-Price, N. Horizontal Gene Transfer in Archaea-From Mechanisms to Genome Evolution. Annu Rev Microbiol, (2022).

6 Blokesch, M. Natural competence for transformation. Curr. Biol. 26, R1126-R1130, (2016).

7 Hileman, T. H. & Santangelo, T. J. Genetics Techniques for Thermococcus kodakarensis. Front Microbiol 3, 195, (2012). PMC3370424

8 Chen, I. & Dubnau, D. DNA uptake during bacterial transformation. Nature reviews. Microbiology 2, 241-249, (2004).

9 Gill, S., Catchpole, R. & Forterre, P. Extracellular membrane vesicles in the three domains of life and beyond. FEMS Microbiol Rev 43, 273-303, (2019). PMC6524685

10 Liu, J., Cvirkaite-Krupovic, V., Commere, P. H., Yang, Y., Zhou, F., Forterre, P., Shen, Y. & Krupovic, M. Archaeal extracellular vesicles are produced in an ESCRT-dependent manner and promote gene transfer and nutrient cycling in extreme environments. ISME J 15, 2892-2905, (2021). PMC8443754

11 Erdmann, S., Tschitschko, B., Zhong, L., Raftery, M. J. & Cavicchioli, R. A plasmid from an Antarctic haloarchaeon uses specialized membrane vesicles to disseminate and infect plasmid-free cells. Nat Microbiol 2, 1446-1455, (2017).

12 Soler, N. & Forterre, P. Vesiduction: the fourth way of HGT. Environmental microbiology 22, 2457-2460, (2020).

13 Bartke, K., Garoff, L., Huseby, D. L., Brandis, G. & Hughes, D. Genetic Architecture and Fitness of Bacterial Interspecies Hybrids. Mol Biol Evol 38, 1472-1481, (2021). PMC8042766

14 Llosa, M., Gomis-Ruth, F. X., Coll, M. & de la Cruz Fd, F. Bacterial conjugation: a two-step mechanism for DNA transport. Mol Microbiol 45, 1-8, (2002).

15 Delavat, F., Miyazaki, R., Carraro, N., Pradervand, N. & van der Meer, J. R. The hidden life of integrative and conjugative elements. FEMS Microbiol Rev 41, 512-537, (2017). PMC5812530

16 Botelho, J. & Schulenburg, H. The Role of Integrative and Conjugative Elements in Antibiotic Resistance Evolution. Trends in microbiology 29, 8-18, (2021).

17 Johnson, C. M. & Grossman, A. D. Integrative and Conjugative Elements (ICEs): What They Do and How They Work. Annu Rev Genet 49, 577-601, (2015). PMC5180612

18 Coluzzi, C., Garcillan-Barcia, M. P., de la Cruz, F. & Rocha, E. P. C. Evolution of Plasmid Mobility: Origin and Fate of Conjugative and Nonconjugative Plasmids. Mol Biol Evol 39, (2022). PMC9185392

19 Cury, J., Abby, S. S., Doppelt-Azeroual, O., Neron, B. & Rocha, E. P. C. Identifying Conjugative Plasmids and Integrative Conjugative Elements with CONJscan. Methods Mol Biol 2075, 265-283, (2020).

20 Prangishvili, D., Albers, S. V., Holz, I., Arnold, H. P., Stedman, K., Klein, T., Singh, H., Hiort, J., Schweier, A., Kristjansson, J. K. & Zillig, W. Conjugation in archaea: frequent occurrence of conjugative plasmids in Sulfolobus. Plasmid 40, 190-202, (1998).

21 Medvedeva, S., Brandt, D., Cvirkaite-Krupovic, V., Liu, Y., Severinov, K., Ishino, S., Ishino, Y., Prangishvili, D., Kalinowski, J. & Krupovic, M. New insights into the diversity and evolution of the archaeal mobilome from three complete genomes of Saccharolobus shibatae. Environmental microbiology 23, 4612-4630, (2021).

22 Erauso, G., Stedman, K. M., van de Werken, H. J. G., Zillig, W. & van der Oost, J. Two novel conjugative plasmids from a single strain of Sulfolobus. Microbiology (Reading) 152, 1951-1968, (2006).

23 Greve, B., Jensen, S., Brugger, K., Zillig, W. & Garrett, R. A. Genomic comparison of archaeal conjugative plasmids from Sulfolobus. Archaea 1, 231-239, (2004). PMC2685578

24 Stedman, K. M., She, Q., Phan, H., Holz, I., Singh, H., Prangishvili, D., Garrett, R. & Zillig, W. pING family of conjugative plasmids from the extremely thermophilic archaeon Sulfolobus islandicus: insights into recombination and conjugation in Crenarchaeota. J Bacteriol 182, 7014-7020, (2000). PMC94828

25 Krupovic, M., Makarova, K. S., Wolf, Y. I., Medvedeva, S., Prangishvili, D., Forterre, P. & Koonin, E. V. Integrated mobile genetic elements in Thaumarchaeota. Environmental microbiology 21, 2056-2078, (2019). PMC6563490

26 van Wolferen, M., Wagner, A., van der Does, C. & Albers, S. V. The archaeal Ced system imports DNA. Proc. Natl. Acad. Sci. U.S.A. 113, 2496-2501, (2016). PMC4780597

27 Frols, S., White, M. F. & Schleper, C. Reactions to UV damage in the model archaeon Sulfolobus solfataricus. Biochemical Society transactions 37, 36-41, (2009).

28 van Wolferen, M., Shajahan, A., Heinrich, K., Brenzinger, S., Black, I. M., Wagner, A., Briegel, A., Azadi, P. & Albers, S. V. Species-Specific Recognition of Sulfolobales Mediated by UV-Inducible Pili and S-Layer Glycosylation Patterns. mBio 11, (2020). PMC7064770

29 Ajon, M., Frols, S., van Wolferen, M., Stoecker, K., Teichmann, D., Driessen, A. J., Grogan, D. W., Albers, S. V. & Schleper, C. UV-inducible DNA exchange in hyperthermophilic archaea mediated by type IV pili. Mol Microbiol 82, 807-817, (2011).

30 Li, Y. G. & Christie, P. J. The Agrobacterium VirB/VirD4 T4SS: Mechanism and Architecture Defined Through In Vivo Mutagenesis and Chimeric Systems. Curr Top Microbiol Immunol 418, 233-260, (2018). PMC7011205

31 Chou, L., Lin, Y. C., Haryono, M., Santos, M. N. M., Cho, S. T., Weisberg, A. J., Wu, C. F., Chang, J. H., Lai, E. M. & Kuo, C. H. Modular evolution of secretion systems and virulence plasmids in a bacterial species complex. BMC Biol 20, 16, (2022). PMC8756689

32 Costa, T. R. D., Harb, L., Khara, P., Zeng, L., Hu, B. & Christie, P. J. Type IV secretion systems: Advances in structure, function, and activation. Mol Microbiol 115, 436-452, (2021). PMC8026593

33 Li, Y. G., Hu, B. & Christie, P. J. Biological and Structural Diversity of Type IV Secretion Systems. Microbiol Spectr 7, (2019). PMC6452883

34 Eisenbrandt, R., Kalkum, M., Lai, E.-M., Lurz, R., Kado, C. I. & Lanka, E. Conjugative Pili of IncP Plasmids, and the Ti Plasmid T Pilus Are Composed of Cyclic Subunits*. Journal of Biological Chemistry 274, 22548-22555, (1999).

35 Lai, E.-M. & Kado, C. I. The T-pilus of Agrobacterium tumefaciens. Trends Microbiol 8, 361-369, (2000).

36 Lai, E.-M. & Kado, C. I. The Agrobacterium tumefaciens T pilus composed of cyclic T pilin is highly resilient to extreme environments. FEMS Microbiology Letters 210, 111-114, (2002).

37 Sako, Y., Nomura, N., Uchida, A., Ishida, Y., Morii, H., Koga, Y., Hoaki, T. & Maruyama, T. Aeropyrum pernix gen. nov., sp. nov., a novel aerobic hyperthermophilic archaeon growing at temperatures up to 100 degrees C. Int J Syst Bacteriol 46, 1070-1077, (1996).

38 Chang, L., Wang, F., Connolly, K., Meng, H., Su, Z., Cvirkaite-Krupovic, V., Krupovic, M., Egelman, E. H. & Si, D. DeepTracer-ID: De novo protein identification from cryo-EM maps. Biophys. J. 121, 2840-2848, (2022).

39 Amo, T., Paje, M. L., Inagaki, A., Ezaki, S., Atomi, H. & Imanaka, T. Pyrobaculum calidifontis sp. nov., a novel hyperthermophilic archaeon that grows in atmospheric air. Archaea 1, 113-121, (2002). PMC2685560

40 Wang, F., Cvirkaite-Krupovic, V., Krupovic, M. & Egelman, E. H. Archaeal bundling pili of Pyrobaculum calidifontis reveal similarities between archaeal and bacterial biofilms. Proc. Natl. Acad. Sci. U.S.A. 119, e2207037119, (2022).

41 Chang, L., Wang, F., Connolly, K., Meng, H., Su, Z., Cvirkaite-Krupovic, V., Krupovic, M., Egelman, E. H. & Si, D. DeepTracer-ID: De novo protein identification from cryo-EM maps. Biophysical Journal 121, 2840-2848, (2022).

42 Almagro Armenteros, J. J., Tsirigos, K. D., Sonderby, C. K., Petersen, T. N., Winther, O., Brunak, S., von Heijne, G. & Nielsen, H. SignalP 5.0 improves signal peptide predictions using deep neural networks. Nat Biotechnol 37, 420-423, (2019).

43 Huang, Q., Liu, L., Liu, J., Ni, J., She, Q. & Shen, Y. Efficient 5'-3' DNA end resection by HerA and NurA is essential for cell viability in the crenarchaeon Sulfolobus islandicus. BMC Mol Biol 16, 2, (2015). PMC4351679

44 Constantinesco, F., Forterre, P., Koonin, E. V., Aravind, L. & Elie, C. A bipolar DNA helicase gene, herA, clusters with rad50, mre11 and nurA genes in thermophilic archaea. Nucleic Acids Res 32, 1439-1447, (2004). PMC390275

45 Atmakuri, K., Cascales, E., Burton, O. T., Banta, L. M. & Christie, P. J. Agrobacterium ParA/MinD-like VirC1 spatially coordinates early conjugative DNA transfer reactions. EMBO J 26, 2540-2551, (2007). PMC1868908

46 Costa, T. R. D., Ilangovan, A., Ukleja, M., Redzej, A., Santini, J. M., Smith, T. K., Egelman, E. H. & Waksman, G. Structure of the Bacterial Sex F Pilus Reveals an Assembly of a Stoichiometric Protein-Phospholipid Complex. Cell 166, 1436-1444.e1410, (2016).

47 Zheng, W., Pena, A., Low, W. W., Wong, J. L. C., Frankel, G. & Egelman, E. H. Cryoelectron-Microscopic Structure of the pKpQIL Conjugative Pili from Carbapenem-Resistant Klebsiella pneumoniae. Structure 28, 1321-1328 e1322, (2020). PMC7710920

48 De Rosa, M., Gambacorta, A. & Gliozzi, A. Structure, biosynthesis, and physicochemical properties of archaebacterial lipids. Microbiol Rev 50, 70-80, (1986). PMC373054

49 Rensen, E. I., Mochizuki, T., Quemin, E., Schouten, S., Krupovic, M. & Prangishvili, D. A virus of hyperthermophilic archaea with a unique architecture among DNA viruses. Proc. Natl. Acad. Sci. U.S.A. 113, 2478-2483, (2016). PMC4780613

50 Yoshida, R., Yoshimura, T. & Hemmi, H. Biosynthetic machinery for C25,C25-diether archaeal lipids from the hyperthermophilic archaeon Aeropyrum pernix. Biochemical and Biophysical Research Communications 497, 87-92, (2018).

51 Wang, F., Cvirkaite-Krupovic, V., Kreutzberger, M. A. B., Su, Z., de Oliveira, G. A. P., Osinski, T., Sherman, N., DiMaio, F., Wall, J. S., Prangishvili, D., Krupovic, M. & Egelman, E. H. An extensively glycosylated archaeal pilus survives extreme conditions. Nat Microbiol 4, 1401-1410, (2019). PMC6656605

52 Amro, J., Black, C., Jemouai, Z., Rooney, N., Daneault, C., Zeytuni, N., Ruiz, M., Bui, K. H. & Baron, C. Cryo-EM structure of the Agrobacterium tumefaciens T-pilus reveals the importance of positive charges in the lumen. bioRxiv, 2022.2004.2028.489814, (2022).

53 Kreida, S., Narita, A., Johnson, M. D., Tocheva, E. I., Das, A., Ghosal, D. & Jensen, G. J. Cryo-EM structure of the Agrobacterium tumefaciens type IV secretion system-associated T-pilus reveals stoichiometric protein-phospholipid assembly. bioRxiv, 2022.2009.2025.509369, (2022).

54 Abu-Arish, A., Frenkiel-Krispin, D., Fricke, T., Tzfira, T., Citovsky, V., Wolf, S. G. & Elbaum, M. Three-dimensional reconstruction of Agrobacterium VirE2 protein with single-stranded DNA. Journal of Biological Chemistry 279, 25359-25363, (2004).

55 Winans, S. C., Burns, D. L. & Christie, P. J. Adaptation of a conjugal transfer system for the export of pathogenic macromolecules. Trends in microbiology 4, 64-68, (1996). PMC4848025

56 Jones, A. L., Lai, E. M., Shirasu, K. & Kado, C. I. VirB2 is a processed pilin-like protein encoded by the Agrobacterium tumefaciens Ti plasmid. J Bacteriol 178, 5706-5711, (1996). PMC178410

57 Holm, L. & Rosenstrom, P. Dali server: conservation mapping in 3D. Nucleic Acids Res 38, W545-549, (2010). PMC2896194

58 Wang, F., Mustafa, K., Suciu, V., Joshi, K., Chan, C. H., Choi, S., Su, Z., Si, D., Hochbaum, A. I., Egelman, E. H. & Bond, D. R. Cryo-EM structure of an extracellular Geobacter OmcE cytochrome filament reveals tetrahaem packing. Nat Microbiol 7, 1291-1300, (2022). PMC9357133

59 Heng, J. B., Aksimentiev, A., Ho, C., Marks, P., Grinkova, Y. V., Sligar, S., Schulten, K. & Timp, G. The electromechanics of DNA in a synthetic nanopore. Biophys. J. 90, 1098-1106, (2006). PMC1367096

60 Wang, F., Cvirkaite-Krupovic, V., Vos, M., Beltran, L. C., Kreutzberger, M. A. B., Winter, J. M., Su, Z., Liu, J., Schouten, S., Krupovic, M. & Egelman, E. H. Spindle-shaped archaeal viruses evolved from rod-shaped ancestors to package a larger genome. Cell 185, 1297-1307 e1211, (2022). PMC9018610

61 Wollman, E. L., Jacob, F. & Hayes, W. Conjugation and genetic recombination in Escherichia coli K-12. Cold Spring Harb Symp Quant Biol 21, 141-162, (1956).

62 Derbyshire, K. M. & Gray, T. A. Distributive Conjugal Transfer: New Insights into Horizontal Gene Transfer and Genetic Exchange in Mycobacteria. Microbiol Spectr 2, (2014). PMC4259119

63 Coros, A., Callahan, B., Battaglioli, E. & Derbyshire, K. M. The specialized secretory apparatus ESX-1 is essential for DNA transfer in Mycobacterium smegmatis. Mol Microbiol 69, 794-808, (2008). PMC2562793

64 Babić, A., Lindner, A. B., Vulić, M., Stewart, E. J. & Radman, M. Direct Visualization of Horizontal Gene Transfer. Science 319, 1533, (2008).

65 Low, H. H., Gubellini, F., Rivera-Calzada, A., Braun, N., Connery, S., Dujeancourt, A., Lu, F., Redzej, A., Fronzes, R., Orlova, E. V. & Waksman, G. Structure of a type IV secretion system. Nature 508, 550-553, (2014).

66 Liu, X., Khara, P., Baker, M. L., Christie, P. J. & Hu, B. Structure of a type IV secretion system core complex encoded by multi-drug resistance F plasmids. Nature Communications 13, 379, (2022).

67 Christie, P. J., Atmakuri, K., Krishnamoorthy, V., Jakubowski, S. & Cascales, E. Biogenesis, architecture, and function of bacterial type IV secretion systems. Annu Rev Microbiol 59, 451-485, (2005). PMC3872966

68 Moncalián, G., Cabezón, E., Alkorta, I., Valle, M., Moro, F., Valpuesta, J. M. a., Goñi, F. M. & de la Cruz, F. Characterization of ATP and DNA Binding Activities of TrwB, the Coupling Protein Essential in Plasmid R388 Conjugation*. Journal of Biological Chemistry 274, 36117-36124, (1999).

69 Hopkins, B. B. & Paull, T. T. The P. furiosus mre11/rad50 complex promotes 5' strand resection at a DNA double-strand break. Cell 135, 250-260, (2008). PMC2581932

70 Blackwood, J. K., Rzechorzek, N. J., Abrams, A. S., Maman, J. D., Pellegrini, L. & Robinson, N. P. Structural and functional insights into DNA-end processing by the archaeal HerA helicase-NurA nuclease complex. Nucleic Acids Res 40, 3183-3196, (2012). PMC3326311

71 De Falco, M., Catalano, F., Rossi, M., Ciaramella, M. & De Felice, M. NurA Is Endowed with Endo- and Exonuclease Activities that Are Modulated by HerA: New Insight into Their Role in DNA-End Processing. PloS one 10, e0142345, (2015). PMC4641729

72 Feng, X., Sun, M., Han, W., Liang, Y. X. & She, Q. A transcriptional factor B paralog functions as an activator to DNA damage-responsive expression in archaea. Nucleic Acids Res 46, 7085-7096, (2018). PMC6101594

73 Koonin, E. V., Makarova, K. S., Wolf, Y. I. & Krupovic, M. Evolutionary entanglement of mobile genetic elements and host defence systems: guns for hire. Nat Rev Genet 21, 119-131, (2020).

74 Lai, E. M. & Kado, C. I. Processed VirB2 is the major subunit of the promiscuous pilus of Agrobacterium tumefaciens. J Bacteriol 180, 2711-2717, (1998). PMC107224

75 Punjani, A., Rubinstein, J. L., Fleet, D. J. & Brubaker, M. A. cryoSPARC: algorithms for rapid unsupervised cryo-EM structure determination. Nature Methods 14, 290-296, (2017).

76 Zhang, K. Gctf: Real-time CTF determination and correction. Journal of Structural Biology 193, 1-12, (2016).

77 Jumper, J., Evans, R., Pritzel, A., Green, T., Figurnov, M., Ronneberger, O., Tunyasuvunakool, K., Bates, R., Žídek, A., Potapenko, A., Bridgland, A., Meyer, C., Kohl, S. A. A., Ballard, A. J., Cowie, A., Romera-Paredes, B., Nikolov, S., Jain, R., Adler, J., Back, T., Petersen, S., Reiman, D., Clancy, E., Zielinski, M., Steinegger, M., Pacholska, M., Berghammer, T., Bodenstein, S., Silver, D., Vinyals, O., Senior, A. W., Kavukcuoglu, K., Kohli, P. & Hassabis, D. Highly accurate protein structure prediction with AlphaFold. Nature 596, 583-589, (2021).

78 Emsley, P., Lohkamp, B., Scott, W. G. & Cowtan, K. Features and development of Coot. Acta crystallographica. Section D, Biological crystallography 66, 486-501, (2010). 2852313

79 Pettersen, E. F., Goddard, T. D., Huang, C. C., Couch, G. S., Greenblatt, D. M., Meng, E. C. & Ferrin, T. E. UCSF Chimera--a visualization system for exploratory research and analysis. J Comput Chem 25, 1605-1612, (2004).

80 Adams, P. D., Afonine, P. V., Bunkoczi, G., Chen, V. B., Davis, I. W., Echols, N., Headd, J. J., Hung, L. W., Kapral, G. J., Grosse-Kunstleve, R. W., McCoy, A. J., Moriarty, N. W., Oeffner, R., Read, R. J., Richardson, D. C., Richardson, J. S., Terwilliger, T. C. & Zwart, P. H. PHENIX: a comprehensive Python-based system for macromolecular structure solution. Acta crystallographica. Section D, Biological crystallography 66, 213-221, (2010). PMC2815670

81 Chen, V. B., Arendall, W. B., 3rd, Headd, J. J., Keedy, D. A., Immormino, R. M., Kapral, G. J., Murray, L. W., Richardson, J. S. & Richardson, D. C. MolProbity: all-atom structure validation for macromolecular crystallography. Acta crystallographica. Section D, Biological crystallography 66, 12-21, (2010). PMC2803126

82 Pei, J. & Grishin, N. V. PROMALS3D: multiple protein sequence alignment enhanced with evolutionary and three-dimensional structural information. Methods Mol Biol 1079, 263-271, (2014). PMC4506754

83 Zallot, R., Oberg, N. & Gerlt, J. A. The EFI Web Resource for Genomic Enzymology Tools: Leveraging Protein, Genome, and Metagenome Databases to Discover Novel Enzymes and Metabolic Pathways. Biochemistry 58, 4169-4182, (2019). PMC7057060

84 Steinegger, M., Meier, M., Mirdita, M., Vohringer, H., Haunsberger, S. J. & Soding, J. HH-suite3 for fast remote homology detection and deep protein annotation. BMC Bioinformatics 20, 473, (2019). PMC6744700

85 Gabler, F., Nam, S. Z., Till, S., Mirdita, M., Steinegger, M., Soding, J., Lupas, A. N. & Alva, V. Protein Sequence Analysis Using the MPI Bioinformatics Toolkit. Curr Protoc Bioinformatics 72, e108, (2020).

86 Bale, N. J., Sorokin, D. Y., Hopmans, E. C., Koenen, M., Rijpstra, W. I. C., Villanueva, L., Wienk, H. & Sinninghe Damsté, J. S. New insights into the polar lipid composition of extremely halo (alkali) philic euryarchaea from hypersaline lakes. Frontiers in microbiology 10, 377, (2019).

87 Sampaio, J. L., Gerl, M. J., Klose, C., Ejsing, C. S., Beug, H., Simons, K. & Shevchenko, A. Membrane lipidome of an epithelial cell line. Proc. Natl. Acad. Sci. U.S.A. 108, 1903-1907, (2011). PMC3033259

88 Ejsing, C. S., Sampaio, J. L., Surendranath, V., Duchoslav, E., Ekroos, K., Klemm, R. W., Simons, K. & Shevchenko, A. Global analysis of the yeast lipidome by quantitative shotgun mass spectrometry. Proc. Natl. Acad. Sci. U.S.A. 106, 2136-2141, (2009). PMC2650121

89 Gerl, M. J., Sampaio, J. L., Urban, S., Kalvodova, L., Verbavatz, J. M., Binnington, B., Lindemann, D., Lingwood, C. A., Shevchenko, A., Schroeder, C. & Simons, K. Quantitative analysis of the lipidomes of the influenza virus envelope and MDCK cell apical membrane. The Journal of cell biology 196, 213-221, (2012). PMC3265945

90 Surma, M. A., Herzog, R., Vasilj, A., Klose, C., Christinat, N., Morin-Rivron, D., Simons, K., Masoodi, M. & Sampaio, J. L. An automated shotgun lipidomics platform for high throughput, comprehensive, and quantitative analysis of blood plasma intact lipids. Eur J Lipid Sci Technol 117, 1540-1549, (2015). PMC4606567

91 Levental, K. R., Surma, M. A., Skinkle, A. D., Lorent, J. H., Zhou, Y., Klose, C., Chang, J. T., Hancock, J. F. & Levental, I. omega-3 polyunsaturated fatty acids direct differentiation of the membrane phenotype in mesenchymal stem cells to potentiate osteogenesis. Sci Adv 3, eaao1193, (2017). PMC5677358

92 Herzog, R., Schuhmann, K., Schwudke, D., Sampaio, J. L., Bornstein, S. R., Schroeder, M. & Shevchenko, A. LipidXplorer: a software for consensual cross-platform lipidomics. PloS one 7, e29851, (2012). PMC3260173

Chapter 3:

Chapter 4:

1. E. Alvarez-Martinez Cristina, J. Christie Peter, Biological Diversity of Prokaryotic Type IV Secretion Systems. *Microbiology and Molecular Biology Reviews* **73**, 775-808 (2009).
2. J. B. Patkowski *et al.*, The F-pilus biomechanical adaptability accelerates conjugative dissemination of antimicrobial resistance and biofilm formation. *Nature Communications* **14**, 1879 (2023).
3. N. Takeuchi, K. Kaneko, E. V. Koonin, Horizontal gene transfer can rescue prokaryotes from Muller's ratchet: benefit of DNA from dead cells and population subdivision. *G3 (Bethesda)* **4**, 325-339 (2014).
4. H. J. Muller, The Relation of Recombination to Mutational Advance. *Mutat Res* **106**, 2-9 (1964).
5. I. P. A. Lee, O. T. Eldakar, J. P. Gogarten, C. P. Andam, Bacterial cooperation through horizontal gene transfer. *Trends Ecol Evol* **37**, 223-232 (2022).
6. C. M. Thomas, K. M. Nielsen, Mechanisms of, and barriers to, horizontal gene transfer between bacteria. *Nature reviews. Microbiology* **3**, 711-721 (2005).
7. U. Gophna, N. Altman-Price, Horizontal Gene Transfer in Archaea-From Mechanisms to Genome Evolution. *Annu Rev Microbiol* 10.1146/annurev-micro-040820-124627 (2022).
8. M. Blokesch, Natural competence for transformation. *Curr. Biol.* **26**, R1126-R1130 (2016).
9. T. H. Hileman, T. J. Santangelo, Genetics Techniques for Thermococcus kodakarensis. *Front Microbiol* **3**, 195 (2012).
10. I. Chen, D. Dubnau, DNA uptake during bacterial transformation. *Nature reviews. Microbiology* **2**, 241-249 (2004).
11. S. Gill, R. Catchpole, P. Forterre, Extracellular membrane vesicles in the three domains of life and beyond. *FEMS Microbiol Rev* **43**, 273-303 (2019).

12. J. Liu *et al.*, Archaeal extracellular vesicles are produced in an ESCRT-dependent manner and promote gene transfer and nutrient cycling in extreme environments. *ISME J* **15**, 2892-2905 (2021).
13. S. Erdmann, B. Tschitschko, L. Zhong, M. J. Raftery, R. Cavicchioli, A plasmid from an Antarctic haloarchaeon uses specialized membrane vesicles to disseminate and infect plasmid-free cells. *Nat Microbiol* **2**, 1446-1455 (2017).
14. N. Soler, P. Forterre, Vesiduction: the fourth way of HGT. *Environmental microbiology* **22**, 2457-2460 (2020).
15. K. Bartke, L. Garoff, D. L. Huseby, G. Brandis, D. Hughes, Genetic Architecture and Fitness of Bacterial Interspecies Hybrids. *Mol Biol Evol* **38**, 1472-1481 (2021).
16. M. Llosa, F. X. Gomis-Ruth, M. Coll, F. de la Cruz Fd, Bacterial conjugation: a two-step mechanism for DNA transport. *Mol Microbiol* **45**, 1-8 (2002).
17. F. Delavat, R. Miyazaki, N. Carraro, N. Pradervand, J. R. van der Meer, The hidden life of integrative and conjugative elements. *FEMS Microbiol Rev* **41**, 512-537 (2017).
18. J. Botelho, H. Schulenburg, The Role of Integrative and Conjugative Elements in Antibiotic Resistance Evolution. *Trends in microbiology* **29**, 8-18 (2021).
19. C. M. Johnson, A. D. Grossman, Integrative and Conjugative Elements (ICEs): What They Do and How They Work. *Annu Rev Genet* **49**, 577-601 (2015).
20. C. Coluzzi, M. P. Garcillan-Barcia, F. de la Cruz, E. P. C. Rocha, Evolution of Plasmid Mobility: Origin and Fate of Conjugative and Nonconjugative Plasmids. *Mol Biol Evol* **39** (2022).
21. J. Cury, S. S. Abby, O. Doppelt-Azeroual, B. Neron, E. P. C. Rocha, Identifying Conjugative Plasmids and Integrative Conjugative Elements with CONJscan. *Methods Mol Biol* **2075**, 265-283 (2020).
22. D. Prangishvili *et al.*, Conjugation in archaea: frequent occurrence of conjugative plasmids in Sulfolobus. *Plasmid* **40**, 190-202 (1998).
23. S. Medvedeva *et al.*, New insights into the diversity and evolution of the archaeal mobilome from three complete genomes of Saccharolobus shibatae. *Environmental microbiology* **23**, 4612-4630 (2021).
24. G. Erauso, K. M. Stedman, H. J. G. van de Werken, W. Zillig, J. van der Oost, Two novel conjugative plasmids from a single strain of Sulfolobus. *Microbiology (Reading)* **152**, 1951-1968 (2006).
25. B. Greve, S. Jensen, K. Brugger, W. Zillig, R. A. Garrett, Genomic comparison of archaeal conjugative plasmids from Sulfolobus. *Archaea* **1**, 231-239 (2004).
26. K. M. Stedman *et al.*, pING family of conjugative plasmids from the extremely thermophilic archaeon Sulfolobus islandicus: insights into recombination and conjugation in Crenarchaeota. *J Bacteriol* **182**, 7014-7020 (2000).
27. M. Krupovic *et al.*, Integrated mobile genetic elements in Thaumarchaeota. *Environmental microbiology* **21**, 2056-2078 (2019).
28. M. van Wolferen, A. Wagner, C. van der Does, S. V. Albers, The archaeal Ced system imports DNA. *Proc. Natl. Acad. Sci. U.S.A.* **113**, 2496-2501 (2016).
29. S. Frols, M. F. White, C. Schleper, Reactions to UV damage in the model archaeon Sulfolobus solfataricus. *Biochemical Society transactions* **37**, 36-41 (2009).
30. M. van Wolferen *et al.*, Species-Specific Recognition of Sulfolobales Mediated by UV-Inducible Pili and S-Layer Glycosylation Patterns. *mBio* **11** (2020).
31. M. Ajon *et al.*, UV-inducible DNA exchange in hyperthermophilic archaea mediated by type IV pili. *Mol Microbiol* **82**, 807-817 (2011).
32. Y. G. Li, P. J. Christie, The Agrobacterium VirB/VirD4 T4SS: Mechanism and Architecture Defined Through In Vivo Mutagenesis and Chimeric Systems. *Curr Top Microbiol Immunol* **418**, 233-260 (2018).
33. L. Chou *et al.*, Modular evolution of secretion systems and virulence plasmids in a bacterial species complex. *BMC Biol* **20**, 16 (2022).
34. T. R. D. Costa *et al.*, Type IV secretion systems: Advances in structure, function, and activation. *Mol Microbiol* **115**, 436-452 (2021).

35. Y. G. Li, B. Hu, P. J. Christie, Biological and Structural Diversity of Type IV Secretion Systems. *Microbiol Spectr* **7** (2019).
36. R. Eisenbrandt *et al.*, Conjugative Pili of IncP Plasmids, and the Ti Plasmid T Pilus Are Composed of Cyclic Subunits*. *Journal of Biological Chemistry* **274**, 22548-22555 (1999).
37. E.-M. Lai, C. I. Kado, The T-pilus of Agrobacterium tumefaciens. *Trends Microbiol* **8**, 361-369 (2000).
38. E.-M. Lai, C. I. Kado, The Agrobacterium tumefaciens T pilus composed of cyclic T pilin is highly resilient to extreme environments. *FEMS Microbiology Letters* **210**, 111-114 (2002).
39. Y. Sako *et al.*, Aeropyrum pernix gen. nov., sp. nov., a novel aerobic hyperthermophilic archaeon growing at temperatures up to 100 degrees C. *Int J Syst Bacteriol* **46**, 1070-1077 (1996).
40. L. Chang *et al.*, DeepTracer-ID: De novo protein identification from cryo-EM maps. *Biophys J* **121**, 2840-2848 (2022).
41. T. Amo *et al.*, Pyrobaculum calidifontis sp. nov., a novel hyperthermophilic archaeon that grows in atmospheric air. *Archaea* **1**, 113-121 (2002).
42. F. Wang, V. Cvirkaite-Krupovic, M. Krupovic, E. H. Egelman, Archaeal bundling pili of Pyrobaculum calidifontis reveal similarities between archaeal and bacterial biofilms. *Proc. Natl. Acad. Sci. U.S.A.* **119**, e2207037119 (2022).
43. L. Chang *et al.*, DeepTracer-ID: De novo protein identification from cryo-EM maps. *Biophysical Journal* **121**, 2840-2848 (2022).
44. J. J. Almagro Armenteros *et al.*, SignalP 5.0 improves signal peptide predictions using deep neural networks. *Nat Biotechnol* **37**, 420-423 (2019).
45. Q. Huang *et al.*, Efficient 5'-3' DNA end resection by HerA and NurA is essential for cell viability in the crenarchaeon Sulfolobus islandicus. *BMC Mol Biol* **16**, 2 (2015).
46. F. Constantinesco, P. Forterre, E. V. Koonin, L. Aravind, C. Elie, A bipolar DNA helicase gene, herA, clusters with rad50, mre11 and nurA genes in thermophilic archaea. *Nucleic Acids Res* **32**, 1439-1447 (2004).
47. K. Atmakuri, E. Cascales, O. T. Burton, L. M. Banta, P. J. Christie, Agrobacterium ParA/MinD-like VirC1 spatially coordinates early conjugative DNA transfer reactions. *EMBO J* **26**, 2540-2551 (2007).
48. T. R. D. Costa *et al.*, Structure of the Bacterial Sex F Pilus Reveals an Assembly of a Stoichiometric Protein-Phospholipid Complex. *Cell* **166**, 1436-1444.e1410 (2016).
49. W. Zheng *et al.*, Cryoelectron-Microscopic Structure of the pKpQIL Conjugative Pili from Carbapenem-Resistant *Klebsiella pneumoniae*. *Structure* **28**, 1321-1328 e1322 (2020).
50. M. De Rosa, A. Gambacorta, A. Gliozzi, Structure, biosynthesis, and physicochemical properties of archaebacterial lipids. *Microbiol Rev* **50**, 70-80 (1986).
51. E. I. Rensen *et al.*, A virus of hyperthermophilic archaea with a unique architecture among DNA viruses. *Proc. Natl. Acad. Sci. U.S.A.* **113**, 2478-2483 (2016).
52. R. Yoshida, T. Yoshimura, H. Hemmi, Biosynthetic machinery for C25,C25-diether archaeal lipids from the hyperthermophilic archaeon Aeropyrum pernix. *Biochemical and Biophysical Research Communications* **497**, 87-92 (2018).
53. J. Amro *et al.*, Cryo-EM structure of the Agrobacterium tumefaciens T-pilus reveals the importance of positive charges in the lumen. *bioRxiv* 10.1101/2022.04.28.489814, 2022.2004.2028.489814 (2022).
54. S. Kreida *et al.*, Cryo-EM structure of the Agrobacterium tumefaciens type IV secretion system-associated T-pilus reveals stoichiometric protein-phospholipid assembly. *bioRxiv* 10.1101/2022.09.25.509369, 2022.2009.2025.509369 (2022).
55. A. Abu-Arish *et al.*, Three-dimensional reconstruction of Agrobacterium VirE2 protein with single-stranded DNA. *Journal of Biological Chemistry* **279**, 25359-25363 (2004).
56. S. C. Winans, D. L. Burns, P. J. Christie, Adaptation of a conjugal transfer system for the export of pathogenic macromolecules. *Trends in microbiology* **4**, 64-68 (1996).

57. A. L. Jones, E. M. Lai, K. Shirasu, C. I. Kado, VirB2 is a processed pilin-like protein encoded by the Agrobacterium tumefaciens Ti plasmid. *J Bacteriol* **178**, 5706-5711 (1996).
58. F. Wang *et al.*, An extensively glycosylated archaeal pilus survives extreme conditions. *Nat Microbiol* **4**, 1401-1410 (2019).
59. L. Holm, P. Rosenstrom, Dali server: conservation mapping in 3D. *Nucleic Acids Res* **38**, W545-549 (2010).
60. F. Wang *et al.*, Cryo-EM structure of an extracellular Geobacter OmcE cytochrome filament reveals tetrahaem packing. *Nat Microbiol* **7**, 1291-1300 (2022).
61. J. B. Heng *et al.*, The electromechanics of DNA in a synthetic nanopore. *Biophys. J.* **90**, 1098-1106 (2006).
62. F. Wang *et al.*, Spindle-shaped archaeal viruses evolved from rod-shaped ancestors to package a larger genome. *Cell* **185**, 1297-1307 e1211 (2022).
63. E. L. Wollman, F. Jacob, W. Hayes, Conjugation and genetic recombination in Escherichia coli K-12. *Cold Spring Harb Symp Quant Biol* **21**, 141-162 (1956).
64. K. M. Derbyshire, T. A. Gray, Distributive Conjugal Transfer: New Insights into Horizontal Gene Transfer and Genetic Exchange in Mycobacteria. *Microbiol Spectr* **2** (2014).
65. A. Coros, B. Callahan, E. Battaglioli, K. M. Derbyshire, The specialized secretory apparatus ESX-1 is essential for DNA transfer in Mycobacterium smegmatis. *Mol Microbiol* **69**, 794-808 (2008).
66. A. Babić, A. B. Lindner, M. Vulić, E. J. Stewart, M. Radman, Direct Visualization of Horizontal Gene Transfer. *Science* **319**, 1533 (2008).
67. H. H. Low *et al.*, Structure of a type IV secretion system. *Nature* **508**, 550-553 (2014).
68. X. Liu, P. Khara, M. L. Baker, P. J. Christie, B. Hu, Structure of a type IV secretion system core complex encoded by multi-drug resistance F plasmids. *Nature Communications* **13**, 379 (2022).
69. P. J. Christie, K. Atmakuri, V. Krishnamoorthy, S. Jakubowski, E. Cascales, Biogenesis, architecture, and function of bacterial type IV secretion systems. *Annu Rev Microbiol* **59**, 451-485 (2005).
70. G. Moncalián *et al.*, Characterization of ATP and DNA Binding Activities of TrwB, the Coupling Protein Essential in Plasmid R388 Conjugation*. *Journal of Biological Chemistry* **274**, 36117-36124 (1999).
71. B. B. Hopkins, T. T. Paull, The P. furiosus mre11/rad50 complex promotes 5' strand resection at a DNA double-strand break. *Cell* **135**, 250-260 (2008).
72. J. K. Blackwood *et al.*, Structural and functional insights into DNA-end processing by the archaeal HerA helicase-NurA nuclease complex. *Nucleic Acids Res* **40**, 3183-3196 (2012).
73. M. De Falco, F. Catalano, M. Rossi, M. Ciaramella, M. De Felice, NurA Is Endowed with Endo- and Exonuclease Activities that Are Modulated by HerA: New Insight into Their Role in DNA-End Processing. *PloS one* **10**, e0142345 (2015).
74. X. Feng, M. Sun, W. Han, Y. X. Liang, Q. She, A transcriptional factor B paralog functions as an activator to DNA damage-responsive expression in archaea. *Nucleic Acids Res* **46**, 7085-7096 (2018).
75. E. V. Koonin, K. S. Makarova, Y. I. Wolf, M. Krupovic, Evolutionary entanglement of mobile genetic elements and host defence systems: guns for hire. *Nat Rev Genet* **21**, 119-131 (2020).
76. E. M. Lai, C. I. Kado, Processed VirB2 is the major subunit of the promiscuous pilus of Agrobacterium tumefaciens. *J Bacteriol* **180**, 2711-2717 (1998).
77. A. Punjani, J. L. Rubinstein, D. J. Fleet, M. A. Brubaker, cryoSPARC: algorithms for rapid unsupervised cryo-EM structure determination. *Nature Methods* **14**, 290-296 (2017).
78. K. Zhang, Gctf: Real-time CTF determination and correction. *Journal of Structural Biology* **193**, 1-12 (2016).
79. J. Jumper *et al.*, Highly accurate protein structure prediction with AlphaFold. *Nature* **596**, 583-589 (2021).
80. P. Emsley, B. Lohkamp, W. G. Scott, K. Cowtan, Features and development of Coot. *Acta crystallographica. Section D, Biological crystallography* **66**, 486-501 (2010).

81. E. F. Pettersen *et al.*, UCSF Chimera--a visualization system for exploratory research and analysis. *J Comput Chem* **25**, 1605-1612 (2004).
82. P. D. Adams *et al.*, PHENIX: a comprehensive Python-based system for macromolecular structure solution. *Acta crystallographica. Section D, Biological crystallography* **66**, 213-221 (2010).
83. V. B. Chen *et al.*, MolProbity: all-atom structure validation for macromolecular crystallography. *Acta Crystallogr D Biol Crystallogr* **66**, 12-21 (2010).
84. J. Pei, N. V. Grishin, PROMALS3D: multiple protein sequence alignment enhanced with evolutionary and three-dimensional structural information. *Methods Mol Biol* **1079**, 263-271 (2014).
85. R. Zallot, N. Oberg, J. A. Gerlt, The EFI Web Resource for Genomic Enzymology Tools: Leveraging Protein, Genome, and Metagenome Databases to Discover Novel Enzymes and Metabolic Pathways. *Biochemistry* **58**, 4169-4182 (2019).
86. M. Steinegger *et al.*, HH-suite3 for fast remote homology detection and deep protein annotation. *BMC Bioinformatics* **20**, 473 (2019).
87. F. Gabler *et al.*, Protein Sequence Analysis Using the MPI Bioinformatics Toolkit. *Curr Protoc Bioinformatics* **72**, e108 (2020).
88. N. J. Bale *et al.*, New insights into the polar lipid composition of extremely halo (alkali) philic euryarchaea from hypersaline lakes. *Frontiers in microbiology* **10**, 377 (2019).
89. J. L. Sampaio *et al.*, Membrane lipidome of an epithelial cell line. *Proc. Natl. Acad. Sci. U.S.A.* **108**, 1903-1907 (2011).
90. C. S. Ejsing *et al.*, Global analysis of the yeast lipidome by quantitative shotgun mass spectrometry. *Proc. Natl. Acad. Sci. U.S.A.* **106**, 2136-2141 (2009).
91. M. J. Gerl *et al.*, Quantitative analysis of the lipidomes of the influenza virus envelope and MDCK cell apical membrane. *The Journal of cell biology* **196**, 213-221 (2012).
92. M. A. Surma *et al.*, An automated shotgun lipidomics platform for high throughput, comprehensive, and quantitative analysis of blood plasma intact lipids. *Eur J Lipid Sci Technol* **117**, 1540-1549 (2015).
93. K. R. Levental *et al.*, omega-3 polyunsaturated fatty acids direct differentiation of the membrane phenotype in mesenchymal stem cells to potentiate osteogenesis. *Sci Adv* **3**, eaao1193 (2017).
94. R. Herzog *et al.*, LipidXplorer: a software for consensual cross-platform lipidomics. *PloS one* **7**, e29851 (2012).
95. W. W. Low *et al.*, Mating pair stabilization mediates bacterial conjugation species specificity. *Nature Microbiology* **7**, 1016-1027 (2022).
96. S. Kreida *et al.*, Cryo-EM structure of the Agrobacterium tumefaciens T4SS-associated T-pilus reveals stoichiometric protein-phospholipid assembly. *Structure* **31**, 385-394.e384 (2023).
97. L. C. Beltran *et al.*, Archaeal DNA-import apparatus is homologous to bacterial conjugation machinery. *Nature Communications* **14**, 666 (2023).
98. W. Zheng *et al.*, Cryoelectron-Microscopic Structure of the pKpQIL Conjugative Pili from Carbapenem-Resistant Klebsiella pneumoniae. *Structure* **28**, 1321-1328.e1322 (2020).
99. K. Macé *et al.*, Cryo-EM structure of a type IV secretion system. *Nature* **607**, 191-196 (2022).
100. D. Ghosal *et al.*, Molecular architecture, polar targeting and biogenesis of the Legionella Dot/Icm T4SS. *Nature Microbiology* **4**, 1173-1182 (2019).
101. D. Ghosal, Y.-W. Chang, K. C. Jeong, J. P. Vogel, G. J. Jensen, In situ structure of the Legionella Dot/Icm type IV secretion system by electron cryotomography. *EMBO reports* **18**, 726-732 (2017).
102. C. L. Durie *et al.*, Structural analysis of the Legionella pneumophila Dot/Icm type IV secretion system core complex. *eLife* **9**, e59530 (2020).
103. J. B. Heng *et al.*, The Electromechanics of DNA in a Synthetic Nanopore. *Biophysical Journal* **90**, 1098-1106 (2006).
104. M. Llosa, F. X. Gomis-Rüth, M. Coll, F. de la Cruz Fd, Bacterial conjugation: a two-step mechanism for DNA transport. *Mol Microbiol* **45**, 1-8 (2002).

105. A. Babić, A. B. Lindner, M. Vulić, E. J. Stewart, M. Radman, Direct Visualization of Horizontal Gene Transfer. *Science* **319**, 1533-1536 (2008).
106. C. C. Brinton, Jr., The structure, function, synthesis and genetic control of bacterial pili and a molecular model for DNA and RNA transport in gram negative bacteria. *Trans N Y Acad Sci* **27**, 1003-1054 (1965).
107. J. Amro *et al.*, Cryo-EM structure of the Agrobacterium tumefaciens T-pilus reveals the importance of positive charges in the lumen. *Structure* **31**, 375-384 e374 (2023).
108. L. C. Harrington, A. C. Rogerson, The F pilus of Escherichia coli appears to support stable DNA transfer in the absence of wall-to-wall contact between cells. *J Bacteriol* **172**, 7263-7264 (1990).
109. E. Roth, A. Glick Azaria, O. Girshevitz, A. Bitler, Y. Garini, Measuring the Conformation and Persistence Length of Single-Stranded DNA Using a DNA Origami Structure. *Nano Lett.* **18**, 6703-6709 (2018).
110. K. Goldlust, A. Couturier, L. Terradot, C. Lesterlin, "Live-Cell Visualization of DNA Transfer and Pilus Dynamics During Bacterial Conjugation" in Chromosome Architecture: Methods and Protocols, M. C. Leake, Ed. (Springer US, New York, NY, 2022), 10.1007/978-1-0716-2221-6_6, pp. 63-74.
111. M. Clarke, L. Maddera, R. L. Harris, P. M. Silverman, F-pili dynamics by live-cell imaging. *Proceedings of the National Academy of Sciences* **105**, 17978-17981 (2008).
112. K. Kishida *et al.*, Contributions of F-specific subunits to the F plasmid-encoded type IV secretion system and F pilus. *Molecular Microbiology* **117**, 1275-1290 (2022).
113. M. B. Dürrenberger, W. Villiger, T. Bächi, Conjugational junctions: Morphology of specific contacts in conjugating Escherichia coli bacteria. *Journal of Structural Biology* **107**, 146-156 (1991).
114. A. Klimke William, S. Frost Laura, Genetic Analysis of the Role of the Transfer Gene,traN, of the F and R100-1 Plasmids in Mating Pair Stabilization during Conjugation. *Journal of Bacteriology* **180**, 4036-4043 (1998).
115. B. Hu, P. Khara, P. J. Christie, Structural bases for F plasmid conjugation and F pilus biogenesis in Escherichia coli. *Proc Natl Acad Sci U S A* **116**, 14222-14227 (2019).
116. J. Patkowski *et al.*, The F-pilus biomechanical adaptability accelerates conjugative dissemination of antimicrobial resistance and biofilm formation. *Nature Communications* **14**, 1-14 (2023).
117. C. K. Ellison, T. N. Dalia, A. B. Dalia, Y. V. Brun, Real-time microscopy and physical perturbation of bacterial pili using maleimide-conjugated molecules. *Nat Protoc* **14**, 1803-1819 (2019).
118. I. Chen, D. Dubnau, DNA uptake during bacterial transformation. *Nature Reviews Microbiology* **2**, 241-249 (2004).
119. H. Gangel *et al.*, Concerted Spatio-Temporal Dynamics of Imported DNA and ComE DNA Uptake Protein during Gonococcal Transformation. *PLOS Pathogens* **10**, e1004043 (2014).
120. N.-J. Krüger, K. Stingl, Two steps away from novelty – principles of bacterial DNA uptake. *Molecular Microbiology* **80**, 860-867 (2011).
121. J. Schindelin *et al.*, Fiji: an open-source platform for biological-image analysis. *Nature Methods* **9**, 676-682 (2012).

Chapter 7: List of all publications

Beltran, L.C., Torsilieri Holly, Patkowski, Yang Jae., Casanova James, Costa, T.R.D,. Wright Elizabeth, Egelman, E.H., The mating pilus of *E.coli* pED208 acts as a conduit for ssDNA during horizontal gene transfer. **mBio**, 0(0), e02857-02823.doi:10.1128/mbio.02857-23

Beltran, L.C., Cvirkaite-Krupovic, V., Miller, J., Wang, F., Kreutzberger M, A. B., Patkowski, J., Costa, T.R.D,. Schouten, S., Levental, I., Conticello V.P., Egelman, E. H., and Krupovic, M. Domesticated conjugation machinery promotes DNA exchange in

hyperthermophilic archaea. **Nature Communications**, 14, 666 (2023), 2041-1723. doi:10.1038/s41467-023-36349-8

Lin, Zhiwei., **Beltran, L.C.,** De los Santos, Z.A., Li, Y., Adel, T., Fagan, J.A., Walker A., Egelman, E.H., Zheng, M. DNA-guided lattice remodeling of carbon nanotubes. **Science**, 29, 377 (2022), PMID: 35901135

Low, W.W., Wong, J.L.C., **Beltran, L.C.,** Seddon, C., David, S., Kwong, HK., Bizeau, T., Wang, F., Pe.a, A., Costa, T.R.D,. Pham, P., Chen, M., Egelman, E.H., Beis, K., Frankel, G. Mating pair stabilization mediates bacterial conjugation species specificity. **Nature Microbiology**, 7, 7 (2022), 1016-1027. doi:10.1038/s41564-022-01146-4

Kreutzberger M, A. B., Wang, S., **Beltran L.C.,** Tuachi, A., Zuo, X., Egelman E.H., & Conticello V.P. Phenol Soluble modulins PSMa3 and PSMb2 form nanotubes that are cross-a amyloids. **PNAS** 119, e2121586119 (2022)

Wang, F., Gnewou, O., Modlin, C., **Beltran, L.C**., Xu, C., Su, Z., Juneja, P., Grigoryan, G., Egelman, E. H. and Conticello, V. P. Structural analysis of cross α-helical nanotubes provides insight into the designability of filamentous peptide nanomaterials. **Nature Communications** 12, 407 (2021). PMCID: PMC7814010

Wang, F., Cvirkaite-Krupovic, V., Vos, M., **Beltran, L.C.,** Kreutzberger, M. A. B., Winter, J.-M., Su, Z., Liu, J., Schouten, S., Krupovic, M and Egelman, E. H. Spindleshaped archaeal viruses evolved from rod-shaped ancestors to package a larger genome. **Cell** 185, 1297-1307 (2022), cover article of 14 April issue.

Wang, F., P. Baquero, D., **Beltran, L.C.,** Su, Z., Osinski, T., Zheng, W., Prangishvili, D., Krupovic, M. and Egelman E.H. Structures of filamentous viruses infecting hyperthermophilic archaea explain DNA stabilization in extreme environments. **PNAS** 117 (33) (2020). PMCID: PMC7443925

Wang, F., Baquero, D. P., Su, Z., **Beltran, L.C**., Prangishvili, D., Krupovic, M., & Egelman, E. H. The structures of two archaeal type IV pili illuminate evolutionary relationships. **Nature Communications** 11, 3424 (2020). PMCID: PMC73478